III. DUBAI INTERNATIONAL CONFERENCE OF PURE, APPLIED AND TECHNOLOGICAL SCIENCES

Rimar Academy
Publishing House

III. Dubai International Conference of Pure, Applied and Technological Sciences

FULL TEXT BOOK

Yayınevi:	دار النشر:	Rimar Academy
Editör:	المحرر:	Prof. Dr. Ghuson H. MOHAMMED
Yayın Koordinatörü:	تنسيق النشر:	AMIR MUAENI
ISBN:	نظام الترميز الدولي لترقيم الكتاب:	978-625-92121-0-4
DOI :	رقم معرف الكائن الرقمي:	http://dx.doi.org/10.47832/Dub.Conf3
Baskı:	تاريخ الطباعة:	29 / 03 / 2026
kongre Tarihi:	تاريخ المؤتمر:	05 - 06 - 07 / 01 / 2026
Sayfalar:	عدد الصفحات:	83
URL:	رابط النشر:	www.rimaracademy.com
No Sertifikası Matbaa:	رقم شهادة المطبعة:	47843

PREFACE

III. Dubai International Conference of Pure, Applied and Technological Sciences was organized by Mardin University in collaboration with Rimar Academy. The primary objective of this event was to compile and disseminate valuable scientific knowledge andmake ameaningful contribution to the future.

A substantial number of researchers from both local and international backgrounds demonstrated their interest in this conference. The scientific committee meticulously reviewed the submissions and ultimately accepted a select group of applicants—**13** in total—of whom **10** were approved by the scientific committee.

The core of this conference was the presentation of **8** full research papers, while the remaining articles and research findings are set to be featured in for the coming issues of the MINAR Journal.

I would like to extend my sincere appreciation to all the contributors and scholars who played an essential role in making this conference a resounding success. Your dedication and valuable contributions are deeply respected and acknowledged.

Editor-in-Chief
Prof. Dr. Ghuson H. MOHAMMED

رئيس المؤتمر
Chair of Congress

Chair of Congress

رئيس المؤتمر

الأستاذ الدكتور غصون حميد محمد

Prof. Dr. Ghuson H. MOHAMMED

جامعة بغداد

Baghdad University

Iraq - العراق

Chairman of Organizing Committee

رئيس الهيئة التحضيرية

الاستاذ الدكتور منير سالم طه

Prof. Dr. Muneer salim TAHA

مساعد رئيس جامعة الموصل للشؤون العلمية

Vice-president for Scientific Affairs of the University of Mosul

Iraq - العراق

General Secretary

الأمين العام للمؤتمر

أ. د. عبد الكريم دهش علي

Prof. Dr. Abdulkareem Dash ALI

جامعة تكريت

Tikrit University

Iraq - العراق

الرؤساء الفخريون
Honorary Committee

Prof. Dr. Mehmet Hakkı ALMA

Rector of Iğdır University

Türkiye

Prof. Dr. Waad Mahmood RAOOF

Rector of Tikrit University

Iraq

Prof. Dr. Alyaa A. Ali Al-ATTAR

Rector of Northern Technical University

Iraq

Prof. Dr. Tariq Hafdhi Abbd Tawfeeq

President of the University of Al-Farhidi

Iraq

Prof. Dr. Khamis A. ZIDAN

Vice Rector of Al-Iraqia University for Scientific Affairs

Iraq

الهيئة الاستشارية
Consultative Committee

Prof.Dr. Tawfiq Mohammed Mustafa Al-ANTARY
University of Jordan
Jordan

Prof.Dr. Nezar Husein Ata Samarah
Jordan university of Science and Technology
Jordan

Prof. Dr. Ahmad Al-Momany.
University of Jordan.
Jordan

Prof. Dr. Mohammed Younis Salim
university of mosul
Iraq

Dr. Osman TÜRK
Harran University
Türkiye

Prof. Dr. Hiyam Adil Ibrahim Ismail ALTAII
University of Mosul
Iraq

Dr. Nabil Mohie Abdel-Hamid ALY
Kafrelsheikh University
Egypt

الهيئة التحضيرية
Organizing Committee

Prof. Dr. Abdelmonnem S. KAHLEL
University of Mosul
Iraq

Dr. Kassem Danach
Al Maaref University
Lebanon

Assist. Prof. Dr.Assma Ahmed Hatem Sultan
Baghdad University
Iraq

Prof. Dr. Nihad Abdul-Lateef ALI
Al-Qasim Green University
Iraq

Prof.Dr.Abbas kadhim Abd Ali
Al-Qasim Green University
Iraq

Rehab Noori Shalan
University of Baghdad
Iraq

Lect. Dr. Zahraa Hussein Kadhim
Al-Qasim Green University
Iraq

Assist. Prof. Iman radha JASIM
University of Mosul
Iraq

Farah T.O.Al-Jumaili
A-l Nahrain University
Iraq

Lect. Dr. Ahmed N. AL-SHAMMAA
University of Baghdad
Iraq

Lect. Dr. Bassim Kareem Mihsin
General Directorate of Education in karbala
Iraq

Prof. Dr. Nawras Abdelah Alwan
Basrah University
Iraq

Assist. Prof. Dr. Methaq Abd Muslim GUDA
University of Kufa
Iraq

Esraa Habeeb Khaleel
Tikrit university
Iraq

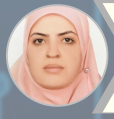

Anas Hashim Sadek
Ibn Sina University
Iraq

Ghufran Mohammed Jassam
Al-Nahrain University
Iraq

الهيئة العلمية

prof.Dr. Ebtehag Zeki Sulyman Al Halim
University of Mosul
Iraq

Dr. Nagwa El-Mobarak
Mansoura University
Egypt

Dr. FOUZIA Youcef
University of Kasdi Merbah Ouargla
Algeria

Assist. prof. intisar ghanim TAHA
University of Mosul
Iraq

Dr. Rana Rezk Drbouli
Al_Baath University
Syria

Dr. Mutasim Ali Mohamed ELAGAB
Gezera University
Sudan

Dr. Riyam Adnan Hammudi Al inizi
wasit university
Iraq

Assist. Prof. Dr. Qusay Kamil Jasim
Northern technical unviersity
Iraq

Dr. Bader AL-AİFAN
Kuwait University
Kuwait

Lect.Dr. Ammar Al-ZUBADE
University of Baghdad
Iraq

prof.Dr. Athraa H.Mohsen alduhaidahawi
Desert Research Center
Egypt

Lect. Ameer kamil hamzah alqaraghuli
Middle technical university
Iraq

Amal Mohamed OmerSalem
Ain Shams University
Egypt

Dr. Fatiha HACHANI
KASDI Merbah University-Ouargla
Algeria

ssistant professor dr.Rusul Alabada
Al-Muthanna University
Iraq

Dr. Ali Farhan Hashoosh
Misan University
Iraq

Asst.Prof.Dr. Hussain Ibrahim Hussain
Tikrit University
Iraq

Assistant Professor Dr.MOHAMMED SHAREEF MOHAMMED
SAMARRA UNIVERSITY
Iraq

Assistant professor Dr Ali Hassan Karim ALHAMMAMI
University of kufa
Iraq

Assistant Professor Dr. Zainab Hadi Mahmoud
University of Baghdad
Iraq

Assistant Teacher Zeina Hadi Saeed
Middle Technical University
Iraq

Dr. May Ahmed Fakhry Farhat Mousa
Alexandria University
Egypt

Dr. Mayson Thafir HADI
University of Baghdad
Iraq

Hussein Ali Mohammed AL_Ukaily
University of Wasit
Iraq

Dr. Shatha Hizem SHAKER
Tikrit University
Iraq

Associate Professor Dr. Nisreen Sulayman
Damascus University
Syria

Dr.Dawood Salman Abd Al-kader
Ministry of Education
Iraq

Lec. Dr. Ali Adil Abbas
University of Baghdad
Iraq

Table of Contents


DUBAI

L-Methionine Γ-Lyase Extracted and Characterized from Streptomyces Maritimus has Microbicidal Activity

Nada Z. Mahdi [1]

Neihaya H. Zaki [2]

Suhair S Al-Siraj [3]

Amr Hassan [4]

Maha F. Lotfy [5]

Eman M. Sharaf [6]

Abstract:

-methionine γ-lyase (MGL) is a biologically active enzyme with recognized antitumor and antimicrobial potential that can be produced from microbial sources. In this study, MGL from the soil isolate *Streptomyces maritimus* MSQ21 was purified, physiochemically characterized, and evaluated for antimicrobial activity against *Escherichia coli* (ATCC 6933), *Salmonella typhimurium* (ATCC 14028), *Pseudomonas aeruginosa* (ATCC 10145), *Staphylococcus aureus* (ATCC 20231), *Bacillus cereus* (ATCC 33018), *Candida albicans* (ATCC 90028), and *Aspergillus niger* obtained from the National Microbial Culture Repository, Ain Shams University. UV-visible spectrophotometry revealed the typical enzyme characteristic absorption peaks (280 and 420 nm). The enzyme showed optimal activity at pH 6.5–7.5 and retained 90% stability at pH 7.0, while mercury and iodoacetate strongly inhibited activity, leaving residual activities of 42.5% and 11.5%, respectively. Kinetic analysis showed Km and Vmax values of 20 µM and 13.041 µM·min^{-1}. The enzyme demonstrated antimicrobial activity against *Bacillus cereus* and *Staphylococcus aureus* with MIC ≤ 8 and 16 µg/ml, while MIC values against *Salmonella typhimurium*, *E. coli*, and *Pseudomonas aeruginosa* were 16, 64, and 64 µg/ml. Additionally, the enzyme exhibited antifungal activity against *Candida albicans* and *Aspergillus niger*, with MIC 8 µg/ml for both organisms. These results indicate that MGL from *Streptomyces maritimus* MSQ21 possesses broad-spectrum microbicidal.

Keywords: *L-Methionine Γ-Lyase; Candida; Streptomyces Maritimus; Fermentation; Gram-Negative; Gram-Positive; Antifungal; Antimicrobial* .

http://dx.doi.org/10.47832/Dub.Conf3-1

[1] Researcher. College of Science, Mustansiriyah University, Iraq smnk@uomustansiriyah.edu.iq

[2] Researcher. College of Science, Mustansiriyah University, Iraq dr.neihayahz@uomustansiriyah.edu.iq

[3] Researcher. College of Science, Mustansiriyah University, Iraq suhair_shaker@uomustansiriyah.edu.iq

[4] Researcher. Genetic Engineering and Biotechnology Research Institute (GEBRI), University of Sadat, Egypt amrhassan.nanotechnology@gmail.com

[5] Researcher. Faculty of Agriculture, Ain Shams University, Egypt maha_fawzy@agr.asu.edu.eg

[6] Researcher. Immunology and Mycology Dept., Animal Health Research Institute, Egypt dr_emansharaf@yahoo.co

1. Introduction

Infectious infections are one of the leading triggers of death worldwide [1], and they impose a significant burden on public health and economy, because the growing problem of antimicrobial resistance has necessitated the re-evaluation of classical chemotherapeutic approaches relying primarily on broad-spectrum antibiotics [2, 3]. Enzymology has been considered as a field of research with wide implications in the various scientific and medical fields, and L-methionine-based therapies were applied as an anticancer treatment for different types of cancer, including colon, lung, prostate, brain, and kidney cancers [4, 5]. For example, oral administration of recombinant methioninase was suggested for COVID-19 treatment with a dual mechanism of action, by limiting methionine supply and distribution in the virus and suppressing the virus growth which is a critical factor of COVID-19-related mortality [6]. However, some bacterial and fungal pathogens are difficult to treat in the clinic, while Staphylococcus aureus, a typical member of the *Staphylococcaceae* family, is known for causing life-threatening bloodstream, respiratory, and skin infections in humans [7, 8], and *Pseudomonas aeruginosa* is known as the main invoker of highly intense acute and chronic infections with 40% as a mortality rate [9]. *Bacillus cereus* has been stated as gram-positive bacterium that causes food-related diseases and has been isolated especially from ready-to-eat foods [10], because the infection of *B. cereus* leads to diarrheal and emetic syndromes, as the bacterium produces several factors in the gastrointestinal tract that contribute to its virulence [11]. *Candida albicans* is the main etiological agent of localized mucosal, disseminated fungal infections and represents more than 70% of mycoses worldwide [12], although antifungal therapy has developed, the mortality rate of *C. albicans* infections still around 40%, especially under clinical conditions such as critically ill or immunocompromised patients [13, 14]. *Aspergillus niger* is widely used in industrial fermentation and food biotechnology, especially in the production of biological acids, as a ubiquitous environmental fungus that is often isolated from soil and other natural habitats, and the spores of *A. niger* show a high resistance to environmental stress, which contributes to survival, spread, and persistence in different environments, including food-related and human-associated niches. In addition, *A. niger* is a medically important opportunistic fungus, because members of the *A. niger* complex have been implicated in human infections, particularly otomycosis, under certain conditions or in immunocompromised individuals [15–17], and consequently, the combination of significant biotechnological importance and environmental persistence with opportunistic pathogenicity underlines the dual importance of *A. niger* for industry and human health. During the last ten years, a tremendous research effort has been devoted to discovery of new strategies to prevent and treat bacterial and fungal infections that are resistant to conventional antibiotics [18], and L-methionine was found to be a promising candidate to target and control different classes of bacterial, fungal, and protozoal pathogens [19, 20]. In the present study, we have isolated, purified, and characterized L-methionine γ-lyase (MGL) from *Streptomyces maritimus*, assayed its activity against different bacterial and fungal species to examine its ability to inhibit microbial growth as compared to the conventional antimicrobial drugs.

2. Materials and Methods

2.1. Microbial isolates and strains:

For the current investigation, a collection of bacterial and fungal microorganisms was sourced out of the National Microbial Culture Repository, Faculty of Agriculture, Ain Shams University, Cairo, Egypt. The selected strains comprised Gram-negative bacteria, including *Escherichia coli* (ATCC 6933), *Salmonella typhimurium* (ATCC 14028), and *Pseudomonas aeruginosa* (ATCC 10145), in addition to Gram-positive species represented by *Staphylococcus aureus* (ATCC 20231) and *Bacillus cereus* (ATCC 33018). The microbial panel also involved the yeast *Candida albicans* (ATCC 90028) and the fungal strain *Aspergillus niger*. Furthermore, *Streptomyces maritimus* (MSQ21), employed as the source organism for enzymex production through fermentation, was isolated from soil samples.

2.2. Preparation and standardization of microbial inoculum:

Fresh bacterial cultures were prepared by overnight growth in appropriate broth media, whereas fungal isolates were cultivated on suitable agar media under optimal conditions. Microbial suspensions were adjusted to 0.5 McFarland standard (approximately 1×10^8 CFU/mL for bacteria) to ensure standardized inoculum density. For minimum inhibitory concentration (MIC) assays, standardized suspensions were further diluted to approximately 5×10^5 CFU/mL according to assay requirements. This procedure ensured reproducible microbial loading and minimized experimental variability during antimicrobial susceptibility assessments.

2.3. Enzyme production using submerged fermentation:

For enzyme biosynthesis, *Streptomyces maritimus* was grown in submerged fermentation in an induction-based production medium designed to induce methioninase expression by the addition of methionine [21], and L-methionine was added as a substrate inducer with balanced nutritional ingredients for microbial growth and extracellular enzyme production. Cultivation was performed at 25°C with aerobic shaking for 72 h, and after incubation, the biomass was harvested by cold centrifugation, washed with phosphate buffer (pH 7.8) to remove the remaining medium components, and used for intracellular enzyme extraction. Cells were disrupted in extraction buffer with phenylmethylsulfonyl fluoride and ultrasonic disintegration, and subsequently, cellular debris has been eliminated by centrifugation, clarified supernatant has been assembled [22].

2.4. Enzyme activity investigation:

Activity was determined using modified version of the DTNB-based spectrophotometric assay originally developed for the detection of thiol [23] in order to measure methanethiol, because reaction mixtures were prepared in phosphate buffer (pH 8.0) using PLP as the cofactor and L-methionine as the substrate. After catalytic cleavage, sulfur-containing product released has reacted with 5,5'-dithiobis-(2-nitrobenzoic acid) to create a chromogenic derivative that was quantified spectrophotometrically, and after incubation at defined

conditions, then absorbance measured at 420 nm. The methanethiol formation rate has been used to estimate the enzyme activity.

2.5. Assessment of Deaminase activity:

Based on the amount of ammonia formed during substrate turnover, the deaminating activity has been assessed, which was performed using a Nessler reagent-based analytical procedure [24]. In this assay, the enzymatically produced ammonia reacts with Nessler reagent to form a colored complex that is measured spectrophotometrically to determine deaminase activity, and the concentration of ammonia was used to calculate the enzymatic activity.

2.6. Estimation of enzyme concentration:

Protein concentration during extraction and purification was estimated using a Folin–Ciocalteu colorimetric protocol adapted for enzyme-containing fractions [25]. Quantification was performed by comparing absorbance values of tested samples against a standard calibration curve generated using reference protein solutions. Purification efficiency of L-methionine γ-lyase was subsequently assessed through progressive analysis of total protein, specific activity, and recovery percentage across sequential purification stages, including fractionation and chromatographic processing [26].

2.7. Enzyme purity:

The implementation of UV–visible spectroscopy was proved to have the efficacy to detect and assess the degree of purity that enzymes possess [27]. Briefly, purified enzyme extract was combined with phosphate buffer that have concentration of 100 mM, in addition, EDTA with a concentration of 1 μM has been added to the mixture. Furthermore, through utilization of UV- visible scanning, the covalent Schiff base formed within the MGL active site has been assessed at the wavelength of 180–560 nm.

2.8. Characterization of L-methioninase:

2.8.1. pH optimization:

Catalytic responsiveness of purified enzyme to pH variation was evaluated over a broad spectrum of acidic, neutral, and alkaline conditions using appropriate buffering systems. Acetate, phosphate, and carbonate buffers were employed to generate pH range of 4 to 10.5. To determine pH stability, enzyme samples have been incubated for one hour at 25 °C in substrate-free buffers of different pH values prior to residual activity determination under standardized assay conditions. This approach enabled assessment of both immediate catalytic response and structural tolerance across variable hydrogen ion concentrations [28].

2.8.2. Influence of temperature:

Temperature optimization was performed by exposing L-methionine γ-lyase to reaction temperatures spanning 30°C to 80°C followed by measurement of catalytic performance under standard assay conditions. Thermal stability further assessed by pre-incubating enzyme aliquots at selected temperatures for defined time intervals prior to residual activity analysis.

These experiments allowed determination of the optimal functional temperature range as well as thermal resistance characteristics of the purified enzyme [28].

2.8.3. Assessment of enzyme responsiveness to chemical inhibitors and metal ions:

To investigate biochemical sensitivity, purified enzyme samples were pretreated with selected metal ions and chemical modifiers before substrate addition. Following incubation, residual catalytic activity was quantified relative to untreated controls to determine the degree of enzymatic inhibition or tolerance induced by each tested compound. This procedure provided functional insight into cofactor dependence, inhibitory susceptibility, and catalytic stability under chemically modified conditions [28].

2.9. Investigation of kinetic parameters:

Kinetic analysis of purified enzyme was carried out by determining the reaction initial velocities at varying substrate concentrations under optimal assay conditions, and data obtained were tailored to the Michaelis–Menten equation to evaluate the substrate affinity and catalytic efficiency. The Km and Vmax were derived out of Lineweaver–Burk double reciprocal plots to assess the enzyme–substrate interaction and maximum catalytic velocity [29].

2.10. Enzyme antimicrobial activity:

2.10.1. In vitro Antimicrobial Susceptibility Testing:

Microbicidal activities of MGL against different types of bacteria were assayed through implementation of agar well diffusion method [30], briefly, the above mentioned Gram-negative and Gram-positive bacterial test strains were individually inoculated into sterile nutrient agar (0.7% w/v). Fresh overnight suspensions (0.1 mL; 105 CFU/mL) of bacteria were mixed with 15 mL of molten nutrient agar cooled to 48°C and then placed into Petri dishes, where 6 mm wells have been punched aseptically in the agar. One hundred microliters of the enzyme extract were added to each well, and tetracycline was employed as antibacterial control. The plates kept at 25°C for 120 min then incubated at 37°C for 24 h.

2.10.2. Antifungal Disk Diffusion Method:

Potato dextrose agar (PDA) was utilized to incubate fungal strains obtained from the culture collection. The agar was melted at a high temperature and then cooled to 48°C. It was then mixed with 0.1 ml of *Candida albicans* and *Aspergillus niger* fresh culture (105 CFU/ml) and placed in a sterile Petri dish. To prepare the agar plate, 6 mm diameter wells were made and 100 µL of enzyme extract was added. The plates were kept at 30°C for two days, and findings were compared to Itraconazole, a control antifungal drug [25].

2.10.3. Minimum inhibitory concentration assay:

Quantitative assay of MIC has been implemented to view capability of the antimicrobial activity of that the enzyme exhibits. In order to run the assay, a preparation of inoculum with a concentration of 5×105 CFU/mL has been formed by inoculum dilution with equivalence to 0.5 McFarland standard to reach the ratio of 1:100. Each inoculum was diluted twice using the tested mixtures, then at wavelength of 540 nm the absorption was assessed after

incubation at 37 °C for one day. Control drugs utilized were composed of tetracycline and itraconazole [3].

2.11. Statistical Analysis:

Data implemented in this study has been analyzed in SPSS v17 (SPSS Inc., USA) using one-way ANOVA. Significance was accepted at $p < 0.05$. Results represent mean ± SD based on analyses performed by three investigators in an independent way [30-32].

3. Results

3.1. Production of *Streptomyces maritimus* L-methioninase:

Crude extracellular L-methioninase fraction obtained had an activity of 12.24 U/mL and protein content of 0.092 mg/mL, which was observed to decrease to 0.080, 0.065, 0.056, and 0.048 mg/mL after purification with acetone precipitation, ammonium sulphite fractionation, Sephadex G100 gel filtration, and DEAE–Sepharose anion-exchange chromatography. The purification fold seemed to increase from 1.0 in the crude extract to 1.082 in the acetone-treated fraction and 1.094 after ammonium sulphite fractionation, and it showed a marked increase to 2.632 and 2.865 after Sephadex G100 and DEAE–Sepharose chromatography, respectively. The enzyme recovery was 100% in the crude extract and decreased progressively during purification, ranging from 40–41% after the DEAE–Sepharose chromatography, because the purification fold and recovery of MGL were observed to be significantly affected by the nature of the purification matrix. Consequently, the enzyme recovery decreased from 100% in the crude preparation to 40.72% after DEAE–Sepharose chromatography. Fig. 1 shows the UV–visible spectrum, which exhibits two typical absorption peaks at 280 and 420 nm, indicating that the purified enzyme was proteinaceous, as the 280 nm peak suggested presence of aromatic amino acid residues. Moreover, the peak at 420 nm suggested presence of pyridoxal 5′-phosphate cofactor at the active site, which is consistent with the formation of an internal Schiff-base linkage between PLP and the ε-amino group of an active-site lysine residue, a characteristic of methionine γ-lyase and other PLP-dependent enzymes.

Table 1. Comprehensive Purification profile of the extracted enzyme

Steps	Total Protein (mg/ml)	Streptomyces maritimus			
		Total Activity (µmol/min)	Specific activity (µmol /mg/min)	Purification fold value	Recovery (%)
Crude enzyme extract	0.09	6.2	64.2	1	100
Acetone precipitation	0.08	5.7	82	1.1	91.1
Ammonium sulfate fractionation	0.06	4.2	82.4	1.1	90.4
Sephadex G-100 gel filtration chromatography	0.05	3.4	92	2.6	65
DEAE-Sepharose anion-exchange chromatography	0.04	3.1	99.7	2.9	40.7

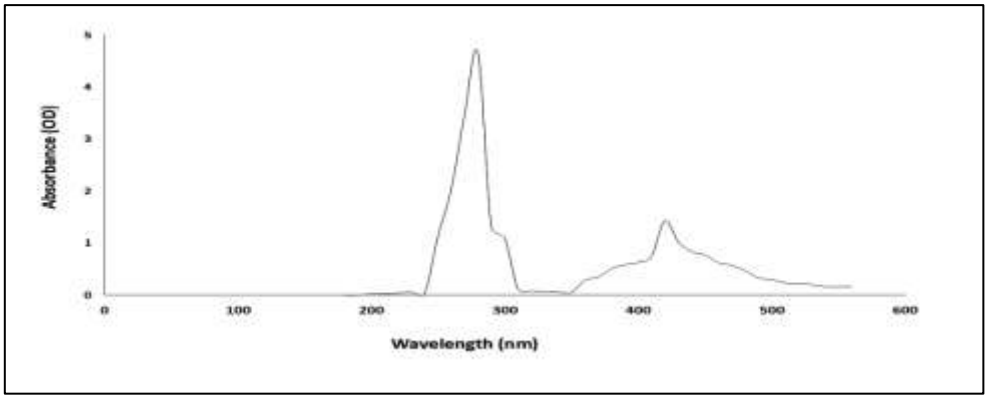

Figure 1. UV spectrum of purified Streptomyces maritimus MSQ21 L-methionine γ-lyase.

3.2. pH-Dependent Changes in Enzyme Activity and Stability:

Catalytic activity and structural stability of purified L-methionine γ-lyase were greatly influenced by pH as shown in Table 2 and Fig. 2. L-methionine γ-lyase showed measurable activity over a wide pH range (4.0–10.5), but the degree of catalysis was dependent on proton concentration, and the enzyme showed lower activity at acidic conditions with 42% activity at pH 4.0, but it increased gradually as pH values were approaching neutral. The highest catalytic activity was observed at pH 6.5–7.5 with 80% activity at pH 6.5 and maximum activity of 88% at pH 7.5; however, activity decreased progressively with increasing pH value and the activity reached 31% at pH 10.5. The structural stability of the enzyme also showed a similar pH dependent profile, because the residual activity increased gradually from acidic pH, reached the maximum of 90% at pH 7.0, and showed that the structure of e is stable at neutral condition. The residual activity was gradually decreased at higher pH values with 45% of the residual activity at pH 10.5; consequently, the combined results indicate that the highest catalytic activity was demonstrated at slightly alkaline pH, whereas the most conformationally stable state of the enzyme was observed at neutral pH.

Table 2. pH value impact on enzyme stability and activity.

pH Value	MGL Activity	MGL Stability (%)
4.0	42.0%	52.0%
4.5	50.0%	56.0%
5.0	58.0%	70.0%
5.5	65.0%	73.0%
6.0	73.0%	78.0%
6.5	80.0%	80.0%
7.0	85.0%	90.0%
7.5	88.0%	85.0%
8.0	75.0%	80.0%
8.5	67.0%	60.0%
9.0	50.0%	54.0%
9.5	44.0%	50.0%
10.0	40.0%	48.0%
10.5	31.0%	45.0%

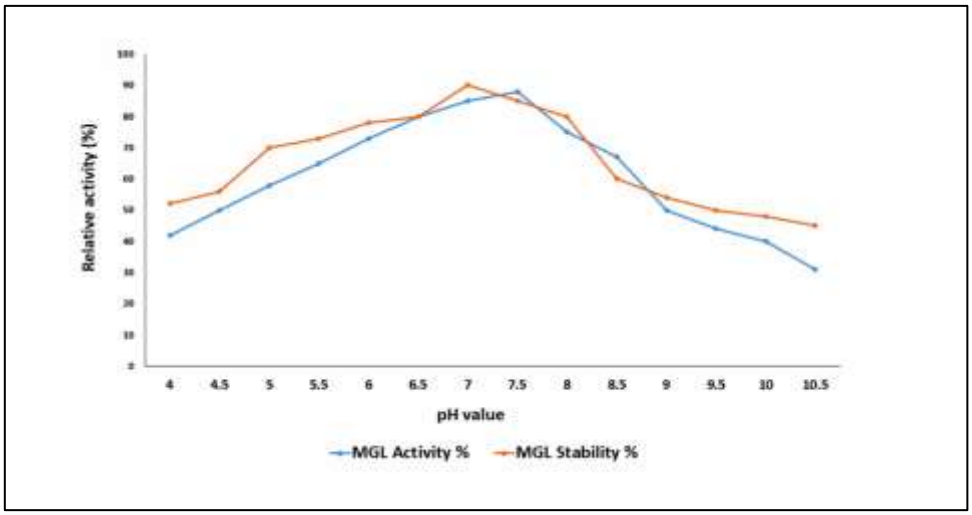

3.3. Effect of temperature on enzyme activity;

Temperature had a notable effect on the catalytic performance of purified enzyme, as presented in Table 3. The enzyme maintained full activity (100%) throughout the temperature range of 30–45°C, indicating that this interval represented the optimal thermal window for catalytic function. A gradual decline in activity was observed above 45°C, with activity remaining relatively high at 50°C (95%) and 55°C (87%), suggesting moderate thermal tolerance. Further temperature elevation resulted in a more substantial reduction in enzymatic activity. Activity declined to 70.2% at 60°C, 50.7% at 70°C, and ultimately reached only 20% at 80°C. This progressive decrease demonstrates increasing thermal sensitivity at elevated temperatures, likely due to temperature-induced structural disruption affecting catalytic efficiency. Overall, L-methionine γ-lyase displayed optimal activity under moderate temperatures between 30°C and 45°C, while temperatures above this range caused progressive thermal inactivation. These findings establish moderate thermal conditions as most suitable for preserving enzymatic functionality.

Table 3. Effect of temperature on enzyme activity.

Reaction temperature	MGL Activity
30.0 °C	100%
35.0 °C	100%
40.0 °C	100%
45.0 °C	100%
50.0 °C	95.0%
55.0 °C	87.0%
60.0 °C	70.2%
65.0 °C	65.0%
70.0 °C	50.7%
75.0 °C	33.0%
80.0 °C	20.0%

3.4. Enzyme thermal stability:

Thermal stability of MGL was estimated by incubation at different temperatures for different periods of time as shown in Table 4. The data presented in Table 3 show that the L-methionine γ-lyase retains 100% activity at 40 °C for 100 min and was stable at 45 °C; however, the enzyme showed a significant loss of activity at higher temperatures: at 70 °C, the activity dropped after 40 min and at 90 °C, the residual activity decreased to 60% after 20 min and was totally lost after 100 min.

Table 4. Thermal stability L-methionine γ-lyase enzyme.

MGL Stability					
Reaction temperature (°C) / time (minutes)	**20 minutes**	**40 minutes**	**60 minutes**	**80 minutes**	**100 minutes**
40.0	100%	100%	100%	100%	100%
45.0	100%	100%	100%	100%	100%
50.0	100%	92.0%	88.0%	58.0%	37.5%
55.0	100%	82.0%	64.0%	48.0%	35.0%
60.0	100%	67.0%	40.0%	25.0%	5.0%
65.0	100%	50.0%	28.0%	10.0%	0.00%
70.0	94.0%	55.0%	10.0%	00.0%	0.00%
75.0	80.0%	29.0%	4.00%	00.0%	0.00%
80.0	75.0%	20.0%	0.00%	00.0%	0.00%
85.0	66.0%	15.0%	0.00%	00.0%	0.00%
90.0	60.0%	10.0%	0.00%	00.0%	0.00%

3.5. Influence of the metal ion on the activity:

The relative activity in presence of calcium, sodium, zinc and potassium ions was 99.6%, 93.0%, 87.5% and 94.8%, respectively, so the enzyme activity was little affected by these ions. However, Ba2+, Hg2+ and Cu+ ions significantly reduced the catalytic efficiency of the enzyme, and the residual activities were 42.7%, 42.5% and 47.5%, respectively. It could be concluded that Hg2+ and Ba2+ ions are strong inhibitory ions that significantly inactivate L-methionine γ-lyase (Table 5).

Table 5. Metal ions dependent variations in L-methionine γ-lyase activity.

Metal ions (Chloride salt, 10 mM)	Relative activity
Control	100%
Sodium ion	99.6%
Potassium ion	94.8%
Magnesium ion	82.3%
Manganese (II) ion	52.0%
Cadmium (II) ion	61.0%
Mercury (II) ion	42.5%

Chromium (III) ion	80.0%
Zinc (II) ion	87.5%
Calcium ion	93.0%
Barium ion	42.7%
Lithium (II) ion	56.1%
Iron (III)	83.0%
Copper (II)	47.5%
Nickel (II) ion	56.8%
Aluminum (III) ion	73.4%
Cobalt (II) ion	73.6 %

3.6. Chemical reagents effects on activity:

Effect of various reagents on MGL activity are presented in Table 6. EDTA, ethanol, methanol, n-butanol, and acetone showed slight effects on L-methionine γ-lyase with residual activities of 91.5%, 99.5%, 96.0%, 85.0%, and 99.2%. while hydroxylamine, H_2O_2, and sodium azide were found to be inhibitors of the enzyme with residual activities of 25.7%, 22.0%, and 40.8%, respectively. Iodoacetate had the strongest inhibition with a residual activity of 11.5%, which indicated that iodoacetate was a major inhibitor of the enzyme.

Table 6. Effect of chemical reagents on L-methionine γ-lyase activity

Chemical reagents (1 mM)	Relative activity
EDTA	91.50%
SDS	50.20%
Ethanol	99.50%
Sodium Azide	40.80%
Methanol	96.00%
Acetone	99.20%
H2O2	22.00%
n-Butanol	85.00%
β- mercabtoethanol	58.00%
Hydroxylamine	25.70%
Iodoacetate	11.50%

3.7. Kinetic properties of L-methionine γ-lyase from Streptomyces maritimus MSQ21:

The kinetic constants (Km and Vmax) were determined by measuring the reaction rates using concentrations of the standard substrate under the standard assay conditions, and the Km and Vmax values were calculated from the Lineweaver-Burk plot (Fig. 3; Table 7). The Lineweaver-Burk analysis showed that Km (affinity constant) was 20 mM and Vmax (maximum velocity) was 13.041 μM·min−1, and therefore, the enzyme showed saturation and maximum activity at substrate concentrations above 30 mM (40, 60, 80 mM, etc.). Moreover, the relationship between reaction velocity and substrate concentration was hyperbolic rather than sigmoidal, indicating that L-methioninase is an allosteric enzyme.

Table 7. Lineweaver–Burk Plot Data.

[S] (L-methionine, mM)	Enzyme Activity (μM·min⁻¹)	1/[S] (1/mM)	1/Enzyme Activity (1/μM·min⁻¹)
5	9.2	0.2	0.1086
10	10.5	0.1	0.0950
20	13.041	0.05	0.0766
30	11.8	0.0333	0.0847
40	11.5	0.025	0.0869
50	10.8	0.02	0.0925
60	8.32	0.016	0.1201
70	6.74	0.014	0.1483
80	5.823	0.0125	0.1717
90	4.932	0.011	0.2027
100	3.672	0.01	0.2723
110	1.362	0.009	0.7342
120	0.796	0.008	1.256

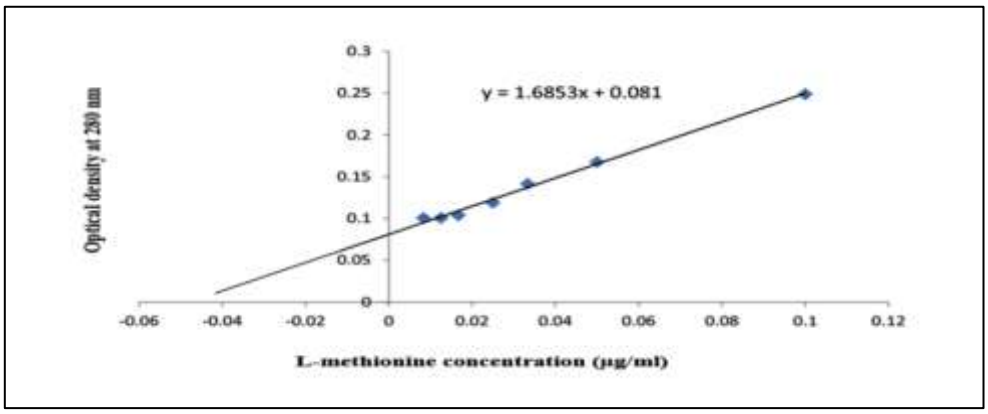

Figure 3. Lineweaver–Burk Plot of L-methionine γ-lyase against L-methionine.

3.8. The antimicrobial activity of L-methioninase:

The antimicrobial activity of purified enzyme is summarized in Table 8. The enzyme demonstrated inhibitory activity against all tested microorganisms. For Gram-negative bacteria, *Escherichia coli*, *Salmonella typhimurium*, and *Pseudomonas aeruginosa* showed inhibition zones of 8.0, 12, and 10 mm, respectively (Figure 4 c–e). These values were lower than those observed for tetracycline (23, 26, and 17 mm). For Gram-positive bacteria, inhibition zones of 22 and 27 mm were recorded for *Bacillus cereus* and *Staphylococcus aureus*, respectively (Figure 4 a–b), compared to 38 and 33 mm for tetracycline. L-methioninase also demonstrated antifungal activity, with inhibition zones of 18 and 16 mm against *Candida albicans* and *Aspergillus niger*, respectively (Figure 4 f–g), while itraconazole showed higher activity (31 and 22 mm). The MIC values are presented in Table 9. For Gram-positive bacteria, MIC values were ≤ 8.0 µg/mL for *Bacillus cereus* and 16.0 µg/mL for *Staphylococcus aureus* (Figure 5 a–b), compared to 4 and 8 µg/mL for tetracycline. For Gram-negative bacteria, MIC values were 16.0 µg/mL for *Salmonella typhimurium* and 64.0 µg/mL for both *Escherichia coli* and *Pseudomonas aeruginosa* (Figure 5 c–e), while tetracycline showed lower values (4–8 µg/mL). For fungal isolates, L-methioninase showed MIC values of 8 µg/mL against both *Candida albicans* and *Aspergillus niger* (Figure 5 f–g), whereas itraconazole exhibited MIC values of 31 and 22 µg/mL, respectively. Overall, the data in Table 8–9 and Figure 4–5 indicate that L-methioninase from *Streptomyces maritimus* possesses broad-spectrum antimicrobial activity, although its potency remains lower than that of standard antimicrobial agents.

Table 8. Detection of MGL antimicrobial activity

Treatments	Inhibition zone diameter (mm)						
	Gram -ve Bacteria			Gram +ve Bacteria		Yeasts and molds	
	Salmonella typhimurium	E. coli	Pseudomonas aeruginosa	Bacillus cereus	Staphylococcus Aureus	Candida albicans	Aspergillus niger
L-methionine γ-lyase (MGL)	12* ± 2.3	8.0* ± 1.4	10* ± 1.5	22* ± 2.5	27*± 1.3	18* ±1.2	16* ± 1.3
Tetracycline antibiotic	23 ± 1.2	26 ± 1.5	17 ± 1.3	38 ± 1.6	33 ± 1.5	NA	NA
Itraconazole antifungal agent	NA	NA	NA	NA	NA	31 ± 1.1	22 ± 1.8

NA: Not applicable (agent not tested against that microorganism)

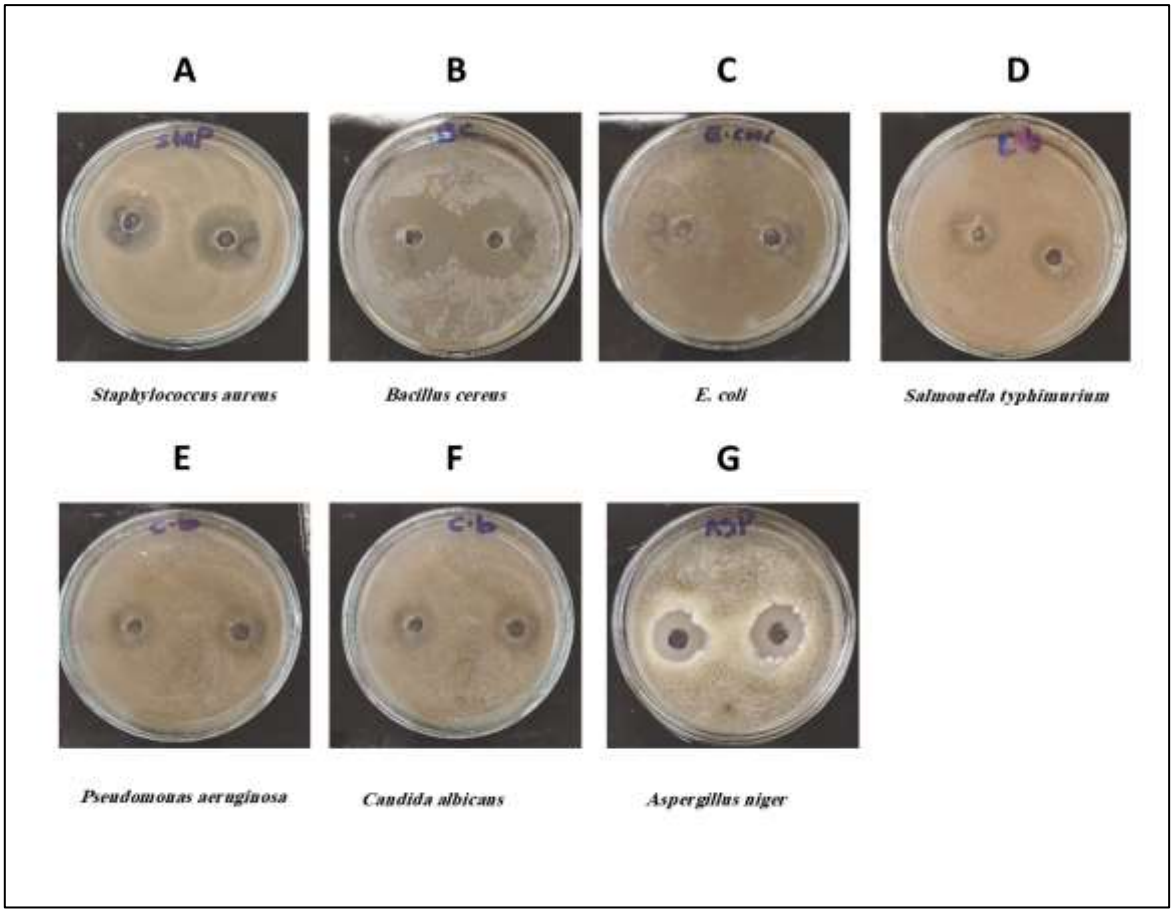

Figure 4. The diffusion disk assay of the L-methionine gamma-lyase displaying different diameters against various types bacteria and fungi

Table 9. Minimum inhibitory concentration (MIC) values of L-methionine gamma lyase

M.O.s	MICs (µg/ml)	
	L-methionine γ-lyase (MGL)	Positive control (Tetracycline, Itraconazole)
Gram +ve bacteria		
Bacillus cereus	≤ 8.00	4.00
Staphylococcus aureus	16.00	8.00
Gram -ve bacteria		
Salmonella typhimurium	16.00	4.00
E. coli	64.00	≤ 8.00
Pseudomonas aeruginosa	64.00	≤ 8.00
Yeasts and molds		
Candida albicans	8.00	4.00
Aspergillus niger	8.00	≤ 4.00

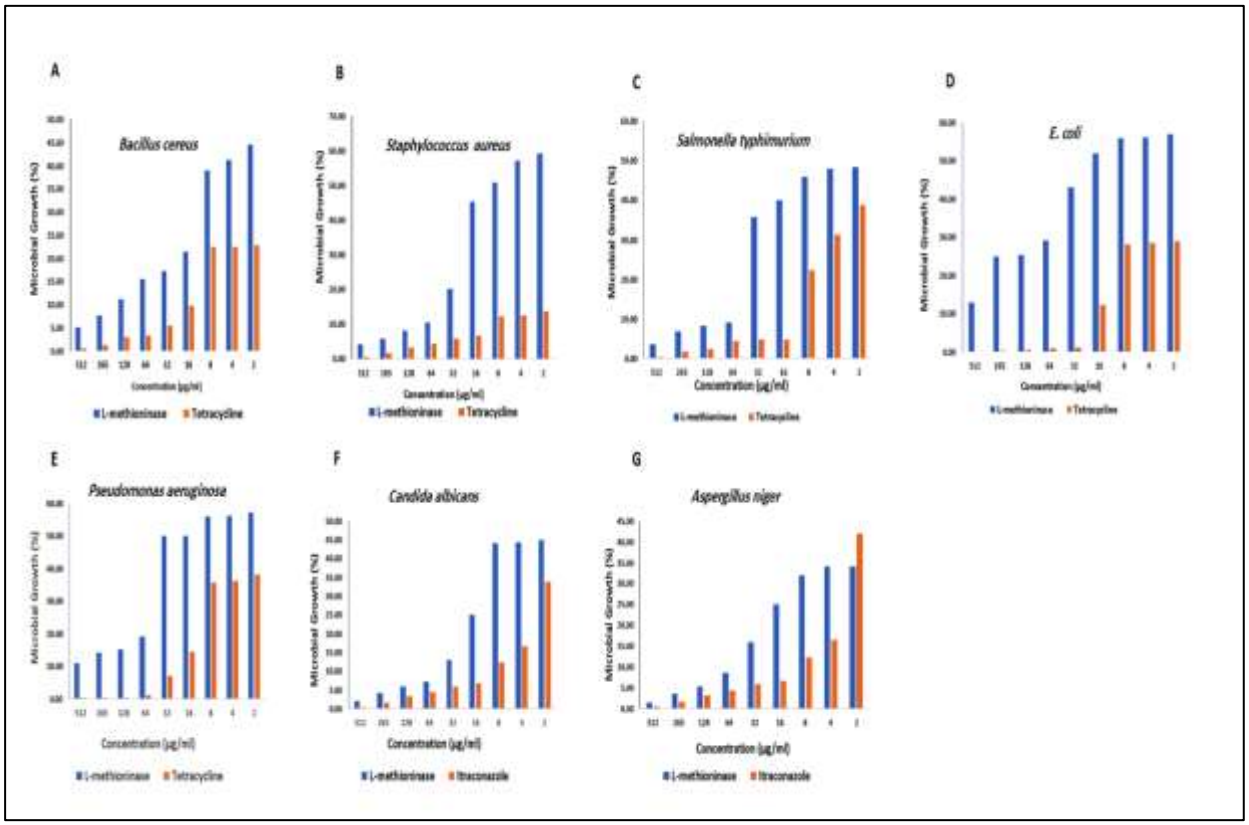

Figure 5. Microbicidal effect of Streptomyces maritimus-derived L-methionine γ-lyase

4. Discussion

Infectious diseases have resulted in serious global health burdens and have also led to a marked decline in the world economy [1]. Therefore, various strategies have been developed to counteract and attenuate microbial infections, which include the design and synthesis of novel drugs. The efficacy of conventional antibiotics has decreased gradually due to the widespread appearance of antimicrobial resistance [2], because L-methionine γ-lyase was identified as a potential target for antimicrobial development. L-methionine γ-lyase catalyzes γ-elimination of L-methionine to methanethiol, α-ketobutyrate and ammonia [33], and MGL was acknowledged to be isolated, identified, purified and characterized from several bacteria [34]. Different production systems have been investigated, and submerged and solid-state fermentation are considered as efficient methods to obtain high yields of L-methionine γ-lyase [35], while high-level L-methioninase synthesis has been reported in Idiomarina, indicating its potential as an anti-leukemic agent, and a recombinant MGL strain was constructed using *Escherichia coli* as the host and a plasmid vector with a kanamycin resistance marker [34]. In this study, *Streptomyces maritimus* was exploited as a fermentative source for L-methionine γ-lyase, because pharmacological activities of *Streptomyces maritimus* were previously detected against carbapenem-resistant *Klebsiella pneumoniae* [36]. Other microorganisms, such as *Aspergillus fumigatus* and *Candida tropicalis*, were also used for the fermentative production of L-methionine γ-lyase and were employed as anticancer agents [37], and the enzyme UV–visible spectrum showed two different peaks (240 and 280 nm) corresponding to lysine amino group of L-methionine (Fig. 1), which is consistent with the findings of Hendy et

al., who reported that L-methionine γ-lyase has peaks at same wavelengths [38]. Consequently, enzyme recovery after treatment of crude extract was 100%, and the purification fold of enzyme is illustrated in Table 1. Optimal pH range of L-methionine γ-lyase from *Streptomyces maritimus* was between 6.5 and 7.5, with 90% residual activity at pH 7.0, and the optimal temperature for catalytic activity was between 35 and 45 °C (Table 2), while Hg2+ and iodoacetate were strong inhibitors of the enzyme, with its activity reduced to 42.5% and 11.5%, respectively (Tables 4 and 5). Moreover, kinetic properties of the L-methioninase of *Streptomyces maritimus*, according to Michaelis–Menten kinetics, showed a Km of 20 mM and a Vmax of 13.041 μM·min−1, and L-methioninase has become a potential target for antimicrobial development because of its unique properties and because it is present in various pathogenic microorganisms [39, 19]. However, L-methionine has been demonstrated to exert antibacterial effects by preventing the formation of key pathogenic determinants of Pseudomonas aeruginosa at low concentrations, and the inhibitory mechanism involves targeting DNA and DNA-associated enzymes, such as DNase [40]. Therefore, in the present work, the microbicidal activity of the enzyme against *Bacillus cereus* and *Staphylococcus aureus* was demonstrated by minimum inhibitory concentrations (MICs) of < 8.0 and 16.0 μg/ml, respectively, and values of L-methioninase against *Salmonella typhimurium*, *E. coli*, and *Pseudomonas aeruginosa* were 16.0, 64.0, and 64.0 μg/ml, respectively, as shown in Table 9 and Figure 5c–e. L-methionine γ-lyase inhibited the growth of the fungal pathogens *Candida albicans* and *Aspergillus niger* with MIC values of 8 μg/ml for both species, thus suggesting that L-methionine γ-lyase produced by *Streptomyces maritimus* is an efficient enzyme that has antimicrobial activity.

5. Conclusion

L-methionine γ-lyase derived from *Streptomyces maritimus* demonstrated stable catalytic behavior under near-neutral conditions and exhibited broad antimicrobial activity against multiple bacterial and fungal pathogens, with comparatively stronger effects against Gram-positive bacteria and fungi. Although its bioactivity showed promising therapeutic potential, further improvement may be required to maximize its practical effectiveness. Future research should focus on mechanistic studies, structural optimization, formulation strategies, and in vivo investigations to further advance its potential biomedical and antimicrobial applications.

Acknowledgments

The authors express their gratitude to Mustansiriyah University (Baghdad, Iraq) for its support of the present work.

Data Availability & Accessibility

All data generated in this study are included in the article. Further details are available upon request.

Declaration of Interest Conflict

The authors confirmed that there were no corporate or financial conflicts

References:

Wehbe, M., Kadah El Habbal, R., Kaj, J., & Karam, P. (2024). Synergistic Dual Antibacterial Activity of Magnetite Hydrogels Doped with Silver. *Langmuir*. https://doi.org/10.1021/acs.langmuir.4c02964

Hassan, A., Al-Salmi, F. A., Saleh, M. A., Sabatier, J. M., Alatawi, F. A., Alenezi, M. A., ... & Sharaf, E. M. (2023). Inhibition mechanism of methicillin-resistant staphylococcus aureus by zinc oxide nanorods via suppresses penicillin-binding protein 2a. ACS omega, 8(11), 9969-9977. https://doi.org/10.1021/acsomega.2c07142

Sharaf, E. M., Hassan, A., Al-Salmi, F. A., Albalwe, F. M., Albalawi, H. M. R., Darwish, D. B., & Fayad, E. (2022). Synergistic antibacterial activity of compact silver/magnetite core-shell nanoparticles core shell against Gram-negative foodborne pathogens. Frontiers in Microbiology, 13, 929491. https://doi.org/10.3389/fmicb.2022.929491

Tan, Y., Xu, M., Tan, X., Tan, X., Wang, X., Saikawa, Y., ... & Hoffman, R. M. (1997). Overexpression and large-scale production of recombinantl-methionine-α-deamino-γ-mercaptomethane-lyase for novel anticancer therapy. Protein expression and purification, 9(2), 233-245. https://doi.org/10.1006/prep.1996.0700

Javia, B. M., Gadhvi, M. S., Vyas, S. J., Ghelani, A., Wirajana, N., & Dudhagara, D. R. (2024). A review on L-methioninase in cancer therapy: Precision targeting, advancements and diverse applications for a promising future. *International Journal of Biological Macromolecules*, 130997. https://doi.org/10.1016/j.ijbiomac.2024.130997

Hoffman, R. M., & Han, Q. (2020). Oral methioninase for Covid-19 methionine-restriction therapy. *in vivo*, *34*(3 suppl), 1593-1596. https://doi.org/10.21873/invivo.11948

Gherardi, G. (2023). *Staphylococcus aureus* infection: pathogenesis and antimicrobial resistance. *International journal of molecular sciences*, *24*(9), 8182. https://doi.org/10.3390/ijms24098182

Lakhundi, S., & Zhang, K. (2018). Methicillin-resistant *Staphylococcus aureus*: molecular characterization, evolution, and epidemiology. *Clinical microbiology reviews*, *31*(4), 10-1128. https://doi.org/10.1128/cmr.00020-18

Wood, S. J., Kuzel, T. M., & Shafikhani, S. H. (2023). *Pseudomonas aeruginosa*: infections, animal modeling, and therapeutics. Cells, 12(1), 199. https://doi.org/10.3390/cells12010199

Yu, S., Yu, P., Wang, J., Li, C., Guo, H., Liu, C., ... & Ding, Y. (2020). A study on prevalence and characterization of *Bacillus cereus* in ready-to-eat foods in China. *Frontiers in Microbiology*, *10*, 3043. https://doi.org/10.3389/fmicb.2019.03043

Song, Z., Zhao, Q., Zhu, L., Zhang, Z., Jiang, L., & Huang, H. (2019). Draft genome sequence of multidrug-resistant β-lactamase-producing Bacillus cereus S66 isolated from

China. *Journal of Global Antimicrobial Resistance*, *17*, 23-24. https://doi.org/10.1016/j.jgar.2019.02.019

Talapko, J., Juzbašić, M., Matijević, T., Pustijanac, E., Bekić, S., Kotris, I., & Škrlec, I. (2021). Candida albicans—the virulence factors and clinical manifestations of infection. *Journal of Fungi*, *7*(2), 79. https://doi.org/10.3390/jof7020079

Morad, H. O., Wild, A. M., Wiehr, S., Davies, G., Maurer, A., Pichler, B. J., & Thornton, C. R. (2018). Pre-clinical imaging of invasive candidiasis using immunoPET/MR. *Frontiers in microbiology*, *9*, 1996. https://doi.org/10.3389/fmicb.2018.01996

Chen, H., Zhou, X., Ren, B., & Cheng, L. (2020). The regulation of hyphae growth in Candida albicans. *Virulence*, *11*(1), 337-348.https://doi.org/10.1080/21505594.2020.1748930

Cortesão, M.; de Haas, A.; Unterbusch, R.; Fujimori, A.; Schütze, T.; Meyer, V.; Moeller, R. Aspergillus niger Spores Are Highly Resistant to Space Radiation. Front. Microbiol. 2020, 11, 560. https://doi.org/10.3389/fmicb.2020.00560

Madika, A., Eugene, U. A., Bishir, M., Sulaiman, M. A., & Hussaini, I. M. (2020). Screening of Aspergillus niger isolated from soil for pectinase production. *FUDMA Journal of Sciences*, *4*(2), 244-249. https://doi.org/10.33003/fjs-2020-0402-165

Bojanović, M.; Stalević, M.; Arsić-Arsenijević, V.; Ignjatović, A.; Ranđelović, M.; Golubović, M.; Živković-Marinkov, E.; Koraćević, G.; Stamenković, B.; Otašević, S. Etiology, Predisposing Factors, Clinical Features and Diagnostic Procedure of Otomycosis: A Literature Review. *J. Fungi* **2023**, *9*, 662. https://doi.org/10.3390/jof9060662.

Rijo, P., Abuamara, T. M., Ali Lashin, L. S., Kamar, S. A., Isca, V. M., Mohammed, T. S., ... & Hassan, A. (2024). Glycyrrhizic Acid Nanoparticles Subside the Activity of Methicillin-Resistant *Staphylococcus aureus* by Suppressing PBP2a. Pharmaceuticals, 17(5), 589. https://doi.org/10.3390/ph17050589

Sato, D., & Nozaki, T. (2009). Methionine gamma-lyase: The unique reaction mechanism, physiological roles, and therapeutic applications against infectious diseases and cancers. *IUBMB life*, *61*(11), 1019-1028. https://doi.org/10.1002/iub.255

Coombs, G. H., & Mottram, J. C. (2001). Trifluoromethionine, a prodrug designed against methionine γ-lyase-containing pathogens, has efficacy in vitro and in vivo against Trichomonas vaginalis. *Antimicrobial agents and chemotherapy*, *45*(6), 1743-1745. https://doi.org/10.1128/aac.45.6.1743-1745.2001

Nasirian, M., Mobini-Dehkordi, M., & Khosravian, P. (2024). The native Iranian soil bacteria with high potential to produce extracellular methionine gamma-lyase. Frontiers in Microbiology, 15, 1504742. https://doi.org/10.3389/fmicb.2024.1504742.

Dayanand, K., & Nadumane, V. K. (2023). Effect of physicochemical parameters on the L-methioninase activity of Methylobacterium sp. and its in vitro anticancer activity

in combination with tamoxifen citrate. Future Journal of Pharmaceutical Sciences, 9, 95. https://doi.org/10.1186/s43094-023-00545-6.

Javia, B. M., Gadhvi, M. S., Vyas, S. J., Dudhagara, P., Shyu, D. J. H., Chen, Y. Y., & Dudhagara, D. R. (2023). Bioprospecting of a thermostable L-methioninase from *Alcaligenes aquatilis* BJ-1 in agro-industrial waste and its anticancer application. *Microbiology Research, 14*(3), 959–976. https://doi.org/10.3390/microbiolres14030066.

Ashkan, M. F., Younis, S. A., & Elazab, N. T. (2023). Isolation and characterization of Trichoderma harzianum L-methioninase with promising powerful anticancer activity. Saudi Journal of Biological Sciences, 30(12), 103870. https://doi.org/10.1016/j.sjbs.2023.103870.

Salim, N., Santhiagu, A., & Joji, K. S. (2020). Purification, characterization and anticancer evaluation of L-methioninase from Trichoderma harzianum. 3 Biotech, 10, 501. https://doi.org/10.1007/s13205-020-02494-w.

Nasirian, M., Arab-SadeghAbadi, A., Mobini-Dehkordi, M., Khosravian, P., & Farhadian, S. (2025). Production and purification of methionine gamma-lyase from Iranian soil molds: investigation of physicochemical properties and anticancer effects. *BMC Cancer, 25*, Article 14754. https://doi.org/10.1186/s12885-025-14754-0.

El-Sayed, A. S. A., Shindia, A., Emam, E., Labib, M., Nour El-Deen, E., Seadawy, M. G., & Yassin, M. A. (2024). Aspergillus flavipes L-methionine γ-lyase-β-cyclodextrin conjugates with improved stability, catalytic efficiency and anticancer activity. Scientific Reports, 14, 27715. https://doi.org/10.1038/s41598-024-78368-5.

Bu, T., Lan, J., Jo, I., Zhang, J., Bai, X., He, S., Jin, X., Wang, L., Jin, Y., Jin, X., Zhang, L., Piao, H., Ha, N.-C., Quan, C., Nam, K. H., & Xu, Y. (2023). Structural basis of the inhibition of L-methionine γ-lyase from Fusobacterium nucleatum. International Journal of Molecular Sciences, 24(2), 1651. https://doi.org/10.3390/ijms24021651.

Al-Owaidi, A. A. N., & Jebor, M. A. (2025). Evaluation of L-methioninase as a targeted anticancer therapy in ovarian cancer and glioblastoma. AIMS Biophysics, 12(2), 197–219. https://doi.org/10.3934/biophy.2025012.

Alhazmi NM, Sharaf EM. Fungicidal Activity of Zinc Oxide Nanoparticles against Azole-Resistant *Aspergillus flavus* Isolated from Yellow and White Maize. *Molecules*. 2023; 28(2):711. https://doi.org/10.3390/molecules28020711

Hassan A, Rijo P, Abuamara TMM, Ali Lashin LS, Kamar SA, Bangay G, Al-Sawahli MM, Fouad MK, Zoair MA, Abdalrhman TI, et al. Synergistic Differential DNA Demethylation Activity of *Danshensu* (*Salvia miltiorrhiza*) Associated with Different Probiotics in Nonalcoholic Fatty Liver Disease. *Biomedicines*. 2024; 12(2):279. https://doi.org/10.3390/biomedicines12020279

Hassan, A., Al-Salmi, F. A., Abuamara, T. M., Matar, E. R., Amer, M. E., Fayed, E. M., ... & Abd El Maksoud, A. I. (2022). Ultrastructural analysis of zinc oxide nanospheres enhances anti-tumor efficacy against Hepatoma. *Frontiers in oncology*, *12*, 933750. https://doi.org/10.3389/fonc.2022.933750

Hassan, A., Mohsen, R., Rezk, A., Bangay, G., Rijo, P., Soliman, M. F., ... & Mohamed, A. F. (2024). Enhancement of Vitamin C's Protective Effect against Thimerosal-Induced Neurotoxicity in the Cerebral Cortex of Wistar Albino Rats: An In Vivo and Computational Study. *ACS omega*, *9*(8), 8973-8984. https://doi.org/10.1021/acsomega.3c07239

Inoue, H., Inagaki, K., Sugimoto, M., Esaki, N., Soda, K., & Tanaka, H. (1995). Structural analysis of the L-methionine γ-lyase gene from Pseudomonas putida. *The journal of biochemistry*, *117*(5), 1120-1125. https://doi.org/10.1093/oxfordjournals.jbchem.a124816

Huang, K. Y., Hu, H. Y., Tang, Y. L., Xia, F. G., Luo, X. Q., & Liu, J. Z. (2015). High-level expression, purification and large-scale production of L-methionine γ-lyase from Idiomarina as a novel anti-leukemic drug. Marine Drugs, 13(8), 5492-5507. https://doi.org/10.3390/md13085492

Khalaf, S. A., & El-Sayed, A. S. (2009). L-Methioninase production by filamentous fungi: I-screening and optimization under submerged conditions. Current microbiology, 58, 219-226. https://doi.org/10.1007/s00284-008-9311-9

Manikkam, R., Ganesan, V., Kaari, M., Venugopal, G., Arumugam, S., & Joseph, J. (2021). Antibacterial efficacy of Streptomyces maritimus SACC-E6 against carbapenem-resistant Klebsiella pneumoniae ATCC BAA-1705. Journal of Applied Pharmaceutical Science, 11(1), 089-094. https://doi.10.7324/JAPS.2021.110110

Selim, M. H., Karm Eldin, E. Z., Saad, M. M., Mostafa, E. S. E., Shetia, Y. H., & Anise, A. A. H. (2015). Purification, Characterization of L-Methioninase from Candida tropicalis, and Its Application as an Anticancer. Biotechnology Research International, 2015(1), 173140. https://doi.org/10.1155/2015/173140

Hendy, M. H., Hashem, A. H., Suleiman, W. B., Sultan, M. H., & Abdelraof, M. (2023). Purification, Characterization and anticancer activity of L-methionine γ-lyase from thermo-tolerant Aspergillus fumigatus. Microbial cell factories, 22(1), 8. https://doi.org/10.1186/s12934-023-02019-z

Gnanadhas, D. P., Elango, M., Datey, A., & Chakravortty, D. (2015). Chronic lung infection by Pseudomonas aeruginosa biofilm is cured by L-Methionine in combination with antibiotic therapy. Scientific reports, 5(1), 16043. https://doi.org/10.1038/srep16043.

On MSEK Transform with Properties and Application

Merna A. Samarchi [1]

Susan H. Mohammad [2]

Ekhlass S. Al-Rawi [3]

Abstract:

In this work, a new general integral transform called the MSEK transform is introduced. The definition of the new approach and proved its main properties related to linearity, shifting, scaling, existence and convergence theorem, and derivatives are presented. Moreover, the proposed transform was applied to solve some examples of nth-order linear ordinary differential equations with constant coefficients as well as systems of ordinary differential equations of nth order to demonstrate the ability of the MESK transform to change ODEs to simple algebraic equations, in addition to the accuracy and efficiency of the proposed transformation in finding the analytical solution.

Keywords: *Integral Transforms, Ordinary Differential Equations, Systems Of Ordinary Differential Equations*.

http://dx.doi.org/10.47832/Dub.Conf3-2

[1] Researcher. College of Computer Sciences and Mathematics, University of Mosul, Iraq
merna_samarchi@uomosul.edu.iq

[2] Researcher. College of Computer Sciences and Mathematics, University of Mosul, Iraq
susan.al-hakam@uomosul.edu.iq

[3] Researcher. College of Computer Sciences and Mathematics, University of Mosul, Iraq
drekhlass-alrawi@uomosul.edu.iq

1. Introduction

Differential equations and systems play an important role in many fields of sciences, since they are used in the mathematical modeling of many problems in applied mathematics and engineering sciences, such as dynamical systems, signal processing, physical chemistry, mathematical biology, fluid mechanics, electrostatics etc. (Braun, 1993; Debnath, 2005; Erkus-Duman & Ciftc, 2018; Khader et al., 2020; Sobczyk, 2001; Younis & Al-Rawi, 2023).

Therefore, there have been many attempts to develop new techniques for solving differential equations. Over the past two centuries, integral transforms have been used effectively to solve differential equations such as ordinary differential equations, partial differential equations, integral differential equations, and fractional differential equations (Davies, 2002). Pierre-Simpon Laplace and Joseph Fourier first introduced integral transforms in 1780 and 1822, respectively, and they became two of the most widely used transformations in the mathematical literature (Ahmadi et al., 2019; Baleanu & Wu, 2019; Cho & Kim, 2013; Kamal & Sedeeg, 2016 ; Kexue & Jigen, 2011; Mohammad & Al-Rozbayani, 2024; Mustafa, 2023).

Recently, new transforms that depend mainly on the development, extended, modified and generalized of the Laplace transform have been discovered by many mathematicians, such as Laplace-Carson transformation (Donolato, 2002), Sumudu transformation (Watugala, 1993), Natural transformation (Khan & Khan, 2008), Elzaki transformation (Elzaki, 2011), Kamal transformation (Kamal & Sedeeg 2016), Polynomial integral transformation (Barnes, 2016), Shehu transform (Shehu & Weidong, 2019), SEE transform (Mansour et al. 2021) , Emad–Sara integral transformation (Maktoof at el., 2021), SUM transform (Hasan et al., 2023), and more other transforms (Aboodh, 2013; Hilmi & Jwamer, 2024; Kharrat & Toma, 2020; Kim, 2017; Mohand & Mahgoub, 2019; Patil et al., 2023; Turab et al., 2024; Wang et al., 2023).

This work proposes a new general developed formula of integral transform known as the MSEK transform by writing the kernel function in its general form. We have given the main definition; the existence and convergence theorem of this transform was proved, in Sec. 2. The basic properties of the proposed transform are provided and the MSEK transform of some elementary functions is illustrated in Sec. 3. Moreover, higher-order ordinary differential equations and systems of ordinary differential equations have been solved for more generality to show the efficiency and accuracy of the proposed new transform for finding the exact solutions of these applications discussed in Sec. 4. At the end, a conclusion is presented in Sec. 5.

2. MSEK integral transform

Definition: The integral transform is defined as

$$M_a\{f(\tau)\} = \mathcal{G}(s) = g(s)\int_0^{\infty} f(\tau)\, a^{-h(s)\tau} d\tau \qquad (1)$$

Where $\tau \geq 0, a > 1$, the function $f(\tau)$ is a piecewise continuous and satisfies $|f(\tau)| \leq Le^{\alpha\tau}$, L and α are positive constants, $g(s)$ and $h(s)$ are positive real functions with $g(s) \neq 0 \; for \; all \; s > 0$.

and the corresponding inverse MSEK transform is given by

$$M_a^{-1}\{\mathcal{G}(s)\} = f(\tau) = \frac{loga}{2\pi i}\int_{c-i\infty}^{c+i\infty}\left[\frac{\mathcal{G}(s)}{g(s)}\right]a^{h(s)\tau}\,h'(s)ds$$

where M_a^{-1} is the inverse operator of MSEK transformation, c is a real constant, the integral is taken along $s = c$ in the complex plane, $\emptyset(s) = \frac{\mathcal{G}(s)}{g(s)}$ is analytic function for $Re(s) > c$, $\emptyset(s)$ converge to 0 as $|s| \to \infty$ and $h(s)$ is injective .

The existence condition of the MSEK transform is provided by studying the convergence below:

Theorem (1): If $f(\tau)$ is a piecewise continuous function in the interval $0 \leq \tau \leq \tau_0$ and has an exponential order $\alpha > 0$ as $\tau \to \infty$, $g(s) \neq 0, g(s)$ and $h(s)$ are positive real functions then $M_a\{f(\tau)\}$ converges and exists for all $h(s) > \frac{\alpha}{loga}$.

Proof: Suppose $\tau_0 > 0$, then (1) can be rewritten as

$M_a\{f(\tau)\} = \mathcal{G}(s) = g(s)\int_{\tau=0}^{\tau_0} f(\tau)e^{-h(s)\tau loga}d\tau \quad + g(s)\int_{\tau=\tau_0}^{\infty} f(\tau)e^{-h(s)\tau loga}d\tau$ (2)Since $f(\tau)$ is piecewise continuous in the interval, $0 \leq \tau \leq \tau_0$, the first part in (2) exists finitely, similarly since $f(\tau)$ has exponential order α as, $\tau \to \infty$, using, $|f(\tau)| \leq Le^{\alpha\tau}$, $\lim_{\tau\to\infty} f(\tau)\, e^{-\alpha\tau}$ is finite.

$$\left|g(s)\int_{\tau=\tau_0}^{\infty} f(\tau)\, e^{-h(s)\tau loga}d\tau\right| \leq g(s)\int_{\tau=\tau_0}^{\infty}\left|f(\tau)\, e^{-h(s)\tau loga}\right|d\tau$$

$$\leq\; g(s)\int_{\tau=\tau_0}^{\infty}|f(\tau)|\, e^{-h(s)\tau loga}d\tau$$

$$\leq g(s)\int_{\tau=\tau_0}^{\infty} Le^{\alpha\tau}e^{-h(s)\tau loga}d\tau$$

$$= g(s)L\int_{\tau=\tau_0}^{\infty} e^{-\{h(s)loga-\alpha\}\tau}d\tau$$

$$= g(s)L\lim_{c\to\infty}\left[\frac{e^{-\{h(s)loga-\alpha\}\tau}}{-h(s)loga+\alpha}\right]_{\tau_0}^{c} = \frac{g(s)Le^{-\{h(s)loga-\alpha\}\tau_0}}{h(s)loga-\alpha}$$

by choosing τ_0 as large enough, thus, $\frac{g(s)Le^{-\{h(s)loga-\alpha\}\tau_0}}{h(s)loga-\alpha}$ will be small for $h(s) > \frac{\alpha}{loga}$, so the second part in Eq.(2) exists finitely and subsequently $M_a\{f(\tau)\}$ converges and exists.

□

Table 1 lists various well-known integral transforms that are generated by equation (1) based on different selections for g(s) and h(s). The convergence of these transforms can also be easily derived from Theorem (1).

Table1: shows the relation between MSEK and other well-known integral transforms

Name	Transform form	Choice of components

Laplace transform (Davies, 2002)	$L\{f(\tau),s\}=\int_0^\infty f(\tau)e^{-s\tau}d\tau$	$g(s)=1,\ h(s)=s\ ,\ a=e$
Laplace - Carson transform (Donolato, 2002)	$LC\{f(\tau),s\}=s\int_0^\infty f(\tau)e^{-s\tau}d\tau$	$g(s)=s\ ,\ h(s)=s,\ a=e$
Sumudu transform (Watugala, 1993)	$S\{f(\tau),s\}=\frac{1}{s}\int_0^\infty f(\tau)e^{-\frac{\tau}{s}}\,d\tau$	$g(s)=\frac{1}{s},\ h(s)=\frac{1}{s}\ ,\ a=e$
Elzaki transform (Elzaki, 2011)	$E\{f(\tau),s\}=s\int_0^\infty f(\tau)e^{-\frac{\tau}{s}}\,d\tau$	$g(s)=\ s\ ,h(s)=\frac{1}{s}\ ,\ a=e$
Aboodh transform (Aboodh, 2013)	$A\{f(\tau),s\}=\frac{1}{s}\int_0^\infty f(\tau)e^{-s\tau}\,d\tau$	$g(s)=\frac{1}{s},\ h(s)=s\ ,a=e$
Kamal transform (Kamal & Sedeeg, 2016)	$K\{f(\tau),s\}=\int_0^\infty f(\tau)e^{-\frac{\tau}{s}}\,d\tau$	$g(s)=1,\ h(s)=\frac{1}{s}\ ,a=e$
Shehu transform (Shehu & Weidong 2019)	$S\{f(\tau),s\}=\int_0^\infty f(\tau)e^{-\frac{s\tau}{u}}\,d\tau$	$g(s)=1,\ h(s)=\frac{s}{u}\ ,a=e$
G- transform (Kim, 2017)	$G\{f(\tau),s\}=s^\beta\int_0^\infty f(\tau)e^{-\frac{\tau}{s}}\,d\tau$	$g(s)=\ s^\beta,\ h(s)=\frac{1}{s}\ ,\ a=e$
Sawi transform (Mohand & Mahgoub, 2019)	$S\{f(\tau),s\}=\frac{1}{s^2}\int_0^\infty f(\tau)e^{-\frac{\tau}{s}}\,d\tau$	$g(s)=\frac{1}{s}\ ,\ h(s)=\frac{1}{s}\ ,a=e$
Kharrat-Toma transform (Kharrat & Toma, 2020)	$B\{f(\tau),s\}=s^3\int_0^\infty f(\tau)e^{-\frac{\tau}{s^2}}\,d\tau$	$g(s)=\ s^3,h(s)=\frac{1}{s^2}\ ,a=e$
SEE transform (Mansour et al. 2021)	$S_a\{f(\tau),s\}=\frac{1}{s^r}\int_0^\infty f(\tau)e^{-s\tau}\,d\tau$	$g(s)=\frac{1}{s^r},\ h(s)=\ s,a=e$
SUM transform (Hasan et al., 2023)	$S_a\{f(\tau),s\}=\frac{1}{s^r}\int_0^\infty f(\tau)a^{-s\tau}\,d\tau$	$g(s)=\frac{1}{s^r},\ h(s)=s$

3. Results of the preliminary study

3.1 Properties of MSEK transform :

Some special properties of the MSEK transform are discussed in this section.

Theorem (2): (Linearity)

Let $u(\tau)$ and $v(\tau)$ are two functions for which MESK transform exists, then

$$M_a\{\delta u(\tau)+\ \mu v(\tau)\}=\delta M_a\{u(\tau)\}+\mu M_a\{v(\tau)\} \qquad (3)$$

Where δ,μ are arbitrary constants.

Proof: The RHS of Eq. (3) can be expressed by

$$M_a\{\delta u(\tau)+\ \mu v(\tau)\}=g(s)\int_0^\infty\{\delta u(\tau)+\ \mu v(\tau)\}a^{-h(s)\tau}d\tau$$

$$=\delta\{g(s)\int_0^\infty u(\tau)a^{-h(s)\tau}d\tau\ \}+\mu\{g(s)\int_0^\infty v(\tau)a^{-h(s)\tau}d\tau\ \}$$

$= \delta M_a\{u(\tau)\} + \mu M_a\{v(\tau)\}$ □

Theorem (3): (First Shifting)

If $M_a\{f(\tau)\} = \mathcal{G}(s)$ is the MSEK transform for the function $f(\tau)$, then

$$M_a\{e^{\beta\tau} f(\tau)\} = \mathcal{G}(h(s)\log a - \beta) \qquad (4)$$

Proof: By using MSEK transform in (1), we have

$M_a\{e^{\beta\tau} f(\tau)\} = g(s)\int_0^\infty f(\tau)e^{\beta\tau}a^{-h(s)\tau}d\tau = g(s)\int_0^\infty e^{-(h(s)\log a-\beta)\tau}d\tau$

$= \mathcal{G}(h(s)\log a - \beta)$ □

Theorem (4): (second Shifting)

If $M_a\{f(\tau)\} = \mathcal{G}(s)$ is the MSEK transform for the function $f(\tau)$ and

$$u(\tau) = \begin{cases} f(\tau-\beta) & if \quad \tau > \beta \\ 0 & if \quad \tau < \beta \end{cases}$$

then

$$M_a\{u(\tau)\} = a^{-h(s)\beta} M_a\{f(\tau)\} \qquad (5)$$

Proof: In view (1), we have

$M_a\{u(\tau)\} = g(s)\int_0^\infty u(\tau)a^{-h(s)\tau}d\tau = g(s)\int_{\tau=\beta}^\infty f(\tau-\beta)a^{-h(s)\tau}\, d\tau$, Setting $\tau - \beta = \gamma$ and change of variables leads to (5). □

Theorem (5): (change of scale)

If $M_a\{f(\tau)\} = \mathcal{G}(s)$, then

$$M_a\{f(\rho\tau)\} = \frac{1}{\rho} M_a\left\{\frac{s}{\rho}\right\} \qquad (6)$$

Proof: Using (1), we get

$M_a\{f(\rho\tau)\} = g(s)\int_0^\infty f(\rho\tau)a^{-h(s)\tau}d\tau$, putting $\rho\tau = \gamma$ and change of variables we have

$M_a\{f(\rho\tau)\} = \frac{1}{\rho}\{g(s)\int_0^\infty f(\tau)a^{-h(s)\tau}d\tau\ \} = \frac{1}{\rho}\mathcal{G}\left\{\frac{s}{\rho}\right\}$

□

3.2 The MSEK transform of some elementary functions:

In this section, Eq. (1) is used to get the generalized transforms for some basic functions as below:

i) If $f(\tau) = k$, where $k$is constant, then:

$$M_a\{k\} = \frac{k g(s)}{h(s)\log a} \qquad (7)$$

ii) If $f(\tau) = \tau^n, n \in N$, then:

$$M_a\{\tau^n\} = g(s)\int_0^\infty \tau^n e^{-h(s)\tau\log a}d\tau$$

and using integrations by part, we get

$$M_a\{\tau^n\} = \frac{g(s)}{[h(s)loga]^{n+1}} \int_0^\infty v^n e^{-v} dv$$

By the definition of the gamma function, Eq. (8) is obtained.

$$M_a\{\tau^n\} = \frac{g(s)\Gamma(n+1)}{[h(s)loga]^{n+1}}, Re(n+1) > 0 \qquad (8)$$

iii) If $f(\tau) = e^{\rho\tau}$, where ρ is constant, then:

$$M_a\{e^{\rho\tau}\} = g(s) \int_0^\infty e^{\rho\tau} a^{-h(s)\tau} d\tau$$

$$= g(s) \int_0^\infty e^{-(h(s)loga-\rho)\tau} d\tau$$

$$M_a\{e^{\rho\tau}\} = \frac{g(s)}{h(s)loga - \rho} \qquad (9)$$

iv) If $f(\tau) = sin(\rho\tau)$, where ρ is constant, then:

$$M_a\{sin(\rho\tau)\} = g(s) \int_0^\infty \left(\frac{e^{\rho i\tau} - e^{-\rho i\tau}}{2i}\right) e^{-h(s)\tau loga} d\tau$$

$$= \frac{g(s)}{2i} \int_0^\infty \{e^{-\{h(s)loga-\rho i\}\tau} - e^{-\{h(s)loga+\rho i\}\tau}\} d\tau$$

$$M_a\{sin(\rho\tau)\} = \frac{\rho\, g(s)}{[h(s)loga]^2 + \rho^2} \qquad (10)$$

v) If $f(\tau) = cos(\rho\tau)$, where ρ is constant, then:

$$M_a\{cos(\rho\tau)\} = g(s) \int_0^\infty \left(\frac{e^{\rho i\tau} + e^{-\rho i\tau}}{2}\right) e^{-h(s)\tau loga} d\tau$$

$$= \frac{g(s)}{2} \int_0^\infty \{e^{-\{h(s)loga-\rho i\}\tau} + e^{-\{h(s)loga+\rho i\}\tau}\} d\tau$$

$$M_a\{cos(\rho\tau)\} = \frac{g(s)h(s)loga}{[h(s)loga]^2 + \rho^2} \qquad (11)$$

vi) If $f(\tau) = sinh(\rho\tau)$, where ρ is constant, then:

$$M_a\{sinh(\rho\tau)\} = g(s) \int_0^\infty \left(\frac{e^{\rho\tau} - e^{-\rho\tau}}{2}\right) e^{-h(s)\tau loga} d\tau$$

$$= \frac{g(s)}{2} \int_0^\infty \{e^{-\{h(s)loga-\rho\}\tau} - e^{-\{h(s)loga+\rho\}\tau}\} d\tau$$

$$M_a\{sinh(\rho\tau)\} = \frac{\rho\, g(s)}{[h(s)loga]^2 - \rho^2} \qquad (12)$$

vii) If $f(\tau) = cosh(\rho\tau)$, where ρ is constant, then :

$$M_a\{cosh(\rho\tau)\} = g(s) \int_0^\infty \left(\frac{e^{\rho\tau} + e^{-\rho\tau}}{2}\right) e^{-h(s)\tau loga} d\tau$$

$$= \frac{g(s)}{2} \int_0^\infty \{e^{-\{h(s)loga-\rho\}\tau} + e^{-\{h(s)loga+\rho\}\tau}\} d\tau$$

$$M_a\{cosh(\rho\tau)\} = \frac{g(s)h(s)loga}{[h(s)loga]^2 - \rho^2} \qquad (13)$$

Theorem (6): suppose $f(\tau)$ is n- times continuously differentiable on $[0,\infty)$ and of exponential order $\alpha > 0$, then $M_a\{f^{(n)}(\tau)\}$, $n = 0,1,2,\dots$ exist for $h(s) > \frac{\alpha}{loga}$ and

$$M_a\{f^{(n)}(\tau)\} = [h(s)loga]^n M_a\{f(\tau)\} - g(s)\sum_{w=0}^{n-1}[h(s)loga]^{(n-1)-w} f^{(w)}(0) \qquad (14)$$

Proof: From the definition in Eq. (1) for $n = 1$, we obtain

$$M_a\{f'(\tau)\} = g(s)\int_0^\infty f'(t)a^{-h(s)t}dt$$

By using the integration by parts and setting $u = a^{-h(s)t}$, $dv = f'(t)dt$, we get that

$$M_a\{f'(\tau)\} = -g(s)f(0) + [h(s)loga]g(s)\int_0^\infty f(\tau)a^{-h(s)\tau}d\tau$$

$$= [h(s)loga]M_a\{f(\tau)\} - g(s)f(0) \qquad (15)$$

Now, suppose Eq. (14) is true for n=k, i.e.

$$M_a\{f^{(k)}(\tau)\} = [h(s)loga]^k M_a\{f(\tau)\}$$

$$- g(s)\sum_{w=0}^{k-1}[h(s)loga]^{(k-1)-w} f^{(w)}(0) \qquad (16)$$

By using Eq. (15) and Eq. (16), yield:

$$M_a\{(f^{(k)}(\tau))'\} = [h(s)loga]M_a\{f^{(k)}(\tau)\} - g(s)f^{(k)}(0)$$

$$= h(s)loga\left\{[h(s)loga]^k M_a\{f(\tau)\} - g(s)\sum_{w=0}^{k-1}[h(s)loga]^{(k-1)-w} f^{(w)}(0)\right\} - g(s)f^{(k)}(0)$$

$$= [h(s)loga]^{k+1} M_a\{f(\tau)\} - g(s)\sum_{w=0}^{k}[h(s)loga]^{k-w} f^{(w)}(0)$$

Which implies that Eq. (14) holds for $n = k + 1$ by induction hypothesis.

□

4. Applications of the MSEK transform

In this part, we employed the proposed new general transform (MSEK) for solving linear equation of order n with constant coefficient as

$$L(D)[y(x)] = D^n y(x) + a_1 D^{n-1} y(x) + a_2 D^{n-2} y(x) + \cdots + a_n y(x) = \varphi(x) \qquad (17)$$

With the initial conditions

$$y(x_0) = y_0\,, Dy(x_1) = y_1, D^2 y(x_2) = y_2\,, \dots, D^{n-1} y(x_{n-1}) = y_{n-1}$$

where $D = \frac{d}{dx}$ is the differential operator. $y_0\,, y_1, y_2\,, \dots, y_{n-1}$ and. $a_1\,, a_2, a_3\,, \dots, a_n$ are constants. The MSEK transform applied on both sides of Eq. (17)

$$M_a\{D^n y(x)\} + a_1 M_a\{D^{n-1} y(x)\} + a_2 M_a\{D^{n-2} y(x)\} + \cdots + a_n M_a\{y(x)\} = M_a\{\varphi(x)\}$$

Using Th. (8), we have

$$\left\{[h(s)\ loga]^n \mathcal{G}(s) - g(s)\sum_{w=0}^{n-1}[h(s)loga]^{n-w-1}y^{(w)}(0)\right\}$$
$$+ a_1\left\{[h(s)\ loga]^{n-1}\mathcal{G}(s) - g(s)\sum_{w=0}^{n-2}[h(s)loga]^{n-w-2}y^{(w)}(0)\right\}$$
$$+\cdots + a_n\mathcal{G}(s) = \varphi(s) \qquad (18)$$

after substituting the initial conditions in Eq. (18), we get

$$p(s)\mathcal{G}(s) = \varphi(s) + \psi(s) \qquad (19)$$

where $p(s) = \{[h(s)\ loga]^n + a_1[h(s)\ loga]^{n-1} + \cdots + a_n\},\ \varphi(s) = M_a\{\varphi(x)\}$ and

$$\psi(s) = g(s)\left[\sum_{w=0}^{n-1}[h(s)loga]^{n-w-1}y_{n-1} + a_1\sum_{w=0}^{n-2}[h(s)loga]^{n-w-2}y_{n-2} + \cdots + y_0\right]$$

From Eq. (18), Eq. (19) will be found.

$$\mathcal{G}(s) = \frac{\varphi(s)}{p(s)} + \frac{\psi(s)}{p(s)}, \qquad \mathcal{G}(s) = M_a\{y(x)\} \qquad (20)$$

By applying the inverse MSEK transform to both sides of Eq. (20), we obtain the exact solution

$$y(x) = M_a^{-1}\left\{\frac{\varphi(s)}{p(s)}\right\} + M_a^{-1}\left\{\frac{\psi(s)}{p(s)}\right\}$$

The MSEK transform's application was also expanded to encompass systems of ordinary differential equations. To get exact solutions of the differential systems, all the MSEK transform's properties and theorems, Cramer's rule, and Maple software are applied.

Example 1. Consider the following third-order ODE

$$y'''(x) - 3y''(x) + 3y'(x) - y(x) = xe^x \qquad (21)$$

With the initial conditions

$$y(0) = 1,\ y'(0) = 0,\ y''(0) = \frac{1}{2} \qquad (22)$$

Applying the MSEK transform to both sides of Eq. (21), we get

$$M_a\{y'''(x)\} - 3M_a\{y''(x)\} + 3M_a\{y'(x)\} - M_a\{y(x)\} = M_a\{xe^x\}$$

Using the initial conditions in (22), Eq. (23) is valid.

$$-\frac{g(s)}{2} - g(s)[h(s)loga]^2 + [h(s)loga]^3\mathcal{G}(s) - 3[h(s)loga]^2\mathcal{G}(s) + 3g(s)\ h(s)loga + 3h(s)loga\mathcal{G}(s)$$
$$- 3g(s) - \mathcal{G}(s) = \frac{g(s)}{[h(s)\ loga - 1]^2} \qquad (23)$$

Simplifying Eq. (23), we get

$$([h(s)loga]^3 - 3[h(s)loga]^2 + 3h(s)loga - 1)\mathcal{G}(s)$$
$$= \frac{g(s)}{[h(s)\ loga - 1]^2} + \frac{7g(s)}{2} + g(s)[h(s)loga]^2 - 3g(s)\ h(s)loga$$

Solving the last equation for $\mathcal{G}(s)$ leads to

$$\mathcal{G}(s) = \frac{g(s)}{[h(s)\,loga - 1]^5} + \frac{7}{2}\frac{g(s)}{[h(s)\,loga - 1]^3} + \frac{g(s)[h(s)loga]^2}{[h(s)\,loga - 1]^3} - \frac{3g(s)h(s)loga}{[h(s)loga - 1]^3}$$

(24)

By using Maple software, we have expanded the partial fractions in Eq. (24) to become

$$\mathcal{G}(s) = \frac{g(s)}{[h(s)\,loga - 1]^5} + \frac{3}{2}\frac{g(s)}{[h(s)loga - 1]^3} - \frac{g(s)}{[h(s)loga - 1]^2} + \frac{g(s)}{h(s)loga - 1}$$

(25)

Taking the inverse M_a^{-1} to both sides of Eq. (25), gives the exact solution of (21) - (22) in the form

$$y(x) = \frac{1}{24}x^4e^x + \frac{3}{4}x^2e^x - xe^x + e^x$$

Example 2. Consider the following fourth-order ODE

$$y^{(4)}(x) - y(x) = sinx \qquad (26)$$

Subject to the initial conditions

$$y(0) = y'(0) = y''(0) = y'''(0) = 0 \qquad (27)$$

Applying the MSEK transform to both sides of Eq. (26), we get

$$M_a\{y^{(4)}(x)\} - M_a\{y(x)\} = M_a\{sinx\}$$

Using the initial conditions in (27), Eq. (28) holds

$$[h(s)loga]^4\mathcal{G}(s) - \mathcal{G}(s) = \frac{g(s)}{[h(s)loga]^2 + 1} \qquad (28)$$

Simplifying and solving Eq. (28) for $G(s)$ leads to

$$\mathcal{G}(s) = \frac{g(s)}{([h(s)loga]^2 + 1)([h(s)loga]^4 - 1)} \qquad (29)$$

The fraction in Eq. (29) has been expanded by using Maple software, to become

$$\mathcal{G}(s) = \frac{g(s)}{4([h(s)loga]^2 - 1)} - \frac{g(s)}{4([h(s)\,loga]^2 + 1)} - \frac{g(s)}{2([h(s)loga]^2 + 1)^2} \qquad (30)$$

Taking M_a^{-1} to both sides of Eq. (30), gives the exact solution of (26) - (27) in the form

$$y(x) = \frac{1}{4}sinhx + \frac{1}{4}xcosx - \frac{1}{2}sinx$$

Example 3. Consider the following fifth-order ODE

$$y^{(5)}(x) - 5y'''(x) + 4y'(x) = 0 \qquad (31)$$

Subject to the initial conditions

$$y(0) = 3, y'(0) = -5, y''(0) = 11, y'''(0) = -23,\ y^{(4)}(0) = 47 \qquad (32)$$

Apply MSEK transform to both sides of Eq. (31), we get

$$M_a\{y^{(5)}(x)\} - 5M_a\{y'''(x)\} + 4M_a\{y'(x)\} = 0$$

Using the initial conditions in (32) to obtain

$$\{[h(s)loga]^5 - 5[h(s)loga]^3 + 4[h(s)loga]\}\mathcal{G}(s) =$$

$$= g(s)\{3[h(s)\,loga]^4 - 5[h(s)loga]^3 - 4[h(s)loga]^2 + 2h(s)loga + 4\}$$

(33)

Simplifying and solving Eq. (33) for $\mathcal{G}(s)$ leads to

$$\mathcal{G}(s) = \frac{g(s)\{3[h(s)loga]^4 - 5[h(s)loga]^3 - 4[h(s)loga]^2 + 2h(s)loga + 4\}}{[h(s)loga]^5 - 5[h(s)loga]^3 + 4[h(s)loga]} \quad (34)$$

By using Maple software for partial fractions method, we have expanded Eq. (34) to become

$$\mathcal{G}(s) = \frac{g(s)}{h(s)loga} - \frac{g(s)}{h(s)loga + 1} + \frac{3g(s)}{h(s)\,loga + 2} \quad (35)$$

Taking M_a^{-1} to both sides of Eq. (35), gives the exact solution of (31) - (32) in the form

$$y(x) = 1 - e^{-x} + 3e^{-2x}$$

Example 4. Consider the following system

$$x_1'' + 3x_1 - 2x_2 = 0$$

$$x_1'' + x_2'' - 3x_1 + 2x_2 = 0 \quad (36)$$

Subject to

$$x_1(0) = x_2(0) = 0,\ \ x_1'(0) = 3, \qquad x_2'(0) = 0 \quad (37)$$

Applying MSEK transformation to both sides of sys. (36), we get

$$M_a\{x_1''\} + 3M_a\{x_1\} - 2M_a\{x_2\} = 0$$

$$M_a\{x_1''\} + M_a\{x_2''\} - 3M_a\{x_1\} + 5M_a\{x_2\} = 0$$

Using the initial conditions in (37) to obtain

$$\{[h(s)loga]^2 + 3\}X_1(s) + 2X_2(s) = 3g(s)$$

$$\{[h(s)loga]^2 - 3\}X_1(s) + \{[h(s)loga]^2 + 5\}X_2(s) = 5g(s) \quad (38)$$

Where $X_1(s)$, $X_2(s)$ is the MSEK transform for $x_1(\tau)$ and $x_2(\tau)$ respectively. Solving the sys. (38) for $X_1(s)$ and $X_2(s)$, we get

$$X_1(s) = \frac{\begin{vmatrix} 3g(s) & -2 \\ 5g(s) & [h(s)loga]^2 + 5 \end{vmatrix}}{\begin{vmatrix} [h(s)loga]^2 + 3 & -2 \\ [h(s)loga]^2 - 3 & [h(s)loga]^2 + 5 \end{vmatrix}} = \frac{3g(s)[h(s)loga]^2 + 25g(s)}{[h(s)loga]^4 + 10[h(s)loga]^2 + 9}$$

$$X_2(s) = \frac{\begin{vmatrix} [h(s)loga]^2 + 3 & 3g(s) \\ [h(s)loga]^2 - 3 & 5g(s) \end{vmatrix}}{\begin{vmatrix} [h(s)\,loga]^2 + 3 & -2 \\ [h(s)\,loga]^2 - 3 & [h(s)loga]^2 + 5 \end{vmatrix}} = \frac{2\,g(s)[h(s)loga]^2 + 24\,g(s)}{[h(s)\,loga]^4 + 10[h(s)\,loga]^2 + 9}$$

(39)

By partial fractions sys. (38) becomes

$$X_1(s) = \frac{g(s)}{4([h(s)\,loga]^2 + 9)} + \frac{11\,g(s)}{4([h(s)\,loga]^2 + 1)}$$

$$X_2(s) = \frac{-3g(s)}{4([h(s)\,loga]^2 + 9)} + \frac{11\,g(s)}{4([h(s)loga]^2 + 1)} \qquad (40)$$

Taking the inverse M_a^{-1} to both sides of sys. (40), gives the exact solution of (36) - (37) in the form

$$x_1(t) = \frac{1}{12}sin3t + \frac{11}{4}sint$$

$$x_2(t) = \frac{11}{4}sint - \frac{1}{4}sin3t$$

Example 5. Consider the following system

$$x_1'' + x_1 - x_2'' - 4x_2 = 0$$

$$x_1' + x_2' = cos\tau + 2cos2\tau \qquad (41)$$

Subject to $$x_1(0) = x_2(0) = 0,\ x_1'(0) = 1,\ x_2'(0) = 2 \qquad (42)$$

Applying MSEK transformation to both sides of sys. (41), we get

$$M_a\{x_1{}''\} + M_a\{x_1\} - M_a\{x_2''\} - 4M_a\{x_2\} = 0$$

$$M_a\{x_1{}'\} + M_a\{x_2'\} = M_a\{cos\tau\} + 2M_a\{cos2\tau\}$$

Using the initial conditions in (42) we obtain

$$\{[h(s)loga]^2 + 1\}X_1(s) - \{[h(s)loga]^2 + 4\}X_2(s) = -g(s)$$

$$[h(s)loga]X_1(s) + [h(s)loga]X_2(s) = \frac{g(s)h(s)loga}{[h(s)loga]^2 + 1} + \frac{2g(s)h(s)loga}{[h(s)loga]^2 + 4} \qquad (43)$$

Where $X_1(s), X_2(s)$ is the MSEK transform for $x_1(\tau)$ and $x_2(\tau)$ respectively. Solving the sys. (43) for $X_1(s)$ and $X_2(s)$, we get

$$X_1(s) = \frac{\begin{vmatrix} -g(s) & -([h(s)loga]^2 + 4) \\ \frac{g(s)h(s)loga}{[h(s)loga]^2 + 1} + \frac{2g(s)h(s)loga}{[h(s)loga]^2 + 4} & h(s)loga \end{vmatrix}}{\begin{vmatrix} [h(s)loga]^2 + 1 & -([h(s)loga]^2 + 4) \\ h(s)loga & h(s)loga \end{vmatrix}} = \frac{g(s)}{[h(s)loga]^2 + 1}$$

$$X_2(s) = \frac{\begin{vmatrix} [h(s)loga]^2 + 1 & -g(s) \\ h(s)loga & \frac{g(s)h(s)loga}{[h(s)loga]^2 + 1} + \frac{2g(s)h(s)loga}{[h(s)loga]^2 + 4} \end{vmatrix}}{\begin{vmatrix} [h(s)loga]^2 + 1 & -([h(s)loga]^2 + 4) \\ h(s)loga & h(s)loga \end{vmatrix}} = \frac{2g(s)}{[h(s)loga]^2 + 4}$$

(44)

Taking the inverse M_a^{-1} to both sides of sys. (44), gives the exact solution of (41) - (42) in the form

$$x_1(\tau) = sin\tau\,,\quad x_2(\tau) = sin2\tau$$

Example 6. Consider the following system

$$x_1'' - x_2 + 2x_3 = 3e^{-\tau}$$

$$-2x_1' + 2x_2' + x_3 = 0$$

$$2x_1' - 2x_2 + x_3' + 2x_3'' = 0 \qquad (45)$$

Subject to

$$x_1(0) = 1, x_2(0) = 2, x_3(0) = 2 \;\; x_1'(0) = 1, \qquad x_3'(0) = -2 \qquad (46)$$

Applying MSEK transformation to both sides of sys. (45), we get

$$M_a\{x_1''\} - M_a\{x_2\} + 2M_a\{x_3\} = 3M_a\{e^{-\tau}\}$$

$$-2M_a\{x_1'\} + 2M_a\{x_2'\} + 3M_a\{x_3\} = 0$$

$$2M_a\{x_1'\} - 2M_a\{x_2\} + M_a\{x_3'\} = 2M_a\{x_3''\}$$

Using the initial conditions in (46) to obtain

$$[h(s)loga]^2 X_1(s) - X_2(s) + 2X_3(s) = \frac{g(s)[h(s)loga]^2 + 2g(s)h(s)loga + 4g(s)}{h(s)loga + 1}$$

$$-2h(s)loga\, X_1(s) + 2h(s)loga\, X_2(s) + X_3(s) = 2g(s)$$

$$2h(s)loga\, X_1(s) - 2X_2(s) + \{2[h(s)loga]^2 + h(s)\}X_3(s) = 4g(s)h(s)loga \qquad (47)$$

In matrix form, sys. (47) becomes

$$\begin{bmatrix} [h(s)loga]^2 & -1 & 2 \\ -2h(s)loga & 2h(s)loga & 1 \\ 2h(s)loga & -2 & \{2[h(s)loga]^2 + h(s)\} \end{bmatrix} \begin{bmatrix} X_1(s) \\ X_2(s) \\ X_3(s) \end{bmatrix} =$$

$$\begin{bmatrix} \frac{g(s)[h(s)loga]^2 + 2g(s)h(s)loga + 4g(s)}{h(s)loga + 1} \\ 2g(s) \\ 4g(s)h(s)loga \end{bmatrix}$$

(48)

Where $X_1(s), X_2(s)$ and $X_3(s)$ are the MSEK transform for $x_1(\tau)$, $x_2(\tau)$ and $x_3(\tau)$ respectively, solving the sys. (48) for $X_1(s)$, $X_2(s)$ and $X_3(s)$ by using Crammer's rule and Maple software to calculate the determinates, we get

$$X_1(s) == \frac{\begin{vmatrix} \frac{g(s)[h(s)loga]^2 + 2g(s)h(s)loga + 4g(s)}{h(s)loga + 1} & -1 & 2 \\ 2g(s) & 2h(s)loga & 1 \\ 4g(s)h(s)loga & -2 & \{2[h(s)loga]^2 + h(s)\} \end{vmatrix}}{\begin{vmatrix} [h(s)loga]^2 & -1 & 2 \\ -2h(s)loga & 2h(s)loga & 1 \\ 2h(s)loga & -2 & \{2[h(s)loga]^2 + h(s)\} \end{vmatrix}}$$

$$= \frac{g(s)}{h(s)loga - 1}$$

$$X_2(s) == \frac{\begin{vmatrix} [h(s)loga]^2 & \frac{g(s)[h(s)loga]^2 + 2g(s)h(s)loga + 4g(s)}{h(s)loga + 1} & 2 \\ -2h(s)loga & 2g(s) & 1 \\ 2h(s)loga & 4g(s)h(s)loga & \{2[h(s)loga]^2 + h(s)\} \end{vmatrix}}{\begin{vmatrix} [h(s)loga]^2 & -1 & 2 \\ -2h(s)loga & 2h(s)loga & 1 \\ 2h(s)loga & -2 & \{2[h(s)loga]^2 + h(s)\} \end{vmatrix}}$$

$$= \frac{2g(s)h(s)loga}{(h(s)loga)^2 - 1}$$

$$X_3(s) == \frac{\begin{vmatrix} [h(s)loga]^2 & 2 & \frac{g(s)[h(s)loga]^2 + 2g(s)h(s)loga + 4h(s)}{h(s)loga + 1} \\ -2h(s)loga & 1 & 2g(s) \\ 2h(s)loga & \{2[h(s)loga]^2 + h(s)\} & 4g(s)h(s)loga \end{vmatrix}}{\begin{vmatrix} [h(s)loga]^2 & -1 & 2 \\ -2h(s)loga & 2h(s)loga & 1 \\ 2h(s)loga & -2 & \{2[h(s)loga]^2 + h(s)\} \end{vmatrix}}$$

$$= \frac{-2g(s)}{h(s)loga+1} \qquad (49)$$

Taking the inverse M_a^{-1} to both sides of sys. (49), gives the exact solution of (45) - (46) in the form

$$x_1(\tau) = e^{\tau}, \quad x_2(\tau) = 2cosh\tau \quad , x_3(\tau) = -2e^{-\tau}$$

5. Discussion and Conclusion

The MSEK transform, a newly designed general integral transform, was implemented into the study. The inverse, convergence, practical characteristics, and applications of the MSEK transform for resolving differential equations and systems have all been examined. It can be readily used for ordinary differential equations of the nth order and systems of ordinary differential equations by transforming them into straightforward algebraic equations that are simple to solve. To demonstrate the transformation's simplicity and efficacy, we provide different numerical examples, the study focuses on solving equations of the third, fourth, and fifth orders, as well as systems of equations, irrespective of the number of equations and orders that are added. In every instance, the approach was successful in determining the exact solutions, indicating the potential for the suggested strategy to further improve knowledge of science. The MSEK transform is a specific instance of all transforms in the Laplace transform class, which was established in the last few decades. Several additional integral transforms can be built by selecting new forms for g(s) and h(s) based on their definitions. The MSEK transform's power lies in its ability to cover nearly all integral transforms, including Laplace, Ezaki, Sumudu, SEE, and others, given a variety of g(s) and h(s) possibilities when $a = e$ these benefits lead us to the conclusion that the suggested integral transform is extremely efficient based on its mathematical formulations, simplicity, and results

References:

Aboodh, K. H. S. (2013). The new integral transform Aboodh transform. *Global Journal of Pure and Applied Mathematics, 9*(1), 35–43.

Ahmadi, S. A. P., Hosseinzadeh, H., & Cherati, A. (2019). A new integral transform for solving higher order linear ordinary Laguerre and Hermite differential equations. *International Journal of Applied and Computational Mathematics, 5*(5),142-142.

Baleanu, D., & Wu, G. (2019). Some further results of the Laplace transform for variable–order fractional difference equations. *Fractional Calculus and Applied Analysis, 22*(1), 1641–1654.

Barnes, B. (2016). Polynomial integral transform for solving differential equations. *European Journal of Pure and Applied Mathematics, 9*(2), 140–151.

Braun, M. (1993). *Differential equation and their application* (4th ed.). Springer Verlag.

Cho, I., & Kim, H. (2013). The solution of Bessel's equation by using integral transform. *Applied Mathematical Sciences, 7*(122), 6069–6075.

Davies, B. (2002). *Integral transforms and their applications* (3rd Ed.), Springer.

Debnath, L. (2005). *Nonlinear partial differential equations for scientists and engineers*. Birkhäuser.

Donolato, D. (2002). Analytical and numerical inversion of the Laplace-Carson transform by a differential method, *Computer Physics Communications, 145*(2), 298–309.

Elzaki, T. M. (2011). The new integral transform Elzaki transform. *Global Journal of Pure and Applied Mathematics, 7*(1), 57–64.

Erkus-Duman, E., & Ciftc, H. (2018). Fibonacci and Lucas differential equations. *Applications and Applied Mathematics, 13*(2), 756–763.

Hasan, S. Q., Abubaker, U. M., & Kaurangini, M. L. (2023). The new integral transform "SUM Transform" and its properties. *Palestine Journal of Mathematics, 12*(1), 30–45.

Hilmi, H., & Jwamer, K. H. F. (2024). A new integral transform and applications HK-Transform. *Zanco Journal of Pure and Applied Sciences, 36*(5), 37–46.

Kamal, A., & Sedeeg, H. (2016). The new integral transform Kamal transform. *Advances in Theoretical and Applied Mathematics, 11*(4), 451–458.

Khan, Z. H., & Khan, W. A. (2008). N-transform properties and applications. *NUST Journal of Engineering Sciences, 1*(1), 127–133.

Khader, M. M., Sweilam, N. H., & Kharrat, B. N. (2020). Numerical simulation for solving fractional Riccati and logistic differential equations as a difference equation. *Applications and Applied Mathematics, 15*(12), 655–663.

Kharrat, B. N., & Toma, G. A. (2020). A new integral transform: Kharrat-Toma transform and its properties. *World Applied Sciences Journal, 38*(5), 436–443.

Kexue, L., & Jigen, P. (2011). Laplace transform and fractional differential equations. *Applied Mathematics Letters, 24*(12), 2019–2023.

Kim, H. (2017). The intrinsic structure and properties of Laplace-typed integral transforms. *Mathematical Problems in Engineering, 2017,* Article ID (8 pages).

Maktoof, S. F., Kuffi, E., & Abbas, E. S. (2021). Emad-Sara transform: A new integral transform. *Journal of Interdisciplinary Mathematics, 24*(7), 1985–1994.

Mansour, E. A., Mehdi, S. A., & Kuffi, E. A. (2021). The new integral transform and its applications. *International Journal of Nonlinear Analysis and Applications, 12*(2), 849–856.

Medina, G. D., Ojeda, N. R., Pereira, J. H., & Romero, L. G. (2017). Fractional Laplace transform and fractional calculus. *Mathematical Forum, 12*(20), 991–1000.

Mohammad, S. H., & Al-Rozbayani, A. M. (2024). Fractional integration via Picard method for solving fractional differential-algebraic systems. *Journal of Applied Mathematics, 2024,* Article ID 8499850, 11 pages.

Mohand, M., & Mahgoub, A. (2019). The new integral transform "Sawi transform". *Advances in Theoretical and Applied Mathematics, 14*(1), 81–87.

Mustafa, J. I. (2023). Employing a modified Sumudu with a modified iteration method to solve the system of nonlinear partial differential equations. *Computational and Mathematical Methods, 2023,* Article ID 6649037.

Patil, D. P., Borse, S. R., & Kapadi, D. P. (2023). Kushare transform for the solution of models in health sciences. *International Journal of Novel Research and Development,* *8*(1), 2456-4184.

Shehu, M., & Weidong, Z. H. (2019). New integral transform: Shehu transform a generalization of Sumudu and Laplace transform for solving differential equations. *International Journal of Analysis and Applications, 17*(2), 167–190.

Sobczyk, K. (2001). *Stochastic differential equations: With applications to physics and engineering.* Springer Science & Business Media.

Turab, A., Hilmi, H., Guirao, J. L. G., Jalil, S., Chorfi, N., & Mohammed, P. O. (2024). The Rishi Transform method for solving multi-high order fractional differential equations with constant coefficients. *AIMS Mathematics, 9*(2), 3798 – 3809.

Wang, P., Peng, X., & Wang, F. (2023). The analysis and application of a new integral transform W transform. *Thermal Science Journal, 27*(5A), 3823-3827.

Watugala, G. K. (1993). Sumudu transform: A new integral transform to solve differential equations and control engineering problems. *International Journal of Mathematical Education in Science and Technology,* *24*(1), 35–43.

Younis, I. Th., & Al-Rawi, Ek. S. (2023). Improved finite difference technique via Adomian polynomial to solve the coupled Drinfeld's–Sokolov–Wilson system. *International Journal of Mathematics and Mathematical Sciences, 2023*, Article ID 6916596, 14 pages.

Morphological and Electrical Properties of PbS Thin Films Prepared by Pulse Laser Deposition Technique

Asmaa N. Mohammed Ali [1]

Abstract:

Pulsed laser deposition (PLD) was used to create PbS thin films with thicknesses of 150 and 250 nm on glass substrates at room temperature. The films were then annealed at 373, 473, and 523 K. AFM, DC conductivity, and Hall Effect measurements were used to examine the effects of annealing temperature and film thickness on the morphological and electrical characteristics of the films. The findings demonstrated that whereas the opposite tendencies were seen with increasing annealing temperature, the grain size decreased with increasing film thickness. The electrical activation energies, carrier concentration, the average velocity of charged particles, Hall mobility, carrier lifetime, and mean free path exhibited similar dependencies on the annealing temperature and film thickness. These findings demonstrate that the PLD technique can be utilized to tune the formation and electrical behavior of PbS thin films for various applications. Because PbS has a straight band gap, electrons may go from the valence band to the conduction band without altering their momentum, producing light. It has potential applications in infrared detectors, solar cells, diodes, lasers, sensors, coatings, photocatalysts, thermoelectric, and biotechnology.

Keywords: *Lead(II) sulfide (PbS) , Structural Properties, Electrical Properties, Pulse Laser Deposition Technique.*

http://dx.doi.org/10.47832/Dub.Conf3-3

[1] Researcher. College of Science, Baghdad University, Iraq asmaa.natiq23@gmail.com

1. Introduction

PbS is the chemical formula for lead sulfide, an inorganic substance. Galena, the primary mineral and significant compound of lead, is another name for it. Because of its propensity to crystallize in sodium chloride, it is among the first materials to be employed as a semiconductor [1]. Lead sulfide is a distinctive straight band gap material that has attracted a lot of scientific interest, particularly in solar cell and infrared sensing applications. It is a semiconductor with a tiny band gap of about 0.4 eV. These two characteristics have led to its widespread application in several sectors. One of the earliest materials for electrical diodes capable of detecting electromagnetic radiation, including infrared light, was PbS [2]. Unlike thermal detectors, which react to a change in detector element temperature brought on by the radiation, PbS is an infrared sensor that directly detects light. Quantum dots and sulfide-containing nanoparticles have been thoroughly investigated [3]. Lead salts and other sulfide sources are traditionally combined to create such compounds [3]. Among the IV-VI semiconductors, lead sulfide (PbS) is one of the better options and has a number of uses. Because of its high light absorption capacity and improved quantum efficiency, PbS is regarded as a strong candidate in nano-optoelectronics. It finds use in photography, lasers, sensors, coatings, photocatalysts, solar cells, biological fields, thermoelectric, etc. [4-7]. In this work, high-quality thin films were deposited, nanoparticles were created, and their characteristics were examined using the pulsed laser deposition technique.

2. Experimental part

PLD was used to create PbS films on glass substrates at room temperature in a 10-3 mbar vacuum. Different temperatures (373, 473, and 523) were applied to the films [8]. Atomic force microscopy (AFM) was used to assess the films' shape and grain size (Scanning probe microscope type AA3000, Angstrom Advanced Company). The AFM data was also used to quantify the films' roughness. An electrical oven and a digital device that can detect and record tiny electric currents (Keithley 616) were used to assess DC conductivity. A device that employs the Van der Pauw approach to ascertain the electrical characteristics of materials (Ecopia HMS-3000) was used to test the Hall Effect parameters of the films. The sample was put in a four-point probe configuration with four ohmic contacts in order to quantify the carrier concentration. The carrier concentration (n_H) was determined using the following formula [9] using the Hall coefficient (R_H), which was derived from the Hall Effect measurements:

$$n_H = 1/R_H.q \quad (1)$$

where the electron charge is denoted by q. The Hall coefficient is a measure of how much the electric current is deflected by a magnetic field in a material. The electron charge is a fundamental constant that represents the amount of electric charge carried by a single electron. According to the equation, the carrier concentration is inversely proportional to both the electron charge and the Hall coefficient, meaning that a lower carrier concentration is implied by either a lower electron charge or a higher Hall coefficient. the Hall mobility(μ_H) is

measure of how easily the electric current can flow in a material under the influence of a magnetic calculate and can be calculated from the (R_H) and the conductivity (σ) [9].

$$\mu_H=R_H.\sigma \quad (2)$$

A greater Hall coefficient or conductivity suggests a larger Hall mobility, since the equation demonstrates that the Hall mobility is directly proportional to the R_H and conductivity. The drift velocity (υd) is measure of how fast the electric current moves in a material under an applied electric field and calculated from equation [9]:

$$\upsilon_d=E.\sigma/\ n_H.q \quad (3)$$

According to the equation, the drift velocity is directly proportional to the electric field and conductivity and varies inversely with the carrier concentration and electron charge. This means that a higher drift velocity is implied by a higher electric field or conductivity, while a lower drift velocity is implied by a higher carrier concentration or a lower electron charge. The carrier lifetime (τ) is measure of how long an electric charge can exist in a material before it recombines with another charge of the opposite sign and calculated from the equation:

$$\tau=m^*.\sigma/N.q^2 \quad (4)$$

The effective mass m*is a measure of how much inertia an electric charge has in a material, which depends on the band structure of the material. The carrier lifetime is directly proportional to the effective mass and conductivity and inversely proportional to the carrier concentration and the square of the electron charge, according to the equation. This means that a higher effective mass or conductivity implies a longer carrier lifetime, while a higher carrier concentration or a lower electron charge implies a shorter carrier lifetime. The mean free path (ℓ) is measure of how far an electric charge can travel in a material before it collides with another particle or impurity and calculated from the equation

$$\ell=\upsilon_d.\tau \quad (5)$$

According to the equation, the mean free path is directly proportional to both the drift velocity and the carrier lifetime; hence, a larger mean free path is implied by either a greater drift velocity or a longer carrier lifetime.

3. Results and discussion

3.1 Morphological Properties:

The morphology of PbS films on glass substrates was examined by AFM. We obtained the roughness and the average dimension of the crystallites in the films from the AFM images. These are important parameters to evaluate the surface quality and light-scattering properties of the films. Figures 1 and 2 show the AFM images of PbS films with thicknesses of 150 nm and 250 nm, respectively, annealed at different temperatures of RT, 373 K, 473 K, and 523 K. The images reveal that the films have nanoscale grains and a homogeneous structure without voids, indicating a high density and a good deposition quality. Table 1 provides an overview of the films' average grain size and roughness characteristics. According to the statistics, the average grain size and roughness increase with the temperature at which the material is heated and cooled. The thinner film (150 nm) has a slightly lower roughness than

the thicker film (250 nm), which can be explained by the lower aggregation of nanoparticles in the thinner film. Table 1 shows that the average grain size of the films has a positive dependence on the annealing temperature and a negative dependence on the film thickness [10, 11].

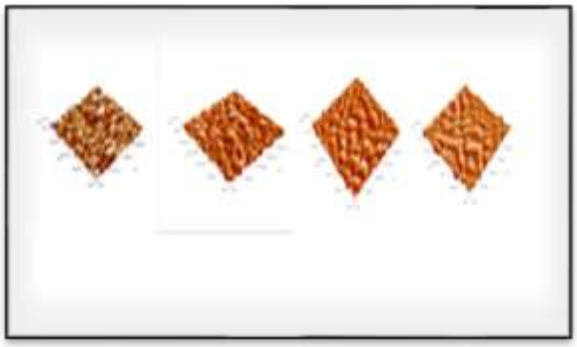

Fig.1 Image taken by AFM for PbS at thickness 150nm at different temperatures a: RT, b: 373K, c: 473and d: 523K

Fig. 2 Image taken by AFM for PbS at thickness 250nm at different temperatures a: RT, b: 373K, c: 473and d: 523K

Table 1: The mean particle diameter, roughness, and height difference of the PbS film particles vary with the film thickness at RT and annealing temperatures (373,473 and 523).

x	T_a(K)	Ave. grain size (nm)	Ave. Roughness (nm)	Peak- Peak (nm)
	295	41.71	3.74	32.86
150nm	373	53.59	8.33	43.71
	473	77.42	10.74	68.31
	523	98.76	14.42	52.11
	295	38.23	6.51	65.94
250nm	373	42.08	7.35	33.93
	473	58.12	10.94	22.45
	523	73.18	12.53	78.52

3.2 Electrical Properties:

As temperature varied, the films' electrical conductivity was measured to investigate the conduction mechanisms and the activation energies in the thin films. For PbS films with thicknesses of 150 nm and 250 nm, respectively, that were produced by pulsed laser deposition (PLD) on glass substrates at room temperature and annealed at 373, 473, and 523 K, Figures 3 and 4 display the logarithmic fluctuation in conductivity ln (σ) with the inverse

of temperature (1000/T). The figures indicate that a pair of energy barriers that need to be overcome Ea1 and Ea2 occurred., corresponding to two different conduction behaviors. The higher activation energy Ea2 in the higher temperature range (413-473 K) was associated with the carrier excitation into the another state above the mobility edge, while the lower energy Ea1 in the lower temperature range (295-408 K) was related to the carrier excitation into the states near the band edge. Increasing the temperature of annealing resulted in higher values of Ea1 and Ea2., which could be attributed to the reduction of defects and the improvement of crystallinity in the films. As film thickness increased, the values of Ea1 and Ea2 likewise fell, which may be explained by the thicker films' increased absorption and lower band gap [8,9]. Table 2 demonstrates that as the thickness of the PbS sheets grew, so did their DC conductivity (σd.c). Additionally, it demonstrates that for all films, the (σd.c) dropped as the temperature rose. This could be due to the lower crystallinity and smaller grain size of the films, as discussed in the previous section. Our results matched the ones that were published by Levechenko et al. and al-Fawade [12,13].

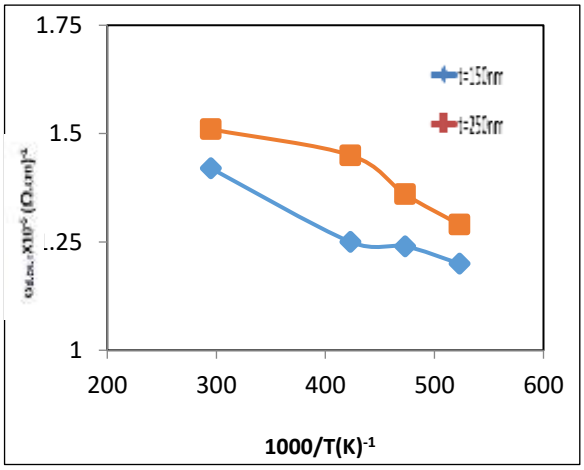

Fig. 3. Plotting the direct current conductivity's natural logarithm against the inverse of temperature for PbS films with varying thicknesses and annealing temperatures is displayed.

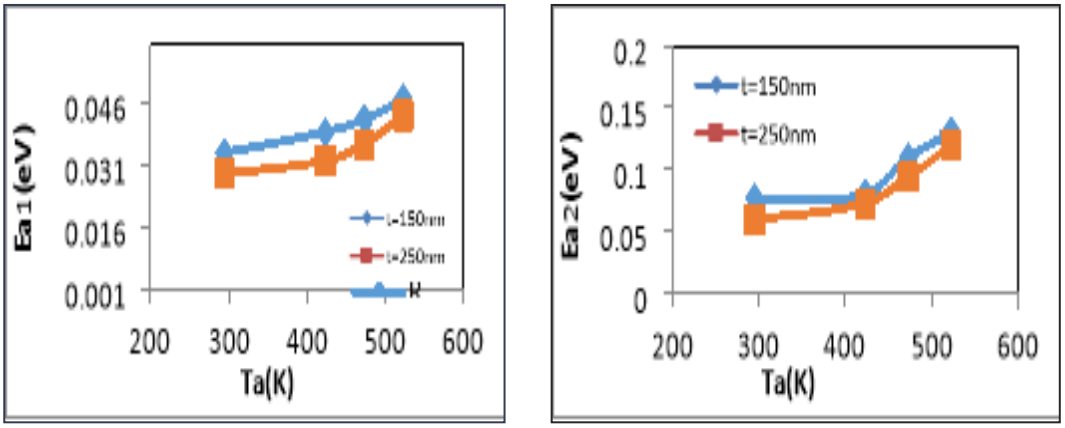

Fig. 4. Displays the change of Ea and Ta for films that had various thicknesses and annealing temperatures.

Table 2: shows the direct current conductivity characteristics of PbS films with varying annealing temperatures and thicknesses.

Thickness (nm)	Ta (K)	$\sigma_{d.c R.T} \times 10^{-5}$ $(\Omega.cm)^{-1}$	Ea1 (eV)	Temp. Range (K)	Ea2 (eV)	Temp. Range (K)
150	295	1.42	0.034	293-403	0.077	408-473
	373	1.25	0.039	293-403	0.08	413-473
	473	1.24	0.042	293-403	0.11	413-473
	523	1.2	0.047	293-403	0.13	413-473
250	295	1.51	0.029	293-403	0.06	413-473
	373	1.45	0.032	293-403	0.073	413-473
	473	1.36	0.036	293-403	0.094	413-473
	523	1.29	0.043	293-403	0.12	413-473

The films' electric behavior was measured and analyzed by Hall Effect measurements. The carrier concentration ($_{nH}$), the Hall mobility (μ_H), the carrier lifetime (τ), the drift velocity (v_d), and the mean free path (ℓ) were determined as functions of film thickness (d) and annealing temperature (Ta). Figure 5 and Table 3 summarize the results of these measurements. Increasing Ta caused the n values to decrease, but increasing d caused the nH values to increase. The μ_H values increased with elevating Ta, while they decreased with d increasing. The τ, vd, and ℓ values were calculated from the μH values using the equations (3), (4) and (5),Figure 5 (c ,d, e) and Table 3 show that these parameters increased with raising Ta, while they decreased with Raising d. The annealing process's effects on the morphology and structure of the film are responsible for the fluctuation in these parameters [14, 15].

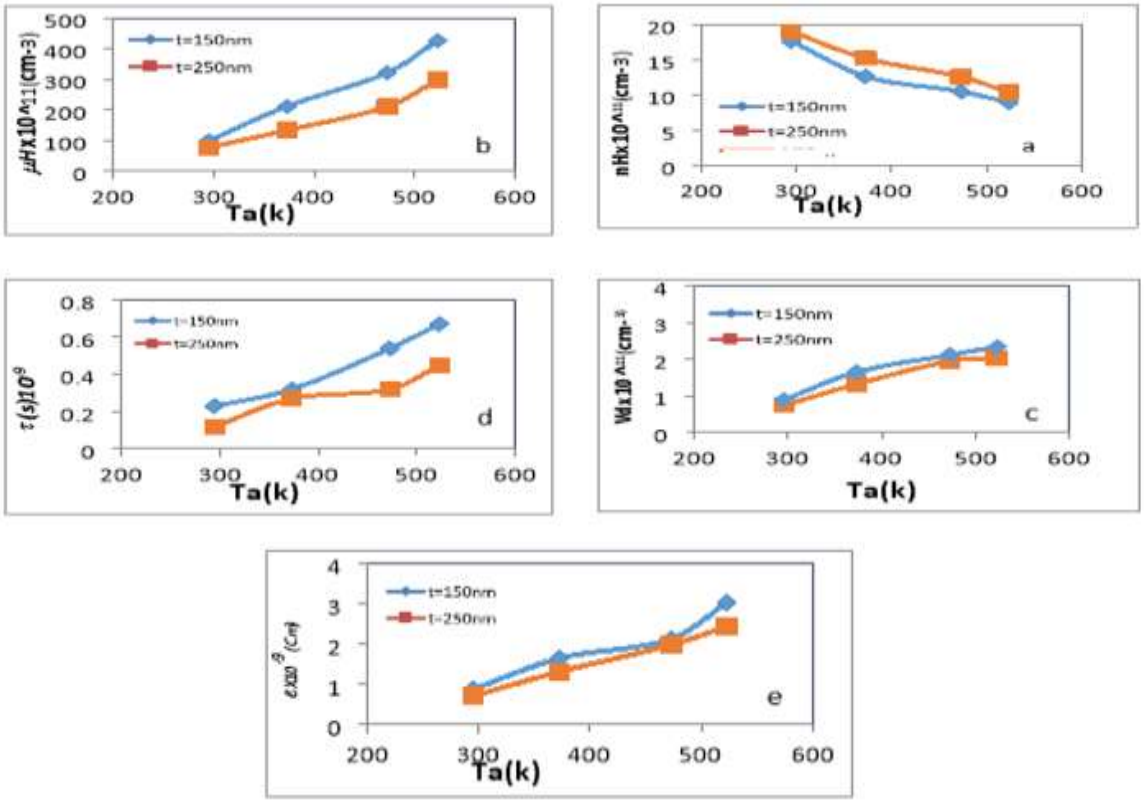

Fig. 5. Shows Hall parameters of PbS thin films. a-(nH), b-(μH), c- (Vd), d-(τ) , e-(ℓ)

Table 3: The variation of the Hall parameters concerning the film thickness and the heat treatment temperature for PbS films.

Thickness (nm)	Ta(K)	6R. T×10-5 (cm.Ω)	nH×1011 (cm-3)	µH×103 (cm2/V.s)	vd (cm/s)	τ (s)´10-9	ℓ × 10-9 (cm)
150	295	.71	17.65	98.77	0.51	.034	.017
	373	7	12.65	212.4	0.69	.049	0.33
	473	6.88	10.51	321.98	0.81	.055	0.44
	523	6.10	8.96	427.11	0.85	.058	0.5
250	295	7.62	18.98	77.75	.050	.033	.016
	373	7.44	15.22	134.23	0.60	.041	0.24
	473	7.21	12.6	211.65	0.72	.048	0.34
	523	6.87	10.42	298.44	0.82	.055	0.45

4. Conclusion

Using a Nd:YAG laser with λ=1064 nm, PbS thin films of 150 and 250 nm thickness were deposited on glass substrates using the PLD technique at room temperature and various annealing temperatures (373, 473, and 523) K. The shape and electric behavior of the films were measured and analyzed in relation to the film thickness (d) and the heat treatment temperature (Ta). AFM was used to examine the films' shape and grain size. The AFM images of the films with different d and Ta values were obtained,. The images were analyzed using the ImageJ software and the average grain size (D) of the films was calculated. D was plotted as a function of d and Ta, as shown in Figure 2. D was directly proportional to Ta, but inversely proportional to d. We performed Hall Effect measurements to determine the carrier concentration (nH), the Hall mobility(µH), the drift velocity (vd), the carrier lifetime (τ), and the average free path (ℓ) of the films. His variation of these parameters with film thickness (d) and annealing temperature (Ta) was investigated. The findings indicated that increasing Ta caused nH to decrease, but increasing d caused n to increase. This indicated that the annealing process reduced n due to the formation of vacancies or defects that act as recombination centers for charge carriers. On the other hand, the increase in d increased nH due to the increased number of PbS molecules per unit area. It was also found that µH, v_d, τ, and ℓ increased with increasing Ta, while they decreased with increasing d. This suggested that the annealing process improved µH, v_d, τ, and ℓ due to the enhanced crystallinity and reduced grain boundary scattering of charge carriers. On the other hand, the decrease in d reduced μ_H, v_d, τ, and ℓ due to the increased surface scattering of charge carriers

Refrence:

Vaughan, D. J.; Craig, J. R. Mineral Chemistry of Metal Sulfides. Cambridge: Cambridge University Press. ISBN 978-0-521-21489-6. (1978).

Arthur, J B (1951). "Lead Sulphide – An Intrinsic Semiconductor". Proceedings of the Physical Society. Series B. 64 (7): 616–618. doi:10.1088/0370-1301/64/7/1102-"Mercuric oxide [ISO]". ChemIDPlus Advanced. United States National Library of Medicine. CAS RN: 21908-53-2. Retrieved 2022-04-14.

The Quantum Mechanics of Larger Semiconductor Clusters ("Quantum Dots")". Annual Review of Physical Chemistry. 41 (1): 477–496. 1990-01-01. Bibcode:1990ARPC...41..477B.

Lee, HyoJoong; Leventis, Henry C.; Moon, Soo-Jin; Chen, Peter; Ito, Seigo; Haque, Saif A.; Torres, Tomas; Nüesch, Frank; Geiger, Thomas "PbS and CdS Quantum Dot-Sensitized Solid-State Solar Cells: "Old Concepts, New Results". Advanced Functional Materials. 19 (17): 2735–2742. (2009-09-09).

Chouldrury, N. and Sarma, K. (2008).Structural characterization of nanocrystrallinePbS thin films: synthesized by CBD method. Indian J. of Pure and Appl. Phys, 46: 261-265.

H.S. Kwok, H.S. Kim, D.H. Kim, W.P. Shen, X.W. Sun, R.F. Xiao, Applied Surface Science,109-110 595-600. (1997).

Robert Eason, “Pulsed Laser Deposition Of Thin Films Applications-led Growth of Functional Materials”, Wiley-Inter science, New Jersey, (2007), pp: 682.

Ali L. Abeda and Mohammed T. Hussein " hin TO Nano x-1Znxernary BeTof Synthesis and Characterization Films prepared by Pulsed Laser Deposition Technique ", Iraqi Journal of Physics, Vol.20, No.2, PP.53-63,(2022).

A. Islam, M. Islam, M. Choudlury& M. Hassan, “Recent Development in Condenced Matter Physics and Nuclear Science,” no. Rajshahi University,Bangladesh, (1998).

Abass, M., Al-Fawadi, E., Al-Samuraee ,A.-K.“Preparation of nanocrystalline PbS thin films by chemical bath deposition”, united states ,vol.4,p.p:2637-2646,(2009).

E.M.N.Al-Fawade and M.F.A.Alias, "Fabrication of PbxS1-x Detector and Studying the Effect of x Content onits some Physical Properties",Iraqi Journal of Physics, Vol. 9, No.15, PP. 31-40,(2011).

VI. Levechenko and LI. Postnov, "Semiconductors", 30, 12, 1996, 13885.

Nasir, E.M , Abass, M.M. "Characterization, morphology and electrical properties of chemically deposited nanocrystalline PbS/Si heterojunction thin films",vol.13,no.6, p.p:271-279,(2016).

VI. Levechenko and LI. Postnov, "Semiconductors", 30, 12, 1996, 13885.

J.F. Wood, "Phys. Rev.", 106, 2, 1957, 235.

Primly Small Retractable Modules

Shaymaa A. Hameed [1]

Rusul Ismail Khalil [2]

Mukdad Qaess Hussain [3]

Abstract:

In this paper we revision primly small retractable module as generalization from small retractable module and we give characterizations of such modules. Also, we investigate relation between this concept and some kinds of modules.

Keywords: *Small Submodules, Prime Modules, Retractable Modules*.

http://dx.doi.org/10.47832/Dub.Conf3-4

[1] Researcher. College of Basic Education, Diyala University, Iraq basicmathte3@uodiyala.edu.iq / orcid.org/0009-0006-2187-3187

[2] Researcher. College of Basic Education, Diyala University, Iraq basicmathte7@uodiyala.edu.iq / orcid.org/0009-0006-2032-9497

[3] Researcher. College of Education for pure science, Diyala University, Iraq mukdadqaess2025@gmail.com / orcid.org/0000-0002-3828-4710

Introduction

Let D be unitary left module over ring with identity R. A sub-module Y of R-module D is small sub-module from D ($Y \ll D$) if for some sub-module X from D such that $D = Y + X$, then $X = D$ [1]. An R-module D is small retractable (S.R) whenever $\mathrm{Hom}_R(D,U) \neq 0$ for every non-zero small sub-module U of D [2]. A sub-module N of R-module D is pure sub-module if for every finitely generated ideal I of R, $ID \cap N = IN$[3]. An R-module D is purely small retractable (Pu.S.R) whenever $\mathrm{Hom}_R(D,U) \neq 0$ for every non-zero pure small sub-module U from D. A ring R is Pu.S.R whenever R as R-module is Pu.S.R, that is $\mathrm{Hom}_R(R,I) \neq 0$ for every non-zero pure ideal I from R. A proper sub-module N of R-module D over ring R is prime sub-module if $re \in N$ for $e \in D$ and $r \in R$ implies that $e \in N$ or $r \in \mathrm{Ann}_R(D,N)$[4]. An R-module D is primly small compressible (Pr.S.C) if D can be embedded in every of its non-zero prime small sub-module. That is D is Pr.S.C if there exists a monomorphism $f : D \to U$ whenever U be non-zero prime small sub-module from D. A ring R is Pr.S.C whenever R as R-module is Pr.S.C.

Primly small retractable modules

Definition1 An R-module D is primly small retractable (Pr.S.R) if $\mathrm{Hom}(D,U) \neq 0$ for every non-zero prime small sub-module U from D.

A ring R is Pr.S.R if R as R-module is Pr.S.R.

Remarks and Examples2

(1) Every S.R module is Pr.S.R, the converse is not true. For example: Q as Z-module is Pr.S.R since the only prime small sub-module from Q is 0, and Q is not S.R since $\mathrm{Hom}(Q,Z) = 0$.

(2) Every fully small prime module D is Pr.S.R if and only if D is S.R.

(3) Every Pr.S.C module is Pr.S.R, the opposite is not correct. For example, Z_{12} as Z-modu is Pr.S.R which is not Pr.S.C.

(4) Every simple module be Pr.S.R but the opposite is not correct.

(5) Let D be R-module. Then D be Pr.S.R R-module if and only if D be Pr.S.RR/annD-module.

(6) Let D be torsion-free module such that $[N:D] = 0$ for each proper small sub-module N from D. Then D be Pr.S.R if and only if D be Pu.S.R.

Proof: Since D be torsion-free and $[N:D] = 0$ for every proper small sub-module N from D implies N be prime small sub-module from D if and only if N be pure small sub-module from D [5]. Hence D is Pr.S.R if and only if D is Pu.S.R.

(7) Let D be prime faithful module such that $[N:D] = 0$ for every proper small sub-module N of D. Then D is Pr.S.R if and only if D be Pu.S.R.

Proof: Since D be faithful prime module implies D be torsion-free [6, Remark 1.1, p.33] thus by (6) D be Pr.S.R if and only if D be Pu.S.R.

(8) Let D be prime module such that annD = $[N:D]$ for each proper small sub-module N of D. Then D is Pr.S.R if and only if D is Pu.S.R .

Proof: From [6, proposition 1.3, p.34] we obtain N be prime small sub-module from D if and only if N be pure small sub-module from D. Therefore D is Pr.S.R if and only if D is Pu.S.R

Proposition3 If D_1 and D_2 are two isomorphic modules, then D_1 is Pr.S.R if and only if D_2 is Pr.S.R.

Proof: Assume that D_1 is Pr.S.R and let $\varphi : D_1 \to D_2$ be an isomorphism and N be non-zero prime small sub-module from D_2.Thus $\varphi(D_1) \not\subset N$, for if $\varphi(D_1) \subset N$ then $D_2 \subseteq N$ implies $D_2 = N$ which is contradiction since N be prime small sub-module from D_2. Thus $\varphi^{-1}(N)$ be prime small sub-module from D_1 [7,proposition 1.2, p.1043]. Put $K = \varphi^{-1}(N)$. since D_1 is Pr.S.R, there exists $f : D_1 \to K$ be non-zero homomorphism with $g = \varphi|_K$ thus $g : K \to D_2$ be homomorphism with $g(k) = \varphi(\varphi^{-1}(N)) = N$, hence $g : K \to N$ be homomorphism. Now, the composition $D_2 \xrightarrow{\varphi^{-1}} D_1 \xrightarrow{f} K \xrightarrow{g} N$. Let $h = gf\varphi^{-1}$, then $h \in \text{Hom}(D_2, N)$.

If $h = 0$, then $0 = g(f(\varphi^{-1}(D_2))) = g(f(D_1))$ then $f(D_1) \subseteq \text{Ker}g \subseteq \text{Ker}\varphi = 0$. Thus $f(D_1) = 0$, which is contradiction. Therefore $\text{Hom}_R(D_2, N) \neq 0$ thus D_2 be Pr.S.R

Proposition4 Let D be R-module satisfying (*) such that $\text{End}_R(D)$ is Boolean ring. If D is Pr.S.R, then every small sub-module from D is Pr.S.R.

Proof: Let U be nonzero small sub-module from D and k be non-zero prime small sub-module of U. Thus $\text{Hom}_R(D, K) \neq 0$. Let $f : D \to K$ be non-zero homomorphism. Therefore $f \circ i : U \to K$ be homomorphism where $i : U \to D$ be inclusion homomorphism. Claim $f \circ i \neq 0$, Suppose $f \circ i = 0$, thus $(f \circ i)(U) = 0 = f(U)$, Also $U \subseteq \text{Ker}f$ implies $K \subseteq \text{Ker}f$, therefore $f(D) \subseteq \text{Ker}\, f$ thus $f(f(D)) = 0$. Let $j : K \to D$ be inclusion homomorphism. Thus $j \circ f \in \text{End}_R(D)$ with $j \circ f(D) = f(D)$ but $(j \circ f)^2(D) = (j \circ f)(j \circ f)(D) = j \circ f(f(D)) = j(f(f(D))) = J(0) = 0$, and $(j \circ f)^2(D) = (j \circ f)(D)$ since $\text{End}_R(D)$ be Boolean ring. implies $j(f(D)) = f(D) = 0$. Thus $f = 0$ which is contradiction, therefore $f \circ i \neq 0$, hence U be Pr.S.R.

Corollary5 Let D be module satisfying (*) such that End(D) be Boolean ring. If D be Pr.S.R, then every direct summand from D be Pr.S.R.

Proposition6 If D is Pr.S.C, then D is generalized small prime module.

Proof: Let D be Pr.S.C module and N be non-zero prime small sub-module from D. To show annD = annN. Let $r \in \text{ann}N$. Thus $rN = 0$. Let $f : D \to N$ be monomorphism, thus $f(rD) = rf(D) \subseteq rN = 0$ implies that $rD = 0$, thus $r \in \text{ann}D$ and therefore annD = annN.

Proposition7 Every Pr.S.C module is primely small uniform

Proof: Let N be prime small sub-module from D. Let $0 \neq x \in D$ such that Rx be prime small sub-module of D. Thus there exists a monomorphism, $f : D \to Rx$. Let $0 \neq m \in N$. Thus $f(m) = wx$ for some $0 \neq w \in R$, with $f(x) = rx$ for some $0 \neq r \in R$, $f(rm) = rf(m) = r(wx) = w(rx) =$

wf(x) = f(wx) then rm = wx ∈ N and wx ≠ 0. So N be` primely small essential in D thus D be primely small uniform.

Proposition8 Let D be Pr.S.R R-module, then D is Pr.S.C.

Proof: Let N be non-zero prime small sub-module from D and $f : D \to N$ be non-zero homomorphism. Thus $i \circ f : D \to D$ be an endomorphism on D, where $i : N \to D$ be inclusion homomorphism. Thus $i \circ f$ is monomorphism and hence f be monomorphism. Then D be Pr.S.C.

Corollary9 Let D be Pr.S.R module. Then D is generalized small prime and primely small uniform.

Proof: By Prop. 8, D is Pr.S.C and from prop. 6 and prop.7, D is generalized small prime and primely small uniform.

Characterizations of Primly Small Retractable Module

Proposition10 Let D be module. Then D is Pr.S.R if and only if there exists $0 \neq \varphi \in \mathrm{End}_R(D)$ such that $\mathrm{Im}\,\varphi \subseteq N$ for each non-zero prime small sub-module N from D.

Proof: (⇒) Suppose D be Pr.S.R. Let N be non-zero prime small sub-module from D. Thus $\mathrm{Hom}_R(D,N) \neq 0$. Let $0 \neq f : D \to N$ be non-zero homomorphism. Let $\varphi = i \circ f$ where $i : N \to D$ be the inclusion homo-morphism, thus $\varphi \in \mathrm{End}_R(D)$, $\varphi \neq 0$ and $\mathrm{Im}\,\varphi = i \circ f(D) = f(D) \subseteq N$.

(⇐) To prove D is Pr.S.R, let N be non-zero prime small sub-module from D, there exists non-zero endomorphism $\varphi : D \to D$ such that $\mathrm{Im}\varphi = \varphi(D) \subseteq N$, thus $\varphi : D \to N$ be non-zero homomorphism, then $0 \neq \varphi \in \mathrm{Hom}(D,N)$, thus D be Pr.S.R.

Proposition11 Let D be module such that every cyclic small sub-module of prime sub-module of D is prime in D. Then D is Pr.S.R if and only if $\mathrm{Hom}(D,Rx) \neq 0$ for each $0 \neq x \in D$.

Proof: (⇒) Clear.

(⇐) Let N be non-zero prime small sub-module from D. Let $0 \neq x \in N$. Thus Rx be prime in D and $\mathrm{Hom}(D,Rx) \neq 0$ hence $\mathrm{Hom}(D,N) \neq 0$, thus D be Pr.S.R.

Corollary12 Let D be modu such that every cyclic small sub-module of D is prime. Then D is Pr.S.R if and only if $\mathrm{Hom}(D,Rx) \neq 0$ for each $0 \neq x \in D$.

Corollary13 Every finitely presented prime module is Pr.S.R.

Proof: Let D be finitely presented prime module and $0 \neq x \in D$. Thus Rx be direct summand from D [8, Exercies 32, p.163]. Thus $\mathrm{Hom}(D,Rx) \neq 0$ then by corollary 12, D be Pr.S.R.

Corollary14 Every prime finitely generated projective module is Pr.S.R.

Proof: Let D be prime finitely generated projective module. Thus D be finitely presented [8, Exercise 1, p. 159]. From corollary 13, D be Pr.S.R.

Proposition15 Let D be module such that every non-zero prime small sub-module from D contains non-zero direct summand from D. Then D is Pr.S.R.

Proof: Let N be non-zero prime small sub-module from D, there is $0 \neq A \leq N$ and A be direct summand from D, thus $D = A \oplus B$ for some $0 \neq B < D$. Let $\rho_A : D \to A$ be the projection homomorphism. Thus $\rho_A \in \mathrm{Hom}(D, A)$ and $i\rho_A \in \mathrm{Hom}(D, N)$ where $i : A \to N$ be inclusion homomorphism. If $i\rho_A = 0$, thus $0 = i\rho_A(D) = \rho_A(D) \simeq A$ implies $A = 0$ which is contradiction thus $\mathrm{Hom}(D, N) \neq 0$, then D be Pr.S.R.

Proposition16 Let D be prime module such that every non-zero small sub-module from D contains non-zero direct summand from D. if D is Pr.S.R, then D is S.R.

Proof: Let $0 \neq N \leq D$, there exist direct summand U from D, $U \subseteq N$. Thus U be prime in D [6, prop. 1.2, p.34]. Since D be Pr.S.R then $\mathrm{Hom}(D, U) \neq 0$ hence $\mathrm{Hom}(D, N) \neq 0$. Thus D be S.R.

Corollary17 Let D be prime module such that every non-zero small sub-module from D contains non-zero direct summand from D. Then D is S.R if and only if D is Pr.S.R.

Remark18 (1) Every commutative ring with identity is retractable.

Proof: Let I be non-zero ideal of commutative ring with identity R. let $0 \neq a \in I$. Define $f : R \longrightarrow I$ by $f(r) = ra \; \forall r \in R$. Clearly f is well-defined R-homomorphism. If $f = 0$. Thus $f(r) = 0$ for all $r \in R$. Thus, $0 = f(1) = 1.a = 0$ which is contradiction. Therefore $\mathrm{Hom}(R, I) \neq 0$.

Proposition19 Let D be finitely generated multiplication R-module. then D is Pr.S.R module.

Proof: Let N be non-zero prime small sub-module from D. Thus $N = ID$ for some non-zero prime ideal I from R[9]. But R be Pr.S.R by Remark18 implies $\mathrm{Hom}(R, I) \neq 0$. Let $0 \neq f : R \to I$ be homomorphism. Let $f(1) = a$. Thus $a \neq 0$. Define $g : D \to N$ by $g(D) = ad$ for all $d \in D$. Clearly, g is well-defined homomorphism, $g \neq 0$ since D be faithful. Thus $\mathrm{Hom}(D, N) \neq 0$ thus D be Pr.S.R module.

Corollary20 Every faithful cyclic R-module is Pr.S.R.

Primly epi-small retractable modules

Definition21 A module D is primly epi-small retractable (Pr.epi-S.R) if every prime small sub-module of D is homomorphic image from D. That is, whenever N is prime small sub-module from D, then there exists an epimorphism from D onto N.

Examples and Remarkes22

(1) Every Pr.epi-S.R module is Pr. S.R.

(2) Q as Z-module is Pr.epi-S.R. Since every prime small sub-module of Q is homomorphic image of Q.

(3) Z_{12} as Z-module is Pr.epi-S.R module. Since every prime small sub-module of Z_{12} is homomorphic image of Z_{12}.

(4) Every semisimple module is Pr.epi-S.R.

(5) Every fully prime module is Pr.epi-S.R if and only epi- S.R.

Proposition23 Let D be module satisfying (*). If D Pr.epi-S.R module, then every non-zero prime small sub-module from D is Pr.epi-S.R.

Proof: Let D be Pr.epi-S.R module and N be non-zero prime small sub-module from D. let K be non-zero prime small sub-module from N. Since D satisfying (*). Thus K be prime in D. Therefore there are epimorphisms $f : D \to N$ and $g : D \to K$. Define $h : N = f(D) \to K = g(D)$ by $h\big(f(d)\big) = g(d)$ for all $d \in D$. Clearly $h \in \mathrm{Hom}(N, K)$. $h \neq 0$, for if $h = 0$. Then $h\big(f(D)\big) = 0 = g(D) = K$ which is contradiction. Also, since $h(N) = h\big(f(D)\big) = g(D) = K$, then h is an epimorphism. Thus N is Pr.epi-S.R.

Corollary24 A direct summand of prime and Pr.epi-S.R module Pr.epi-S.R is Pr.epi-S.R.

Proposition25 Let D be Pr.epi-S.R module. Then D/N is Pr.epi-S.R.

Proof: Let $\bar{0} \neq K/N$ be prime small sub-module from D/N, where K be proper small sub-module from D containing N properly. K/N be prime in D/N implies K be prime in D [10, corollary 3.9]. Since D be Pr.epi-S.R, thus there exists an epimorphism, $f : D \to K$, f induces homomorphism $\bar{f} : D/N \to K/N$ with $\bar{f}(d + N) = f(d) + N$ for all $d \in D$, $\bar{f} \neq 0$, for if $\bar{f} = 0$, then $\bar{0} = \bar{f}(D/N) = f(D) + N = K + N$, since f be an epimorphism. Thus $K + N = N$ implies $K = N$ which is contradiction. Hence $\mathrm{Hom}(D/N, K/N) \neq 0$. Moreover $\bar{f}(D/N) = K/N$. Thus D/N is Pr.epi-S.R.

Lemma26 Let D_1 and D_2 be two R-module. If $N_1 \oplus N_2$ is prime small sub-module of $D_1 \oplus D_2$. Then N_1 is prime small sub-module of D_1 and N_2 is prime small sub-module of D_2.

Proof: Let $r \in R$ and $x \in D_1$ such that $rx \in N_1$. Since $N_1 \oplus N_2$is prime sub-module of $D_1 \oplus D_2$ Thus $r(x, 0) \in N_1 \oplus N_2$ So either$(x, 0) \in N_{1\oplus} N_2$ or $r \in [N_1 \oplus N_2 : D_1 \oplus D_2]$. If $(x, 0) \in N_1 \oplus N_2$ implies $x \in N_1$. If $r \in [N_1 \oplus N_2 : D_1 \oplus D_2]$, then $r(d_1, d_2) \in N_1 \oplus N_2$ for all $d_1 \in D_1$, for all $d_2 \in D_2$.Therefore $rd_1 \in N_1$ for all $d_1 \in D_1$, So $r \in [N_1 : D_1]$ and hence N_1 is prime small sub-module of D_1. Similarly we prove that N_2 is prime small sub-module of D_2.

Proposition27 Let D_1 and D_2 be two Pr.epi-S.R modules such that $\mathrm{ann}D_1 + \mathrm{ann}D_2 = R$. Then $D_1 \oplus D_2$ is Pr.epi-S.R.

Proof: Let N be non-zero prime small sub-module from $D_1 \oplus D_2$. Thus $N = N_1 \oplus N_2$ for some small sub-module N_1 of D_1 and N_2 of D_2. From [11, proposition 4.2] and Lemma 26 N_1 be prime in D_1 and N_2 be prime in D_2.Thus there exist epimorphisms $f : D_1 \to N_1$and $g : D_2 \to N_2$. Define $h : D_1 \oplus D_2 \to N$ by $h(d_1, d_2) = (f(d_1), g(d_2))$ for all $(d_1, d_2) \in D_1 \oplus D_2$. Clearly, h be an epimorphism. Thus $D_1 \oplus D_2$ be Pr.epi-S.R.

Corollary28 Let $\{D_i\}_{i=1}^{n}$be finite family of Pr.epi-S.R modules such that $\sum_{i=1}^{n} \mathrm{ann}D_i = R$. Then $\oplus_{i=1}^{n} D_i$ is Pr.epi-S.R

Refrences:

Abdoul Djibril Diallo, Papa Cheikhou Diop, Mamadou Barry "On S-quasi-Dedekind Modules", Journal of Mathematics Research; 2017, 97-107.

Marhoon, H. K. (2014). Some generalizations of monoform modules, Ms. C Thesis, University of Baghdad.

D.J.Fieldhouse, Pure theories. Math. Ann. 184 (1969),1-18.

Prime submodules of modules, Chin –Pi Lu, Commentarll mathematicl universitatis sancti pauli,vol 33,no1,1984.

Lu, C. P. (1984). Prime submodules of modules. Commentarii Mathematici Universitatis Sancti Pauli, 33(1), 61-69.

AL-Bahraany, B. (1996). A Note on Prime Modules and Pure Submodules. Science, 37, 1431-1441.

McCasland, R. L., & Smith, P. (1993). Prime submodules of Noetherian modules. The Rocky Mountain Journal of Mathematics, 23(3), 1041-1062.

Lam, T. Y. (2012). Lectures on modules and rings (Vol. 189). Springer Science & Business Media.

Athab, E. A. (1996). Prime and semi prime submodules M. SC (Doctoral dissertation, Thesis, university of Baghdad).

Saymeh, S. A. (1979). On prime R-submodules. Univ. Ndc. Tucuma'n Rev. Ser. A, 29, 129-136.

Abbas, M. S. (1990). " On fully stable modules", Ph. D. Thesis. Baghdad: Baghdad University.

Qualitative Analysis of Generalized Caputo Volterra-Fredholm Integro-Differential Equations

Riyam Bassim Abdulmaged [1]

Ihab Hadi Jumaah [2]

Ali Farhan Hashoosh [3]

Alan Jalal Abdulqader [4]

Abstract:

The fractional generalized Caput Volterra-Fredholm integra-differential equation (GFCV-FIDE) with non-local condition is investigated in this work. It uses the Banach's fixed-point theorem (FPT) to demonstrate the existence and uniqueness of solutions. Additionally, it illustrates a noteworthy finding on the presence of a minimum of one solution, supported by criteria derived from the Kwasniewski FPT. Ulam stability of the GFCV-FIDE is also investigated by using the Gronvall inequality. An example is shown to demonstrate the findings' robustness and practical usefulness. 2020 AMS Classification: 45J05; 47H10; 45M10.

Keywords: *Volterra-Fredholm; Generalized Caputo Fractional, Derivative; Fixed-Point.*

http://dx.doi.org/10.47832/Dub.Conf3-5

[1] Researcher. College of Education, Mustansiriyah University, Iraq riyam.basim2023@uomustansiriyah.edu.iq

[2] Researcher. College of Education, Mustansiriyah University, Iraq ihabhadi5@uomustansiriyah.edu.iq

[3] Researcher. College of Basic Education, Misan University, Iraq ali_fr@uomisan.edu.iq

[4] Researcher. College of Education, Mustansiriyah University, Iraq alanjalal515@uomustansiriyah.edu.iq

1. Introduction

Fractional calculus extends the classical concepts of integration and differentiation of integer order to derivatives and integrals of arbitrary real (or even complex) order. Although fractional calculus has gained considerable attention in recent decades due to its wide range of applications, its origins date back to the correspondence between L'Hôpital and G.W. Leibniz in 1695. The theory was further developed by several mathematicians, including Euler, Laplace, Liouville, Riemann, Grünwald, Letnikov, Weyl, and Caputo (see [8,9] for historical details). Over time, these contributions established the theoretical foundation of modern fractional calculus.

One of the best mathematical instruments for characterizing the memory characteristics of certain materials and complicated systems is fractional calculus [22]. The integer-order derivative is commonly used in the classical framework to represent a system's memory:

$$\frac{dQ(z)}{dz} = \lim_{\Delta z \to 0} \frac{Q(z) - Q(z - \Delta z)}{\Delta z}, \qquad 0 < z$$

Because it only uses the function's values at two places, this definition accurately describes the system's short memory characteristics. On the other hand, the fractional approach uses the fractional order derivative to express a system's memory [19]:

$$\frac{d^{\theta}Q(z)}{dz^{\theta}} = \lim_{\mu \to 0} \mu^{-\theta} \sum_{r=0}^{n} (-1)^r \binom{\theta}{r} Q(z - r\mu), \qquad n\mu = z\ , \qquad 0 < \theta < 1$$

where the fractional derivative (FD) order is θ. The fractional derivative, in contrast to the classical derivative, takes into consideration the history of the function. In order to calculate the FD at a particular time t, the system's long memory qualities must be reflected by taking into account all of the function $\Phi(t)$'s prior values. For further information, see [23].

The large number of derivatives and integrals that are available in classical fractional calculus is one of its advantages. To improve our comprehension of the cosmos, fresh developments and advancements in this sector have always been required. Atangana and Baleanu presented a FD in the sense of Caputo in [7], which is notable as the ABC-fractional derivative, using the Mittag-Leffler function with non-singular kernels. Refer to [4, 12, 20, 25] for further information on FDs with non-singular kernels. In order to unify the Hadamard and Riemann-Liouville fractional operators, Katugampola presented what he dubbed generalized fractional operators [1, 2, 3, 18, 26]. Later, the Caputo and Caputo-Hadamard fractional derivatives were included in these generalized derivatives [11].

The authors in [14] introduced fractional operators derived from proportionate derivatives of one function relative to another. The kernel in the proposed fractional operators incorporates an exponential function, contingent upon the specific function employed.In many scientific domains, including physics, engineering, medicine, electrochemistry, control theory, and more, fractional differential equations (FDEs) naturally occur (see [10, 27, 28]). Many scholars have been inspired to examine both the quantitative and qualitative elements

of these equations due to their efficacy in simulating a wide range of real-world phenomena. Furthermore, FDEs with non-local conditions are a very interesting and pertinent field of study. The growing number of published works addressing the existence and uniqueness of solutions for this sort of equation is proof that scholars are becoming more and more interested in studying these equations. The vitality of research in this field is reflected in this trend. We can mention the following publications about the existence and uniqueness of solutions to fractional differential equations:

The existence and uniqueness of solutions to the following two Deformable FDEs were examined by the authors in [16]:

$$\begin{cases} {}^{\mathcal{D}\mathcal{D}}D^{\mathcal{T}}E(r) = \mathscr{F}(r, E(r)), \quad r \in [0, b] \\ E(0) + h(E) = E_0 \end{cases}$$

and

$$\begin{cases} {}^{\mathcal{D}\mathcal{D}}D^{T}E(r) = \mathscr{B}\big(E(r)\big) + \mathscr{F}\big(r, E[r]\big) + \int_0^r \mathcal{K}\big(r, s, E(r)\big)ds \, , r \in [0, b] \\ E(0) = E_0 \end{cases}$$

where the Deformable fractional derivative of order $0 < \tau < 1$ is represented by ${}^{\mathcal{D}\mathcal{D}}D^{T}$.

The subsequent fractional perturbed neutral integra-differential problem concerning the Deformable derivative

was examined by the authors of [24] to determine whether a solution exists and whether it is unique in a Banach space $\mathcal{X}$:

$$\begin{cases} {}^{\mathcal{D}\mathcal{D}}D^{T}E(r) - \mathscr{M}(r, E(\mu))) = \mathscr{L}(r, E(r), \int_0^r \mathcal{K}(r, Z, E(r))dz) + \mathscr{F}\left(r, E(r), \int_0^r \mathcal{K}\big(r, z, E(r)\big)dz\right) \\ E(0) = E_0 \in X \, , r \in [0, b] \, , 0 < T < 1 \end{cases}$$

where. $\mathscr{M}: [0, B] \times X \to X$ in sominanuly diffronsiable lunction, $\mathscr{L}, \mathscr{F}: [\beta, b] \times X \times X \to X$ be continuous functions, and $K \in (c(\mathcal{Z}, X)$ *where* $\mathcal{Z} = \{(r, z): 0 < z < r < b\}$.

Building on the aforementioned works, this paper examines the eiders and uniqueness of the elution to the GIVI-FIDE with a now-local condition :

$$\begin{cases} {}_{\rho}^{C}D_{0^+}^{\tau,\mathscr{R}}\big({}_{\rho}^{C}D_{0^+}^{\delta,\mathscr{R}}\mathscr{H}(\mu) - \mathscr{B}(\mu, \mathscr{H}(\mu), \mathcal{GH}(\mu)), \mathcal{UH}(\mu)\big) = \mathscr{F}(\mu, \mathscr{H}(\mu), \mathcal{GH}(\mu), \mathcal{UH}(\mu)), \\ (\mathscr{H}(\mu) - \mathscr{B}(\mu, \mathscr{H}(\mu), \mathcal{GH}(\mu), \mathcal{UH}(\mu)))_{\mu=0} = u_0, \\ \big(\mathscr{H}(\mu) - \mathscr{B}(\mu, \mathscr{H}(\mu), \mathcal{GH}(\mu), \mathcal{UH}(\mu))_{\mu=0}^{'} = 0, \\ (\mathscr{H}(\mu) - \mathscr{B}(\mu, \mathscr{H}(\mu), \mathcal{GH}(\mu), \mathcal{UH}(\mu)))_{\mu=b} + \varphi(\mathscr{H}) = u_1, \mu \in \chi = [0, b], \end{cases}$$

where $1 < \tau < 2, 0 < \delta < 1$, ${}_{\rho}^{C}D_{0^+}^{\tau,\mathscr{R}}(\cdot)$ is the generalized Caputo proportional FD of order $\tau, \mathscr{R}: \chi \to \mathbb{R}, \mathscr{B}, \mathscr{F}: \chi \times \mathcal{X} \times \mathcal{X} \longrightarrow \mathcal{X}$ are continuous functions, $\varphi \in C(\mathcal{X}, \mathcal{X})$, and $u_0, u_1 \in \mathcal{X}$, where $\mathcal{X}$ is a Banach space. The operators $\mathcal{GH}(\mu), \mathcal{UH}(\mu)$ be given by

$$\mathcal{GH}(\mu) := \int_0^{\mu} \Pi(\mu, s)\mathscr{H}(s)ds, \mathcal{UH}(\mu) = \int_0^{b} \Pi_1(\mu, s)\mathscr{H}(s)ds$$

such that $\Pi_1\Pi_1 \in C(\mathfrak{D}, x)$, where $\mathfrak{D} := \{(\mu, \mathrm{s}): 0 < s < \mu < b\}$. We consider

$$\mathcal{G}^* = \max_{\mu \in [0,b]} \int_0^{\mu} \|\Pi(\mu, s)\|ds, \mathcal{U}^* = \max_{\mu \in [0,b]} \int_0^{b} \|\Pi_1(\mu, s)\|ds$$

The following is a summary of this study's main contributions:

1. We use the FD instead of the classical derivative based on the previously described benefits and results of the fractional derivative.

2. To our know ledge, this is the first attempt to analyze the structure of the system introduced in (1) with a non-local condition.

3. We provide the integral solution to the specified system (1) (Lemma 2.5) utilizing the characteristics of the generalized Caputo fractional derivative type.

4. Banach and Kwasniewski's alternative FPTs are used to establish the main existence theorems. Additionally, section 4 presents an instructive instance to show how the major results might be used.

5. Furthermore, this work builds upon and improves upon earlier research that has been published in the literature, such as that which is cited in [6,21].

2. Preliminaries

This section presents the solution formula for the nonlinear GFCV-FIDE (1) as well as definitions and lemmas pertaining to the generalized Caputo proportional FD. The subsequent sections of this work will make consistent use of these definitions and lemmas.

• Let $\chi = [0, b]$ be a finite interval of R . We denote by $C(\chi, \mathcal{X})$ the Banach space of all continuous functions with the norm $\|\mathcal{H}\| = \sup\{|\mathcal{H}(\mu)|: \mu \in \chi\}$.

• In this study, we consider the function $\mathcal{R}: \chi \to \mathbb{R}$ to be increasing, strictly positive, and differentiable.

Definition 2.1. [14]. Let $0 < \rho < 1, \tau > 0$, and f be a continuous function. The left-sided generalized proportional fractional integral of order τ with respect to $\mathcal{R}$ of the function f is determined by

$$ {}_{\rho}I_{0^+}^{\tau,\mathcal{R}} f(\mu) = \frac{1}{\rho^{\tau}\Gamma(\tau)} \int_0^{\mu} e^{\frac{\rho-1}{\rho}(\mathcal{R}(\mu)-\mathcal{R}(s))} \mathcal{R}'(s)(\mathcal{R}(\mu) - \mathcal{R}(s))^{\tau-1} f(s) ds $$

where $\Gamma(\tau) = \int_0^{+\infty} e^{-t} t^{\tau-1} dt$ is the Euler gamma function.

Dufinition 2.2. Let $p \in [\Phi, \Psi], 4, W: |0,1| \times \mathbb{R} \to |0, \infty\rangle$ be cretinumse flunctions with $\lim_{p+0^+} \Phi(\beta, \mu) = 0$, $\lim_{p+1^-} \Phi(\beta, \mu) = 1$, $\lim_{p+0^+} \Psi(\beta, \mu) = 1$, $\lim_{p\to 1^-} \Psi(\beta, \mu) = 0$, and $\Phi(\beta, \mu) \neq 0, \rho \in (0,1), \Psi(\beta, \mu) \neq 0,\ p \in (0,1), a \in \mathbb{R}$. The properticrial detivalive of order ρ with respect to $\mathcal{R}$ of the function f is cheleminal by

$$ {}_{\rho}D^{\mathcal{R}} f(\mu) = \Psi(\rho, \mu) f(\mu) + \Phi(\rho, \mu) \frac{f'(\mu)}{\mathcal{R}'(\mu)} $$

In particular, if $\Phi(\rho, \mu) = \rho$ and $\Psi(\rho, \mu) = 1 - \rho$, then we have

$$ {}_{\rho}D^{\mathcal{Q}} f(\mu) = (1 - \rho) f(\mu) + \rho \frac{f'(\mu)}{\mathcal{A}'(\mu)} $$

Definition 2.3. [14]. Let $\rho \in (0,1]$. The left-sided generalized Caputo proportional fractional derivative of order $n - 1 < \tau < n$ for the continuous function f is defined by

$$
\begin{aligned}
{}_{\rho}^{C}D_{0^+}^{\tau,\mathcal{P}} f(\mu) &= \rho I_{0^+}^{n-\tau,\mathcal{Q}}\left({}_{\rho}D^{n,\mathcal{P}} f(\mu)\right) \\
&= \frac{1}{\rho^{n-\tau}\Gamma(n-\tau)} \int_0^{\mu} e^{\frac{\rho-1}{\rho}(\mathcal{P}(\mu)-\mathcal{R}(s))} \mathcal{R}'(s)(\mathcal{R}(\mu)-\mathcal{R}(s))^{n-\tau-1}\left({}_{\rho}D^{n,\mathcal{R}} f\right)(s)ds
\end{aligned}
$$

where $n = [\tau] + 1$ and ${}_{\rho}D^{n\mathcal{Q}} = \underbrace{\rho D^{\mathcal{Q}}\ {}_{\rho}D_{\rho}^{\mathcal{P}} \ldots D^{\mathcal{Q}}}_{n-\text{ times}}$;

For the sake of simplification, this manuscript posits

$$\Omega_{\underline{Z}}^{\tau-1}(\mu,0) = e^{\frac{\rho-1}{\rho}(\mathcal{R}(\mu)-g(0))}(\mathcal{R}(\mu)-g(0))^{\tau-1}.$$

Lemma 2.1. [13]. Let $\mu \in \chi, \rho \in (0,1], \tau, \delta > 0$, and f be a continuous function. Then, we have

$$\rho I_{0+}^{\tau,\mathcal{B}}\left({}_{\rho}I_{0+}^{\delta,\mathcal{R}} f(\mu)\right) = \rho I_{0+}^{\tau,\mathcal{R}}\left({}_{\rho}I_{0+}^{\delta,\mathcal{P}} f(\mu)\right) = \rho I_{0+}^{\tau+\delta,\mathcal{P}} f(\mu)$$

Lemma 2.2. [13]. Let $\rho \in (0,1]$ and $\tau, \delta > 0$. Then, we have

(i). $\left({}_{\rho}I_{0+}^{T,\mathcal{R}} e^{\frac{\rho-1}{\rho}(\mathcal{B}(t)-\mathcal{Q}(0))}(\mathcal{R}(t)-\mathcal{R}(0))^{\delta-1}\right)(\mu) = \frac{\Gamma(\delta)}{\rho^{\Gamma}\Gamma(\tau+\delta)}\Omega_{\mathcal{R}}^{\tau+\delta-1}(\mu,0).$

(ii). ${}_{\rho}^{C}D_{0^+}^{\tau,\mathcal{R}} e^{\frac{\rho-1}{\rho}(\mathcal{R}(t)-\mathcal{Q}(0))}(\mathcal{R}(t)-\mathcal{R}(0))^{\delta-1}\Big)(\mu) = \frac{\rho^{\sigma}\Gamma(\delta)}{\Gamma^{(\delta-\tau)}}\Omega_{\mathcal{R}}^{\delta-\tau-1}(\mu,0).$

Lemma 2.3. [13]. Let $\rho \in (0,1], \tau > 0$, and f be a continuous function. Then, we have

$$\lim_{\mu\to 0}\left(\rho I_{0+}^{\tau,\mathcal{P}} f(\mu)\right) = 0$$

Lemma 2.4. [15]. Let $\rho \in (0,1], n-1 < \tau < n, (n = [\tau]+1)$. Then, we have

$$\rho I_{0+}^{\tau,\mathcal{Q}}\left({}_{\rho}^{C}D_{0+}^{\tau,\mathcal{Q}} f(\mu)\right) = f(\mu) - \sum_{k=0}^{n-1} \frac{\left({}_{\rho}D^{k,\mathcal{P}} f\right)(0)}{\rho^{k}\Gamma(k+1)}\Omega_{\mathcal{B}}^{k}(\mu,0).$$

To simplify problem (1), we take the following problem and determine its solution formula:

$$
\begin{cases}
{}_{\rho}^{C}D_{0^+}^{\tau,\mathcal{R}}\left({}_{\rho}^{C}D_{0+}^{\delta,\mathcal{R}}(\mathcal{H}(\mu)-h(\mu))\right) = f(\mu), t \in \chi = [0,b] \\
(\mathcal{H}(\mu)-h(\mu))_{\mu=0} = u_0, (\mathcal{H}(\mu)-h(\mu))'_{\mu=0} = 0 \\
(\mathcal{H}(\mu)-h(\mu))_{\mu=b} + \varphi(\mathcal{H}) = u_1
\end{cases}
$$

where $0 < \tau < 1, 1 < \delta < 2$, ${}_{\rho}^{C}D_{0^+}^{\tau,\&}(\cdot)$ is the generalized Caputo proportional fractional derivative of order $\tau, h, f: \chi \longrightarrow \mathcal{X}$ be continuous functions, and $\varphi \in C(\mathcal{X},\mathcal{X})$.

Lemma 2.5. Let $h, f: \chi \longrightarrow \mathcal{X}$ be continuous functions. Hence, the system (3) has a solution provided by

$$
\begin{aligned}
\mathcal{H}(\mu) =& \frac{(\Delta-\varphi(\mathcal{H}))}{\Omega_{\mathcal{R}}^{\delta}(b,0)}\Omega_{\mathcal{R}}^{\delta}(\mu,0) + u_0 e^{\frac{\rho-1}{\rho}(\mathcal{R}(\mu)-\mathcal{R}(0))} + \frac{(1-\rho)u_0}{\rho}\Omega_{\mathcal{R}}^{1}(\mu,0) \\
&+ \frac{1}{\rho^{\delta+\tau}\Gamma(\delta+\tau)}\int_0^{\mu} \Omega_{\mathcal{R}}^{\delta+\tau-1}(\mu,s)\mathcal{R}'(s)f(s)ds + h(\mu), \mu \in [0,b]
\end{aligned}
$$

where $\Omega_{\mathcal{R}}^{(\cdot)}(\mu,.) and \Delta$ are given by (2) and (4), respectively.

Proof. Let $\mathcal{H}(\mu)$ be a solution of the problem (1). Applying the operator $\rho_{0^+}^{\tau,\mathcal{R}}(\cdot)$ to both sides of (3) and from Lemma 2.4, we get

$${}_{\rho}^{C}D_{0^+}^{\delta,\mathcal{R}}(\mathcal{H}(\mu)-h(\mu)) = \beta_1 e^{\frac{\rho-1}{\rho}(\mathcal{R}(\mu)-\mathcal{R}(0))} + {}_{\rho}I_{0^+}^{\tau,\mathcal{R}} f(\mu)$$

with $\beta_1 \in \mathbb{R}$. Next, Applying the operator ${}_{\rho}I_{0+}^{\delta,\mathscr{R}}(\cdot)$ to both sides of (5), we get

$$\mathscr{H}(\mu) - h(\mu) = \beta_1 {}_{\rho}I_{0+}^{\delta,\mathscr{R}}\Omega_{\mathscr{R}}^{0}(\mu,0) + \beta_2\Omega_{\mathscr{R}}^{0}(\mu,0) + \beta_3\frac{\Omega_{\mathscr{R}}^{1}(\mu,0)}{\rho} + \rho I_{0+}^{\tau+\delta,\mathscr{R}}f(\mu),$$

with $\beta_1, \beta_2, \beta_3 \in \mathbb{R}$. Using Lemma 2.2$(i)$, then the integral equation (6) becomes

$$\begin{aligned}\mathscr{H}(\mu) - h(\mu) = \beta_1\frac{e^{\frac{\rho-1}{\rho}(\mathscr{R}(\mu)-\mathscr{R}(0))}(\mathscr{R}(\mu)-\mathscr{R}(0))^{\delta}}{\rho^{\delta}\Gamma(\delta+1)} + \beta_2 e^{\frac{\rho-1}{\rho}(\mathscr{R}(\mu)-\mathscr{R}(0))}\\ +\beta_3\frac{e^{\frac{\rho-1}{\rho}(\mathscr{R}(\mu)-\mathscr{R}(0))}(\mathscr{R}(\mu)-\mathscr{R}(0))}{\rho}\\ +\frac{1}{\rho^{\delta+\tau}\Gamma(\delta+\tau)}\int_0^{\mu} e^{\frac{\rho-1}{\rho}(\mathscr{R}(\mu)-\mathscr{R}(s))}(\mathscr{R}(\mu)-\mathscr{R}(s))^{\delta+\tau-1}\mathscr{R}'(s)f(s)ds\end{aligned}$$

Putting $\mu = 0$ in the integral equation (7), we get $\beta_2 = (\mathscr{H}(\mu) - h(\mu))_{\mu=0} = u_0$. From the integral equation (7), with $\beta_2 = u_0$, we get

$$\begin{aligned}(\mathscr{H}(\mu) - h(\mu))' =& \frac{\beta_1}{\rho^{\delta}\Gamma(\delta+1)}\left(\frac{\mathscr{R}'(\mu)(\rho-1)}{\rho}\Omega_{\mathscr{R}}^{\delta}(\mu,0) + \delta'(\mu)\Omega_{\mathscr{R}}^{\delta-1}(\mu,0)\right)\\ &+\frac{u_0\mathscr{R}'(\mu)(\rho-1)}{\rho}e^{\frac{\rho-1}{\rho}(\mathscr{R}(\mu)-\mathscr{R}(0))}\\ &+\frac{\beta_3}{\rho}\left(\mathscr{R}'(\mu)e^{\frac{\rho-1}{\rho}(\mathscr{R}(\mu)-\mathscr{R}(0))} + \frac{\mathscr{R}'(\mu)(\rho-1)\Omega_{\mathscr{R}}^{1}(\rho,0)}{\rho}\right)\\ &+\frac{\mathscr{R}'(\mu)(\rho-1)}{\rho^{\delta+\tau+1}\Gamma(\delta+\tau)}\int_0^{\mu}\Omega_{\mathscr{R}}^{\delta+\tau-1}(\mu,s)\mathscr{R}'(s)f(s)ds\\ &+\frac{\mathscr{R}'(\mu)}{\rho^{\delta+\tau}\Gamma(\delta+\tau-1)}\int_0^{\mu}\Omega_{\mathscr{R}}^{\delta+\tau-2}(\mu,s)\mathscr{R}'(s)f(s)ds\end{aligned}$$

Taking $\mu = 0$ in the integral equation (8), we obtain $\beta_3 = u_0(1-\rho)$. Now, taking $\mu = b, \beta_2 = u_0$, and $\beta_3 = u_0(1-\rho)$ in the integral equation (7), we obtain

$$\begin{aligned}(\mathscr{H}(\mu) - h(\mu))_{\mu=b} =& \beta_1\frac{\Omega_{\mathscr{R}}^{\delta}(b,0)}{\rho^{\delta}\Gamma(\delta+1)} + u_0 e^{\frac{\rho-1}{\rho}(\mathscr{R}(b)-\mathscr{R}(0))}\\ &+u_0(1-\rho)\frac{\Omega_{\mathscr{R}}^{1}(b,0)}{\Omega} + \rho I_{0+}^{\delta+\tau,\mathscr{R}}f(b)\end{aligned}$$

Using the condition $(\mathscr{H}(\mu) - h(\mu)\mu{=}b + \varphi(\mathscr{H}) = u_1$, we obtain

$$\begin{aligned}\beta_1 &= \frac{\rho^{\delta}\Gamma(\delta+1)}{\Omega_{Z}^{\delta}(b,0)}\left(u_1 - \varphi(\mathscr{H}) - u_0 e^{\frac{\rho-1}{\rho}(\mathscr{P}(b)-\mathscr{H}(0))} - u_0(1-\rho)\frac{\Omega_{Z}^{1}(b,0)}{\rho} - \rho I_{0^+}^{\delta+\tau,\mathscr{R}}f(b)\right)\\ &= \frac{\rho^{\delta}\Gamma(\delta+1)}{\Omega_{\mathscr{R}}^{\delta}(b,0)}(\Delta - \varphi(\mathscr{H}))\end{aligned}$$

where

$$\Delta = u_1 - u_0\left(e^{\frac{\rho-1}{\rho}(\mathscr{R}(b)-\mathcal{Q}(0))} + (1-\rho)\frac{\Omega_{Z}^{1}(b,0)}{\rho}\right) - \rho I_{0^+}^{\delta+\tau,\mathcal{Q}}f(b)$$

Substituting β_1, β_2, and β_3 in (7) we have

$$\begin{aligned}\mathscr{H}(\mu) =& \frac{(\Delta - \varphi(\mathscr{H}))}{\Omega_{Z}^{\delta}(b,0)}\Omega_{Z}^{\delta}(\mu,0) + u_0 e^{\frac{\rho-1}{\rho}(\mathscr{P}(\mu)-\mathscr{P}(0))} + \frac{(1-\rho)u_0}{\rho}\Omega_{Z}^{1}(\mu,0)\\ &+\frac{1}{\rho^{\delta+\tau}\Gamma(\delta+\tau)}\int_0^{\mu}\Omega_{\mathcal{G}}^{\delta+\tau-1}(\mu,s)\mathscr{R}'(s)f(s)ds + h(\mu)\end{aligned}$$

The evidence is now complete.

We can now define the solution to the GCFV-FIDE (1) using the data from the preceding lemma.

Definition 2.4. If $\mathscr{H}$ solves the problem (1), then $\mathscr{H}$ also solves the integral equation that follows:

$$\mathscr{H}(\mu) = \frac{(\Delta - \varphi(\mathscr{H}))}{\Omega^{\delta}_{\mathscr{B}}(b,0)}\Omega^{\delta}_{\mathscr{B}}(\mu,0) + u_0 e^{\frac{\rho-1}{\rho}(\mathscr{R}(\mu)-\mathscr{E}(0))} + \frac{(1-\rho)u_0}{\rho}\Omega^{1}_{\mathcal{G}}(\mu,0) + \frac{1}{\rho^{\delta+\tau}\Gamma(\delta+\tau)} \times \int_0^{\mu} \Omega^{\delta+\tau-1}_{\mathcal{G}}(\mu,s)\mathscr{R}'(s)\mathscr{F}(s,\mathscr{H}(s),\mathcal{GH}(s),\mathcal{UH}(s))ds + \mathscr{H}(\mu,\mathscr{H}(\mu),\mathcal{GH}(\mu),\mathcal{UH}(\mu)),$$

as long as the integral mentioned above is finite.

3. Existence and uniqueness results

In this section, we present and study the existence of solutions for the given nonlinear GCFV-FIDE (1) under the Krasnoselskiis FPT.

Theorem 3.1. [5] Let $\mathcal{X}$ be a convex, closed, and nonempty subset of the Banach algebra $\mathcal{X}$. We consider the two operators $\mathcal{N}, \mathcal{S}: \mathcal{X} \to \mathcal{X}$ such that:

(a). $\mathcal{N}u + \mathcal{S}v \in \mathcal{X}, \forall u, v \in \mathcal{X}$.

(b). $\mathcal{N}$ is a contraction on $\mathcal{X}$.

(c). $\mathcal{Y}$is completely continuous on $\mathcal{X}$.

Then, the operator $\mathcal{P}u = \mathcal{N}u + \mathcal{Y}u$ has at least a fixed point in $\mathcal{X}$.

The following presumptions are necessary in order to apply the Krasnoselskiis FPT:

(A_1) The function $\mathscr{F}: \chi \times \mathcal{X}^3 \longrightarrow \mathcal{X}$ is continuous and there are constants $L_{\mathcal{Y}}, \hat{L}_{\mathcal{Y}}$, and $\bar{L}_{\mathcal{Y}}$ such that for all $v, w, z, v', w', z' \in \mathcal{X}$ and for all $\mu \in \chi$, we have

(i). $\|\mathscr{F}(\mu, v, w, z) - \mathscr{F}(\mu, v', w', z')\| \leq L_{\mathcal{S}}[\|v - v'\| + \|w - w'\| + \|z - z'\|]$.

(ii). $\|\mathscr{F}(\mu, v, w, z)\| \leq \hat{L}_{\mathcal{S}} + \bar{L}_{\mathcal{S}}[\|v\| + \|w\| + \|z\|]$.

(A_2) The function $\mathscr{B}: \chi \times \mathcal{X}^3 \longrightarrow \mathcal{X}$ is continuous and there are constants $M_{\mathcal{A}}, \hat{M}_{\mathscr{B}}$, and $\bar{M}_{\mathscr{B}}$ such that for all $v, w, v', w', z' \in \mathcal{X}$ and for all $\mu \in \chi$, we have

(i). $\|\mathscr{B}(\mu, v, w, z) - \mathscr{B}(\mu, v', w', z')\| \leq M_{\mathcal{SB}}[\|v - v'\| + \|w - w'\| + \|z - z'\|]$.

(ii). $\|\mathscr{B}(\mu, v, w, z)\| \leq \hat{M}_{\mathscr{B}} + \bar{M}_{\mathscr{B}}[\|v\| + \|w\| + \|z\|]$.

(A_3) The function $\bar{\varphi}: \mathcal{X} \longrightarrow \mathcal{X}$ is continuous and there are constants $K_{\varphi}, \hat{K}_{\varphi}$, and $\bar{K}_{\varphi}$ such that for all $v, w, z \in \mathcal{X}$ and for all $\mu \in \chi$, we have

(i). $\|\varphi(v) - \varphi(w)\| \leq K_{\varphi}\|v - w\|$.

(ii). $\|\varphi(v)\| \leq \hat{K}_{\varphi} + \bar{K}_{\varphi}\|v\|$.

Let the Banach space $\mathcal{Q} := (C(\chi, \mathcal{X}), \|\cdot\|)$. Then we consider the subset $\mathcal{S}$ of $\mathcal{Q}$ given by:

$$\mathcal{S} = \{\mathscr{H} \in \mathcal{Q}: \|\mathscr{H}\| \leq \Theta\}$$

with

$$\Theta > \frac{\hat{\Psi}}{1 - \Phi}, \text{ such that } 1 - \bar{\Psi} \neq 0$$

where

$$\hat{\Psi}' = \frac{(\mathscr{R}(b)-\mathscr{R}(0))^{\delta}}{\Omega^{\delta}_{\mathscr{B}}(b,0)}\left(\|\Delta\|+\hat{K}_{\varphi}\right)+\|u_0\|\left|1-\frac{1-\rho}{\rho}(\mathscr{R}(b)-\mathscr{R}(0))\right| + \frac{(\mathscr{R}(b)-\mathscr{R}(0))^{\delta+\tau}\hat{L}_{\mathcal{S}}}{\rho^{\delta+\tau}\Gamma(\delta+\tau+1)}+\hat{M}_{\mathscr{B}}$$

$$\bar{\Psi}' = \frac{(\mathscr{R}(b)-\mathscr{R}(0))^{\delta}\bar{K}_{\varphi}}{\Omega^{\delta}_{\mathscr{B}}(b,0)}+\frac{(\mathscr{R}(b)-\mathscr{R}(0))^{\delta+\tau}\bar{L}_{\mathcal{S}}(1+\mathcal{G}^*+\mathcal{Z}^*)}{\rho^{\delta+\tau}\Gamma(\delta+\tau+1)}+\bar{M}_{\mathcal{C}}(1+\mathcal{G}^*+\mathcal{C}^*)$$

An obvious subset of the Banach space $\mathcal{Q}$ is $\mathcal{S}$, which is convex, bounded, closed, and nonempty. We now possess all the arguments required to prove the existence results for the specified system (1). As a result, the following existence theorem is presented.

Theorem 3.2. Suppose that all assumptions $(A_1)-(A_3)$ hold and

$$\frac{(\mathscr{R}(b)-\mathscr{R}(0)))^{\delta}}{\Omega^{\delta}_{\mathscr{B}}(b,0)}K_{\varphi}<1$$

where $\Omega^{(\cdot)}_{\mathscr{B}}(.,0)$ is given by (2). Then, the system (1) has at least a solution $\mathscr{H}\in\mathcal{C}(\chi,\mathcal{X})$. Proof. To apply the Krasnoselskiis FPT, we define the operators $\mathcal{Y}:\mathcal{S}\longrightarrow\mathcal{X},\mathcal{W}:\mathcal{S}\longrightarrow\mathcal{X}$, and $\mathcal{P}:\mathcal{S}\longrightarrow\mathcal{X}$ as follows:

$$(\mathcal{V}\mathcal{H})(\mu)=\frac{(\Delta-\varphi(\mathscr{H}))}{\Omega^{\delta}_{\mathscr{B}}(b,0)}\Omega^{\delta}_{\mathscr{R}}(\mu,0)+u_0e^{\frac{\rho-1}{\rho}(\mathscr{B}(\mu)-\mathscr{B}(0))}+\frac{(1-\rho)u_0}{\rho}\Omega^{1}_{\mathscr{H}}(\mu,0)$$

$$(\mathscr{H}\mathscr{H})(\mu)=\frac{1}{\rho^{\delta+\tau}\Gamma(\delta+\tau)} \times\int_0^{\mu}\Omega^{\delta+\tau-1}_{\mathscr{R}}(\mu,s)\mathscr{R}'(s)\mathscr{F}(s,\mathscr{H}(s),\mathcal{G}\mathcal{H}(s),\mathcal{Z}\mathcal{H}(s))ds+\mathscr{B}(\mu,\mathscr{H}(\mu),\mathcal{G}\mathcal{H}(\mu),\mathcal{Z}\mathcal{H}(\mu))$$

$$(\mathcal{P}\mathcal{H})(\mu)=((\mathcal{V}+\mathscr{H})\mathscr{H})(\mu)$$

The proof is then provided in the subsequent steps: Step 1: Let $\mu\in[0,b]$ and $\mathscr{H},v\in\mathcal{S}$. By using the assumptions $(A_1)(ii),(A_2)(ii),(A_3)(ii)$, and the fact that

$$e^{\frac{p-1}{p}(\mathscr{B}(\mu)-\mathscr{B}(0))}<1,$$

we get

$$
\begin{aligned}
&\|\mathcal{V}(\mu)+\mathcal{W}v(\mu)\|\\
&=\|\frac{(\Delta-\varphi(\mathcal{H}))}{\Omega^{\delta}_{\mathcal{B}}(b,0)}\Omega^{\delta}_{\underline{Z}}(\mu,0)+u_0e^{\frac{\rho-1}{\rho}(\mathcal{B}(\mu)-\mathcal{B}(0))}+\frac{(1-\rho)u_0}{\rho}\Omega^{1}_{\underline{Z}}(\mu,0)\\
&+\frac{1}{\rho^{\delta+\tau}\Gamma(\delta+\tau)}\int_0^{\mu}\Omega^{\delta+\tau-1}_{\mathcal{A}}(\mu,s)\mathcal{R}'(s)\mathcal{F}(s,v(s),\mathcal{G}v(s),\mathcal{Z}v(s))ds+\mathcal{B}(\mu,v(\mu),\mathcal{G}v(\mu),\mathcal{Z}v(\mu))\|\\
&\leq\frac{(\mathcal{R}(b)-\mathcal{R}(0))^{\delta}}{\Omega^{\delta}_{\mathcal{B}}(b,0)}\left(\|\Delta\|+\hat{K}_{\varphi}+\bar{K}_{\varphi}\|\mathcal{H}\|\right)+\|u_0\|\left|1-\frac{1-\rho}{\rho}(\mathcal{R}(b)-\mathcal{B}(0))\right|\\
&+\frac{1}{\rho^{\delta+\tau}\Gamma(\delta+\tau)}\int_0^{\mu}(\mathcal{R}(\mu)-\mathcal{R}(s))^{\delta+\tau-1}\mathcal{R}'(s)\left(\hat{L}_{\mathcal{S}}+\bar{L}_{\mathcal{S}}[\|v\|+\|\mathcal{G}v\|+\|\mathcal{Z}v\|]\right)ds\\
&+\hat{M}_{\mathcal{SB}}+\bar{M}_{\mathcal{SB}}[\|v\|+\|\mathcal{G}v\|+\|\mathcal{Z}v\|]\\
&\leq\frac{(\mathcal{R}(b)-\mathcal{R}(0))^{\delta}}{\Omega^{\delta}_{\mathcal{B}}(b,0)}\left(\|\Delta\|+\hat{K}_{\varphi}+\bar{K}_{\varphi}\Theta\right)+\|u_0\|\left|1-\frac{1-\rho}{\rho}(\mathcal{R}(b)-\mathcal{R}(0))\right|\\
&+\frac{(\mathcal{R}(b)-\mathcal{R}(0))^{\delta+\tau}}{\rho^{\delta+\tau}\Gamma(\delta+\tau+1)}\left(\hat{L}_{\mathcal{S}}+\bar{L}_{\mathcal{S}}\Theta(1+\mathcal{G}^*+\mathcal{U}^*)\right)+\hat{M}_{\mathcal{B}}+\bar{M}_{\mathcal{S}}\Theta(1+\mathcal{G}^*+\mathcal{U}^*)\Bigg)\\
&\leq\frac{(\mathcal{R}(b)-\mathcal{R}(0))^{\delta}}{\Omega^{\delta}_{\mathcal{B}}(b,0)}\left(\|\Delta\|+\hat{K}_{\varphi}\right)+\|u_0\|\left|1-\frac{1-\rho}{\rho}(\mathcal{B}(b)-\mathcal{B}(0))\right|\\
&+\frac{(\mathcal{R}(b)-\mathcal{R}(0))^{\delta+\tau}\hat{L}_{\mathcal{S}}}{\rho^{\delta+\tau}\Gamma\left(\delta+\tau+\hat{M}_{\mathcal{S}}\right.}\\
&+\Theta\left[\frac{(\mathcal{R}(b)-\mathcal{R}(0))^{\delta}\bar{K}_{\varphi}}{\Omega^{\delta}_{\mathcal{B}}(b,0)}+\frac{(\mathcal{R}(b)-\mathcal{R}(0))^{\delta+\tau}\bar{L}_{y}(1+\mathcal{G}^*+\mathcal{U}^*)}{\rho^{\delta+\tau}\Gamma(\delta+\tau+1)}+\bar{M}_{\mathcal{B}}(1+\mathcal{G}^*+\mathcal{U}^*)\right]\\
&\leq\hat{\Psi}+\Theta\bar{\Psi}<\Theta.
\end{aligned}
$$

Therefore, $\mathcal{V}(\mathcal{H})+\mathcal{W}(v)\in\mathcal{S}$ for all $\mathcal{H},v\in\mathcal{S}$.

Step 2: We show that $\mathcal{V}$ is a contraction. Let $\mu\in[0,b]$ and $\mathcal{H},v\in\mathcal{S}$. By using the assumption $(A_3)(i)$,

and the fact that

$$e^{\frac{p-1}{p}(\mathcal{R}(\mu)-\mathcal{R}(0))}<1,$$

we get

$$\|\mathcal{V}\mathcal{H}(\mu)-\mathcal{V}v(\mu)\|=\frac{\Omega^{\delta}_{\mathcal{B}}(\mu,0)}{\Omega^{\delta}_{\mathcal{G}}(b,0)}\|\varphi(\mathcal{H})-\varphi(v)\|\leq\frac{(\mathcal{R}(b)-\mathcal{R}(0)))^{\delta}}{\Omega^{\delta}_{\mathcal{R}}(b,0)}K_{\varphi}\|\mathcal{H}-v\|.$$

From the condition (11), we can deduce that the operator $\mathcal{Y}$ is a contraction. Step 3: We show that the operator $\mathcal{W}$ is completely continuous. (i) $\mathcal{W}$ is continuous:

Let $\mu\in[0,b]$ and $\mathcal{H}_n$ be a sequence of $\mathcal{S}$ such that $\mathcal{H}_n\longrightarrow\mathcal{H}$ as $n\longrightarrow\infty$ in $\mathcal{S}$. Then, we get

$$
\begin{aligned}
&\|\mathcal{W}\mathcal{H}_n(\mu)-\mathcal{W}\mathcal{H}(\mu)\|\\
&\leq\frac{1}{\rho^{\delta+\tau}\Gamma(\delta+\tau)}\\
&\times\int_0^{\mu}\Omega^{\delta+\tau-1}_{\mathcal{Q}}(\mu,s)\mathcal{E}'(s)\|\mathcal{F}(s,\mathcal{H}_n(s),\mathcal{G}\mathcal{H}_n(s),\mathcal{U}\mathcal{H}_n(s))-\mathcal{F}(s,\mathcal{H}(s),\mathcal{G}\mathcal{H}(s),\mathcal{U}\mathcal{H}(s))\|ds\\
&+\|\mathcal{B}(\mu,\mathcal{H}_n(\mu),\mathcal{G}\mathcal{H}_n(\mu),\mathcal{U}\mathcal{H}_n(\mu))-\mathcal{B}(\mu,\mathcal{H}(\mu),\mathcal{G}\mathcal{H}(\mu),\mathcal{U}\mathcal{H}(\mu))\|
\end{aligned}
$$

The Lebesgue dominated convergence theorem and the continuity of the functions $\mathcal{F}$ and $\mathcal{B}$ allow us to obtain

$$\|\mathcal{W}\mathcal{H}_n(\mu)-\mathcal{W}\mathcal{H}(\mu)\|\longrightarrow 0,\text{ as }n\longrightarrow\infty.$$

This implies that the operator $\mathcal{W}$ is continuous.

(ii) $\mathcal{W}$ is uniformly bounded:

Let $\mu \in [0,b]$ and $\mathcal{H} \in \mathcal{S}$. Then, by using the assumptions $(A_1)(ii),(A_2)(ii)$, and the fact that

$$e^{\frac{P-1}{P}(\mathcal{R}(\mu)-\mathcal{P}(0))} < 1,$$

we get

$$\begin{aligned}
&\|\mathcal{W}\mathcal{H}(\mu)\| \\
&\leq \frac{1}{\rho^{\delta+\tau}\Gamma(\delta+\tau)} \\
&\times \int_0^{\mu} \Omega_{\mathcal{R}}^{\delta+\tau-1}(\mu,s)\mathcal{W}'(s)\|\mathcal{F}(s,\mathcal{H}(s),\mathcal{G}\mathcal{H}(s),\mathcal{Z}\mathcal{H}(s))\|ds + \|\mathcal{B}(\mu,\mathcal{H}(\mu),\mathcal{G}\mathcal{H}(\mu),\mathcal{Z}\mathcal{H}(\mu))\| \\
&\leq \frac{1}{\rho^{\delta+\tau}\Gamma(\delta+\tau)}\int_0^{\mu} (\mathcal{B}(\mu)-\mathcal{B}(s))^{\delta+\tau-1}\mathcal{B}'(s)\big(\hat{L}_y + \bar{L}_y[\|\mathcal{H}\| + \|\mathcal{G}\mathcal{H} + \|\mathcal{U}\mathcal{H}\|]\big)ds \\
&+\hat{M}_{\mathcal{C}} + \bar{M}_{\mathcal{C}}[\|\mathcal{H}\| + \|\mathcal{H}\| + \|\mathcal{Z}\mathcal{H}\|] \\
&\leq \frac{(\mathcal{R}(b)-\mathcal{R}(0))^{\delta+\tau}}{\rho^{\delta+\tau}\Gamma(\delta+\tau+1)}\Big(\hat{L}_y + \bar{L}_y\Theta(1+\mathcal{G}^*+\mathcal{Z}^*)\Big) + \hat{M}_{\mathcal{B}} + \bar{M}_{\mathcal{B}}\Theta(1+\mathcal{G}^*+\mathcal{Z}^*)
\end{aligned}$$

Then, the operator $\mathcal{W}$ is uniformly bounded.

(iii) $\mathcal{W}$ is equicontinuous:

Let $\mu_1,\mu_2 \in [0,b],(\mu_1<\mu_2)$, and $\mathcal{H} \in \mathcal{S}$, by using our assumptions, we get

$$\begin{aligned}
&\|(\mathcal{W}\mathcal{H})(\mu_2)-(\mathcal{W}\mathcal{H})(\mu_1)\| \\
&= \|\frac{1}{p^{\delta+\tau}\Gamma(\delta+\tau)} \\
&\times \int_0^{\mu_2} \Omega_{\mathcal{B}}^{\delta+1}(\mu_2,s)\mathcal{R}'(s)\mathcal{F}(s,\mathcal{H}(s),\mathcal{G}\mathcal{H}(s),\mathcal{U}\mathcal{H}(s))ds + \mathcal{B}\big(\mu_2,\mathcal{H}(\mu_2),\mathcal{G}\mathcal{H}(\mu_2),\mathcal{U}\mathcal{H}(\mu_2)\big) \\
&-\frac{1}{\rho^{\delta+\tau}(\delta+\tau)} \\
&\times \int_0^{\mu_1} \Omega_{\mathcal{B}}^{\delta+\tau-1}(\mu_1,s)\mathcal{H}'(s)\mathcal{F}(s,\mathcal{H}(s),\mathcal{G}\mathcal{H}(s),\mathcal{U}\mathcal{H}(s))ds - \mathcal{B}\big(\mu_1,\mathcal{H}(\mu_1),\mathcal{G}\mathcal{H}(\mu_1),\mathcal{Z}\mathcal{H}(\mu_1)\big)\| \\
&= \|\frac{1}{\rho^{\delta+\tau}\Gamma(\delta+\tau)} \\
&\times \int_{\mu_1}^{\mu_2} \Omega_{\mathcal{B}}^{\delta+\tau-1}(\mu_2,s)^{\mathcal{B}}(s)\mathcal{F}(s,\mathcal{H}(s),\mathcal{G}\mathcal{H}(s),\mathcal{U}\mathcal{H}(s))ds + \mathcal{B}\big(\mu_2,\mathcal{H}(\mu_2),\mathcal{G}\mathcal{H}(\mu_2),\mathcal{U}\mathcal{H}(\mu_2)\big) \\
&+\frac{1}{\rho^{\delta+\tau}\Gamma(\delta+\tau)}\int_0^{\mu_1}\Big(\Omega_{\mathcal{G}}^{\delta+\tau-1}(\mu_2,s)-\Omega_{\mathcal{B}}^{\delta+\tau-1}(\mu_1,s)\Big)\mathcal{H}'(s)\mathcal{F}(s,\mathcal{H}(s),\mathcal{G}\mathcal{H}(s),\mathcal{Z}\mathcal{H}(s))ds \\
&-\mathcal{B}^{\big(\mu_1,\mathcal{H}'(\mu_1),\mathcal{Z}\mathcal{H}'(\mu_1),\mathbb{Z}\cdot\mathcal{H}'(\mu_1)\big)|} \\
&\leq \frac{\Big(\hat{L}_{\mathcal{S}}+\bar{L}_{\mathcal{S}}\Theta(1+\mathcal{G}^*+\mathcal{U}^*)\Big)}{\rho^{\delta+\tau}\Gamma(\delta+\tau)}\|\int_{\mu_1}^{\mu_2}(\mathcal{R}(\mu_2)-\mathcal{R}(s))^{\delta+\tau-1}\mathcal{R}'(s)ds \\
&+\int_0^{\mu_1}\big((\mathcal{R}(\mu_2)-\mathcal{R}(s))^{\delta+\tau-1}-(\mathcal{R}(\mu_1)-\mathcal{R}(s))^{\delta+\tau-1}\big)\mathcal{R}'(s)ds\| \\
&+\big\|\mathcal{B}\big(\mu_2,\mathcal{H}(\mu_2),\mathcal{G}\mathcal{H}(\mu_2),\mathcal{U}\mathcal{H}(\mu_2)\big)-\mathcal{B}\big(\mu_1,\mathcal{H}(\mu_1),\mathcal{G}\mathcal{H}(\mu_1),\mathcal{U}\mathcal{H}(\mu_1)\big)\big\| \\
&\leq \frac{\Big(\hat{L}_y+\bar{L}_y\Theta(1+\mathcal{G}^*+\mathcal{U}^*)\Big)}{\rho^{\delta+\tau}\Gamma(\delta+\tau+1)}\big\|(\mathcal{R}(\mu_2)-\mathcal{R}(0))^{\delta+\tau}-(\mathcal{R}(\mu_1)-\mathcal{R}(0))^{\delta+\tau}\big\| \\
&+\big\|\mathcal{B}\big(\mu_2,\mathcal{H}(\mu_2),\mathcal{G}\mathcal{H}(\mu_2),\mathcal{Z}\mathcal{H}(\mu_2)\big)-\mathcal{B}\big(\mu_1,\mathcal{H}(\mu_1),\mathcal{G}\mathcal{H}(\mu_1),\mathcal{U}\mathcal{H}(\mu_1)\big)\big\|
\end{aligned}$$

By using the continuity of the functions $\mathscr{B},\mathscr{R},\mathscr{H}$, and by Lebesgue dominated convergence theorem, from the above inequality, we get $\|(\mathcal{W}\mathcal{H})(\mu_2)-(\mathcal{W}\mathcal{H})(\mu_1)\|\to 0$ as $\mu_1\to\mu_2$. Hence, the operator W is Equi continuous. From (ii) and (iii), and by the Arzela-Ascoli theorem, it follows that $\mathcal{W}(\mathcal{S})$ is relatively compact. Moreover, since $\mathcal{W}(\mathcal{S})$is continuous, it is completely continuous. From Theorem 3.1, the operator P has at least one fixed point in S. Therefore, the system (1) has at least one solution $H\in C(\chi,X)$.

We then go on to show that the solution to the system (1) is unique. This results in the subsequent theorem.

Theorem 3.3. Let assumptions $(A_1)-(A_3)$ hold. Then the system (1) has a unique solution $\mathscr{H}\in C(\chi,\mathcal{X})$ provided that

$$\Lambda=\frac{(\mathscr{R}(b)-\mathscr{R}(0))^{\delta}}{\Omega^{\delta}_{\mathscr{R}}(b,0)}K_{\varphi}+M_{\mathscr{B}}(1+\mathcal{G}^{*}+\mathcal{Z}^{*})+\frac{(\mathscr{R}(b)-\mathscr{R}(0))^{\delta+\tau}}{\rho^{\delta+\tau}\Gamma(\delta+\tau+1)}L_{\mathscr{F}}(1+\mathcal{G}^{*}+\mathcal{Z}^{*})<1$$

Proof. Suppose that (12) provides the operator 9. Using the same justifications as in Step 1, we have that $\mathcal{P}(\mathcal{S})\subset\mathcal{S}$, where $\mathcal{S}=\{\mathscr{H}\in\mathcal{Q}:\|\mathscr{H}\|\le\Theta\}$, and Θ satisfied (10). Let $\mu\in[0,b],\mathscr{H},v\in\mathcal{S}$, by using the assumptions $(A_1)(i),(A_2)(i)$, and $(A_3)(i)$, we have

$$\begin{aligned}
&\|\mathcal{P}\mathcal{H}(\mu)-\mathcal{P}_{v}(\mu)\|\\
&=\|\frac{\Omega^{\delta}_{\mathcal{Z}}(\mu,0)\varphi(\mathscr{H})}{\Omega^{\delta}_{\mathcal{Z}}(b,0)}+\frac{1}{\rho^{\delta+\tau}\Gamma(\delta+\tau)}\\
&\times\int_0^{\mu}\Omega^{\delta+\tau-1}_{\mathscr{H}}(\mu,s)\mathscr{H}'(s)\mathcal{F}(s,\mathscr{H}(s),\mathcal{G}\mathcal{H}(s),\mathcal{Z}\mathcal{H}(s))ds+\mathscr{H}(\mu,\mathscr{H}(\mu),\mathcal{G}\mathcal{H}(\mu),\mathcal{U}\mathcal{H}(\mu))\\
&-\frac{\Omega^{\delta}_{\mathcal{Z}}(\mu,0)\varphi(v)}{\Omega^{\delta}_{\mathcal{Z}}(b,0)}-\frac{1}{\rho^{\delta+\tau}\Gamma(\delta+\tau)}\\
&\times\int_0^{\mu}\Omega^{\delta+\tau-1}_{\mathscr{R}}(\mu,s)\mathcal{W}'(s)\mathcal{F}(s,v(s),\mathcal{G}v(s),\mathcal{Z}v(s))ds-\mathscr{B}(\mu,v(\mu),\mathcal{G}v(\mu),\mathcal{Z}v(\mu))\|\\
&\le\frac{(\mathscr{R}(b)-\mathscr{R}(0))^{\delta}}{\Omega^{\delta}_{\mathcal{Z}}(b,0)}\|\varphi(\mathscr{H})-\varphi(v)\|+\|\mathscr{B}(\mu,\mathscr{H}(\mu),\mathcal{G}\mathcal{H}(\mu),\mathcal{Z}\mathcal{H}(\mu))-\mathscr{B}(\mu,v(\mu),\mathcal{G}v(\mu),\mathcal{Z}v(\mu))\|\\
&+\frac{1}{\rho^{\delta+\tau}\Gamma(\delta+\tau)}\\
&\times\int_0^{\mu}(\mathscr{R}(\mu)-\mathscr{R}(s))^{\delta+\tau-1}\mathscr{B}'(s)\|\mathcal{F}(s,\mathscr{H}(s),\mathcal{G}\mathcal{H}(s),\mathcal{Z}\mathcal{H}(s))-\mathcal{F}(s,v(s),\mathcal{G}v(s),\mathcal{Z}v(s))\|ds\\
&\le\frac{(\mathscr{R}(b)-\mathscr{R}(0))^{\delta}K_{\varphi}}{\Omega^{\delta}_{\mathscr{R}}(b,0)}\|\mathscr{H}-v\|+M_{\mathcal{A}}\left[\|\mathscr{H}-v\|+\int_0^{s}\|\Pi(s,t)\|\|\mathscr{H}-v\|dt+\int_0^{T}\|\Pi_1(s,t)\|\|\mathscr{H}-v\|dt\right]\\
&+\frac{L_{s}}{\rho^{\delta+\tau}\Gamma(\delta+\tau)}\int_0^{\mu}(\mathscr{B}(\mu)-\mathscr{B}(s))^{\delta+\tau-1}\mathscr{R}'(s)\\
&\times\left[\|\mathscr{H}-v\|+\int_0^{s}\|\Pi(s,t)\|\|\mathscr{H}-v\|dt+\int_0^{T}\|\Pi_1(s,t)\|\|\mathscr{H}-v\|dt\right]ds\\
&\le\left(\frac{(\mathscr{R}(b)-\mathscr{R}(0))^{\delta}}{\Omega^{\delta}_{\mathcal{Z}}(b,0)}K_{\varphi}+M_{\mathcal{A}}(1+\mathcal{G}^{*}+\mathcal{Z}^{*})+\frac{(\mathscr{E}(b)-\mathscr{R}(0))^{\delta+\tau}}{\rho^{\delta+\tau}\Gamma(\delta+\tau+1)}L_{\mathcal{S}}(1+\mathcal{G}^{*}+\mathcal{Z}^{*})\right)\|\mathscr{H}-v\|\\
&=\Lambda\|\mathscr{H}-v\|.
\end{aligned}$$

In accordance with condition (14), $\mathcal{P}$ is a contraction. Because of this, $\mathcal{P}$ has a unique fixed point $\mathscr{H}\in C(\chi,\mathcal{X})$, which is the only solution to the system (1) in $C(\chi,\mathcal{X})$.

4. Applications

A real-world example is presented in this section to demonstrate how our key findings can be used.

Example 1. We examine the subsequent nonlinear GCFV-FIDE:

$$\begin{cases} {}_{\frac{1}{2}}^{C}D_{0^+}^{\frac{3}{2},\mu}\left({}_{\frac{1}{2}}^{C}D_{0^+}^{\frac{1}{2},\mu}\left(\mathcal{H}(\mu)-\frac{\mu^2}{8}\left(1+\frac{|\mathcal{H}^e(\mu)|}{2\left(1+\left|\mathcal{H}^2(\mu)\right|\right)}\right)+\frac{1}{(\mu+4)^2}\mathcal{GH}(\mu)+\frac{1}{2(e^\mu+2)^3}\mathcal{UH}(\mu)\right)\right) \\ =\frac{\mu^2}{2}\left(e^\mu+\frac{\chi}{16(\mu^2+2)}\frac{|\mathcal{H}^e(\mu)|}{(1+|\mathcal{H}(\mu)|)}\right)+\frac{\chi}{64}\mathcal{GH}(\mu)+\frac{\mu^2}{2}\frac{\chi}{32}\mathcal{UH}(\mu), \mu\in\chi=[0,1] \\ \left(\mathcal{H}(\mu)-\frac{\mu^2}{8}\left(1+\frac{|\mathcal{H}(\mu)|}{2\left(1+\left|\mathcal{H}^2(\mu)\right|\right)}\right)+\frac{1}{(\mu+4)^2}\mathcal{GH}(\mu)+\frac{1}{2(e^\mu+2)^3}\mathcal{UH}(\mu)\right)_{\mu=0}=u_0\in\mathbb{R} \\ \left(\mathcal{H}(\mu)-\frac{\mu^2}{8}\left(1+\frac{|\mathcal{H}(\mu)|}{2\left(1+\left|\mathcal{H}^2(\mu)\right|\right)}\right)+\frac{1}{(\mu+4)^2}\mathcal{GH}(\mu)+\frac{1}{2(e^\mu+2)^3}\mathcal{UH}(\mu)\right)_{\mu=0}=0 \\ \left(\mathcal{H}(\mu)-\frac{\mu^2}{8}\left(1+\frac{|\mathcal{H}(\mu)|}{2(1+|\mathcal{H}(\mu)|)}\right)+\frac{1}{(\mu+4)^2}\mathcal{GH}(\mu)+\frac{1}{2(e^\mu+2)^3}\mathcal{UH}(\mu)\right)_{\mu=1}+\frac{\left|\mathcal{H}^2\left(\frac{1}{2}\right)\right|}{9\left(1+\left|\mathcal{H}\left(\frac{1}{2}\right)\right|\right)}+\frac{3}{17}=u_1\in\mathbb{R}, \end{cases}$$

where $\tau=\frac{3}{2},\rho=\delta=\frac{1}{2},\mathcal{R}(\mu)=\mu,$

$$\mathcal{F}(\mu,\mathcal{H}(\mu),\mathcal{GH}(\mu),\mathcal{ZH}(\mu))=\frac{\mu^2}{2}\left(e^\mu+\frac{\chi}{16(\mu^2+2)}\frac{|\mathcal{H}(\mu)|}{(1+|\mathcal{H}(\mu)|)}\right)+\frac{\chi}{64}\mathcal{GH}(\mu)+\frac{\mu^2}{2}\frac{\chi}{32}\mathcal{ZH}(\mu),$$

$$\mathcal{B}(\mu,\mathcal{H}(\mu),\mathcal{GH}(\mu),\mathcal{ZH}(\mu))=\frac{\mu^2}{8}\left(1+\frac{|\mathcal{H}(\mu)|}{2(1+|\mathcal{H}(\mu)|)}\right)+\frac{1}{(\mu+4)^2}\mathcal{GH}(\mu)+\frac{1}{2(e^\mu+2)^3}\mathcal{ZH}(\mu),$$

$$\varphi(\mathcal{H})=\frac{\left|\mathcal{H}\left(\frac{1}{2}\right)\right|}{9\left(1+\left|\mathcal{H}\left(\frac{1}{2}\right)\right|\right)}+\frac{3}{17},$$

and

$$\mathcal{GH}(\mu)=\int_0^\mu \mu^2 e^s|\mathcal{H}(s)|ds$$

$$\mathcal{UH}(\mu)=\int_0^1 \frac{s}{\mu^2+3}|\mathcal{H}(s)|ds$$

$$\mathcal{G}^*=\max_{\mu\in[0,1]}\int_0^\mu \mu^2 e^s ds=e-1\approx 1.718$$

$$\mathcal{U}^*=\max_{\mu\in[0,1]}\int_0^1 \frac{s}{\mu^2+3}ds=\frac{e^2-1}{6}\approx 1.065.$$

Let's first verify the hypotheses $(A_1),(A_2)$, and $(A_3).\forall\mu\in[0,1]$ and $v,w,m\in\mathbb{R}$, we get

$$\begin{aligned} &\|\mathcal{F}(\mu,v,\mathcal{G}v,\mathcal{Z}v)-\mathcal{F}(\mu,w,\mathcal{G}w,\mathcal{Z}w)\| \\ &\leq\frac{\mu^2}{2}\frac{\chi}{16(\mu^2+2)}\frac{\|v-w\|}{(1+\|v\|)(1+\|w\|)}+\frac{\chi}{64}\|\mathcal{G}v-\mathcal{G}w\|+\frac{\mu^2}{2}\frac{\chi}{32}\|\mathcal{Z}v-\mathcal{Z}w\| \\ &\leq\frac{\chi}{64}[\|v-w\|+\|\mathcal{G}v-\mathcal{G}w\|]. \end{aligned}$$

$$\begin{aligned} \|\mathcal{F}(\mu,v,\mathcal{G}v,\mathcal{Z}v)\|&=\left\|\frac{\mu^2}{2}\left(e^\mu+\frac{\chi}{16(\mu^2+2)}\frac{|v|}{(1+|v|)}\right)+\frac{\chi}{64}\mathcal{G}v+\frac{\mu^2}{2}\frac{\chi}{32}\mathcal{Z}v\right\| \\ &\leq\frac{e}{2}+\frac{\chi}{64}[\|v\|+\|\mathcal{G}v\|+\|\mathcal{Z}v\|]. \end{aligned}$$

Hence, hypotheses (A_1) holds with $L_{\mathcal{F}}=\bar{L}_{\mathcal{F}}=\frac{\chi}{64}$ and $\hat{L}_{\mathcal{F}}=\frac{e}{2}$. We get

$$\|\mathscr{B}(\mu,v,\mathcal{G}v,\mathcal{Z}v)-\mathscr{B}(\mu,w,\mathcal{G}w,\mathcal{Z}w)\|$$
$$\leq \frac{\mu^2}{16}\frac{\|v-w\|}{(1+\|v\|)(1+\|w\|)}+\frac{1}{(\mu+4)^{2)}}\|\mathcal{G}v-\mathcal{G}w\|+\frac{1}{2(e^{\mu}+2)^3}\|\mathcal{Z}v-\mathcal{Z}w\|$$
$$\leq \frac{1}{16}[\|v-w\|+\|\mathcal{G}v-\mathcal{G}w\|+\|\mathcal{Z}v-\mathcal{Z}w\|].$$
$$\|\mathscr{B}(\mu,v,\mathcal{G}v)\|=\left\|\frac{\mu^2}{8}\left(1+\frac{|v|}{2(1+|v|)}\right)+\frac{1}{(\mu+4)^2}\mathcal{G}v+\frac{1}{2(e^{\mu}+2)^3}\mathcal{Z}v\right\|$$
$$\leq \frac{1}{8}+\frac{1}{16}[\|v\|+\|\mathcal{G}v\|+\|\mathcal{Z}v\|].$$

Then, hypotheses (A_2) holds with $M_{\mathscr{B}}=\bar{M}_{\mathscr{B}}=\frac{1}{16}$ and $\hat{M}_{\mathscr{B}}=\frac{1}{8}$. We get

$$\|\varphi(v)-\varphi(w)\|\leq\frac{1}{9}\frac{\|v-w\|}{(1+\|v\|)(1+\|w\|)}\leq\frac{1}{9}\|v-w\|$$
$$\|\varphi(v)\|=\left\|\frac{|v|}{9(1+|v|)}+\frac{3}{17}\right\|\leq\frac{3}{17}+\frac{1}{9}\|v\|$$

Then, hypotheses (A_3) holds with $K_{\varphi}=\bar{K}_{\varphi}=\frac{1}{9}$ and $\hat{K}_{\varphi}=\frac{3}{17}$. Condition (11) also holds:

$$\frac{(\mathscr{R}(1)-\mathscr{R}(0)))^{\delta}}{\Omega^{\delta}_{\mathscr{R}}(1,0)}K_{\varphi}=\frac{1}{e^{-1}}\frac{1}{9}\approx 0.302<1$$

There is at least one solution to the nonlinear system (15) with $\mathscr{H}\in C(\chi,\mathbb{R})$. The following is the uniqueness of the solution to the nonlinear system (15) based on condition (14):

$$\Lambda=\frac{(\mathscr{R}(1)-\mathscr{R}(0))^{\delta}}{\Omega^{\delta}_{\mathcal{G}}(1,0)}K_{\varphi}+M_{\mathcal{G}}(1+\mathcal{G}^*+\mathcal{Z}^*)+\frac{(\mathscr{R}(1)-\mathscr{R}(0))^{\delta+\tau}}{\rho^{\delta+\tau}\Gamma(\delta+\tau+1)}L_{\mathcal{Y}}(1+\mathcal{G}^*+\mathcal{Z}^*)$$
$$=\frac{1}{e^{-1}}\frac{1}{9}+\frac{3.783}{16}+\frac{1}{\frac{1}{4}\Gamma(3)}\frac{\chi}{64}3.783\approx 0.90987<1$$

This implies that the nonlinear system (15) has one solution with $\mathscr{H}\in C(\chi,\mathbb{R})$.

5. Conclusions and Recommendations

The existence and uniqueness of solutions for a class of nonlinear fractional Volterra–Fredholm integro differential systems subject to non-local conditions using the generalized Caputo proportional fractional derivative were examined in this work. The use of Krasnoselskii's fixed-point theorem proved the existence of solutions, and Banach's contraction principle guaranteed the uniqueness of the solution under proper circumstances. The theoretical analysis was conducted inside a suitable functional framework.

By adding generalized fractional derivatives and non-local boundary conditions to the Volterra–Fredholm framework, the obtained results go beyond a number of previous research in the literature. Illustrative examples were provided to support the theoretical conclusions and show how the generated results were useful and applicable.

6.Suggestions

Several suggestions can be made in light of the study's findings:

1. Researchers are urged to adapt the theoretical framework that has been presented to more complicated nonlinear fractional systems that occur in practical applications, especially in population dynamics, control theory, and viscoelasticity.

2. To estimate solutions of nonlinear fractional Volterra–Fredholm systems, it is advised to look into numerical approaches that are compatible with the generalized Caputo proportional fractional derivative.

3. To increase the applicability of the given results, additional analytical research can take into account loosening some of the restrictive assumptions on nonlinear terms or kernel functions.

7. Future Works

The current study may be extended in a number of ways in future research lines. Studying stability characteristics for nonlinear fractional Volterra–Fredholm systems with generalized fractional operators, such as Ulam–Hyers stability, Mittag–Leffler stability, or asymptotic stability, is one potential avenue. Lastly, other kinds of fractional integro differential equations, such as impulsive systems, coupled systems, and systems with time-dependent kernels, which are still difficult and open problems in the field of fractional calculus, can be solved using the theoretical framework created in this study.

References:

E.Y. Salah, B. Sontakke, A.A. Hamoud, H. Emadifar, A. Kumar, A fractal–fractional order modeling

approach to understanding stem cell-chemotherapy combinations for cancer, Scientific Reports15 (1), 3465 (2025).

A.A. Sharif, A.A. Hamoud, M. M. Hamood and K.P. Ghadle, On New Uniqueness Results for Riemann-Liouville Fractional Volterra-Fredholm Integro-Differential Equations with Deviating Arguments, DCDIS: Dynamics of Continuous, Discrete and Impulsive Systems, 2025, 25-40.

S.M. Atshan, A.A. Hamoud, Eexistence results for boundary value problems of Volterra-Fredholm systems involving Caputo derivatives, Nonlinear Functional Analysis and Applications, 2024, 545-558.

A. Atangana, D. Baleanu, New fractional derivative with non-local and non-singular kernel, Therm. Sci. 20 (2016) 757.

T.A. Burton, Fixed-point theorem of Krasnoselskii, Appl. Math. Lett. 11 (1998) 85-88.

M. Bohner, S. Hristova, Stability for generalized Caputo proportional fractional delay integrodifferentialequations, Bound. Value Probl. 2022 (2022) 14.

M. Caputo, M. Fabrizio, A new definition of fractional derivative without singular kernel, Prog.Fract. Differ. Appl. 1 (2015) 73–85.

S.A. David, J.L. Linares, E.M.D.J.A. Pallone, Fractional order calculus: historical apologia, basicconcepts and some applications, Rev. Bras. Ensino Fis. 33 (2011) 4302–4302.

R. Gorenflo, F. Mainardi, Fractional Calculus: Integral and Differential Equations of Fractional Order, Springer Vienna, 1997

K. Hilal, A. Kajouni, S. Zerbib, Hybrid fractional differential equation with nonlocal and impulsive conditions, Filomat 37 (2023) 3291–3303.

F. Jarad, T. Abdeljawad, D. Baleanu, On the generalized fractional derivatives and their Caputo modification J. Nonlinear Sci. Appl. 10 (2017) 2607–2619.

F. Jarad, T. Abdeljawad, Z. Hammouch, On a class of ordinary differential equations in the frame of Atangana-Baleanu fractional derivative, Chaos Solit. Fractals 117 (2018) 16–20.

F. Jarad, T. Abdeljawad, S. Rashid, Z. Hammouch, More properties of the proportional fractional integrals and derivatives of a function with respect to another function, Adv. Differ. Equ. 2020 (220) 303.

F. Jarad, M.A. Alqudah, T. Abdeljawad, On more general forms of proportional fractional operators,Open Math. 18 (2020) 167–176.

I. Mallah, I. Ahmed, A. Akgul, F. Jarad, S. Alha, On ψ-Hilfer generalized proportional fractional operators, AIMS Math. 7 (2021) 82–103.

M. Mebrat, G.M.N. Guerekata, A Cauchy problem for some fractional differential equation via deformable derivatives J. Nonlinear Evol. Equ. Appl. 4 (2020) 55–63.

U.N. Katugampola, New approach to generalized fractional integral, Appl. Math. Comput. 218 (2011) 860-865.

U.N. Katugampola, A new approach to generalized fractional derivatives, Bull. Math. Anal. Appl. 6 (2014) 1–15.

I. Podlubny, Matrix approach to discrete fractional calculus, Fract. Calc. Appl. Anal. 3 (2000) 359–386.

K. Shah, M.A. Alqudah, F. Jarad, T. Abdeljawad, Semi-analytical study of pine wilt disease model with convex rate under Caputo-Fabrizio fractional order derivative,Chaos Solit. Fractals 135 (2020) 109754.

A. Rahmani, W.S. Du, M.T. Khalladi, M. Kostic, D. Velinov, Proportional Caputo Fractional Differential Inclusions in Banach Spaces, Symmetry 14 (2022) 1941.

S.Z. Rida, A.M.A. El-Sayed, A.A.M. Arafa, Effect of bacterial memory dependent growth by using fractional derivatives reaction-diffusion chemotactic model, J. Stat. Phys. 140 (2010) 797–811.

H.G. Sun, W. Chen, H. Wei, Y.Q. Chen, A comparative study of constant-order and variableorder fractional models in characterizing memory property of systems, Eur. Phys. J. Spec. Top.193 (2011) 185–192.

R. Sreedharan, S.R. Balachandar, R. Udhayakumar, S. Etemad, I. Avc, S. Rezapour, On the fractional perturbed neutral integro-differential systems via deformable derivatives: an existence study, Bound. Value Probl. 2024 (2024) 74.

M. Yavuz, N. Ozdemir, Comparing the new fractional derivative operators involving exponential and Mittag-Leffler kernel, Discrete Contin. Dyn. Syst. 13 (2020) 995–1006.

M. Yavuz, N. Ozdemir, European vanilla option pricing model of fractional order without singular kernel, Fractal Fract. 2 (2018) 3.

S. Zerbib, N. Chefnaj, K. Hilal, A. Kajouni, Study of p-Laplacian hybrid fractional differential equations involving the generalized Caputo proportional fractional derivative, Comput. Methods. Differ Equ., 2024, https://doi.org/10.22034/cmde.2024.61552.2665.

S. Zerbib, K. Hilal, A. Kajouni, Some new existence results on the hybrid fractional differential equation with variable order derivative, Results Nonlinear Anal. 6 (2023) 34–48.

Physiological Mechanisms and Predictive Models Based on Biomarkers for Early Risk Stratification in Diabetic Kidney Disease

Eman H. Al-Fadhili [1]

Nada H.A. AL-Badri [2]

Abstract:

Diabetic Nephropathy is one of the most dangerous chronic complications of diabetes mellitus, which is a progressive weakening of the structure and functioning of the kidneys, the end result of which is end-stage renal failure. Although significant achievements have been made in the management of diabetes, the renal burden of the disease is ever-increasing around the world, thus the necessity to design better approaches to the diagnosis and prognosis of this disease. This paper aims to investigate the biology of Diabetic kidney disease (DKD) alongside the interaction of glycemic dysregulation, lipid abnormalities, inflammatory pathways, and oxidative stress. Particular attention is given to new biomarkers, such as new protein markers and omics-based signatures, which show significant potential of meaningfulness in predicting disease progression and disease course.This work will combine both proven and new diagnostic methods to help with the proper risk stratification, inform individualized clinical decisions, and eventually facilitate the earlier therapeutic intervention to slow down the catastrophic development of diabetic nephropathy in the affected patients.

Keywords: *Customized Medicine, Pathophysiology, Risk Assessment, Diabetic Nephropathy, Diabetes Mellitus, Kidney Failure*.

http://dx.doi.org/10.47832/Dub.Conf3-6

[1] Researcher. College of Science, Wasit University, Iraq emanhamzabio@gmail.com

[2] Researcher. College of Science, Wasit University, Iraq nada@uowasit.edu.iq

1. Introduction

The Diabetic kidney disease (DKD) is one of most disastrous microvascular complications of Diabetic mellitus that has overtaken the most world prevalent conditions in the form of end-stage renal disease and close to 40 percent of diabetes population has this condition currently (Alicic *et al.,* 2017). The DKD burden is growing exponentially worldwide, epidemiological reports show a 33 % rise in the prevalence of chronic kidney disease between 1990 and 2017, with diabetic nephropathy contributing a big share of this rise (Saeedi *et al.,* 2019). This is especially the case in developing countries where the rate of diabetes is increasing at an unprecedented rate because people are moving into urban areas, changing their lifestyles and aging (Cho *et al.,* 2018). The issue of high-quality management of this pathology requires not only an adequate diagnosis of potential cases but also the ability to determine the trajectory of the course of the disease in a particular person, which will allow timely introducing nephron-protective measures and increasing the quality of long-term patient outcomes by many times (Tuttle *et al.,* 2014).

Biomarkers The main biomarkers that are utilized currently in clinical practice are considered to be traditional, such as serum creatinine and estimated glomerular filtration rate (eGFR) and albuminuria, which are used to assess and monitor DKD. These primary indicators exhibit a significant weakness in the early signs of kidney damage and inaccuracy in forecasting the disease course trajectories (Coca *et al.,* 2012). The application of newer biomarkers has a great potential in terms of earlier diagnosis and risk stratification, which appear to provide a good source of better clinical decision-making and potential patient outcome improvement (Satirapoj & Adler, 2014).

1.1 Pathophysiological Mechanisms of Diabetic kidney disease:

Pathogenesis and evolution of DKD includes interplays of several pathophysiological pathways; metabolic disturbances, hemodynamics, inflammatory, and oxidant stress exist (Sagoo & Gnudi, 2020). An initial feature of Diabetes mellitus, hyperglycemia triggers a series of molecular processes that eventually lead to structural and functional kidney architecture degradation Preservation of renal architecture depends mainly on the ability to prevent hyperglycemia but also in homeostasis and renal remodeling processes through renal straitening (Reidy *et al.,* 2014), reduction of blood pressure, prevention of micro-albuminuria and maintenance of cellular structure and tissue repair processes Pathogenesis includes complex crosstalk between glomerular endothelial cells, podocytes, mesangial cell, and tubular epithelial cells, all of which play the part in the progressive nature of kidney damage (Najafian *et al.,* 2011).

1.2 Induced Renal Damage Hyperglycemia*:*

Hyperglycemia is the major contributor of DKD pathogenesis by various interrelated mechanisms. High glucose levels induce a number of adverse mechanisms, such as the polyol pathway, advanced glycation end-product (AGE) formation, activation of protein kinase C, and flux through the hexosamine pathway (Forbes & Cooper, 2013). AGE accumulation, in

response to methylglyoxal and other reactive carbonyl species, is important in early-onset diabetic nephropathy development (Rabbani & Thornalley, 2018). The result is glomerulosclerosis and tubulointerstitial fibrosis through oxidative stress, stimulated inflammatory responses and induced structural changes in glomerular and tubular functions (Yamazaki et al., 2021).

1.3 Vascular Changes, Hemodynamic Changes:

In addition to metabolic alterations, DKD has been typified by severe hemodynamic aberrations and vascular changes that lead to a progressive renal dysfunction (Vallon & Thomson, 2020). This trait is usually characterized by glomerular hyperfiltration, which is a compensative process that arises in response to low renal perfusion and loss of nephrons, and is usually the defining characteristic of the early phases of DKD. Although this adaptive hyperfiltration response seems to maintain normal kidney function initially, the development of albuminuria and progressive nephron loss in the long run occur due to causing elevated intraglomerular pressure and shear stress enhancement (Ruggenenti *et al.,* 2010).

1.4 Disorders of Oxidative Stress and Inflammatory Cascades:

DKD pathogenesis is directly associated with oxidative stress and chronic inflammatory mechanism further causing kidney damage (Jha *et al.,* 2016). Endothelial dysfunction as a result of hyperglycemia produces reactive oxygen species that trigger inflammatory cascades and attract immune cells and further activate pro-inflammatory cytokines such as tumor necrosis factor-alpha, interleukin-1beta, and transforming growth factor-beta (Wada & Makino, 2013). The continuous occurrence of such inflammatory mediators along with the buildup of AGEs, enhances subsequent damage of the renal parenchymal tissues, and these include glomeruli the tubules and the interstitium (Tesch, 2008)..

1.5 New Biomarkers in the Early Risk Stratification:

Suboptimal assessment of the current diagnostics markers has spurred the case of novel ones that could lead to better early DKD detection and risk stratification (Pena *et al.,* 2015). The new biomarkers offer greater potential to clinicians in identifying structural and functional changes in the kidney at early stages of the disease so that therapeutic measures can be undertaken in time with precision. The growing capacities of proteomics, metabolomics, and genomics have yielded many promising candidates, such as kidney injury molecule-1 (KIM-1),neutrophil gelatinase-associated lipocalin (NGAL), and a variety of inflammatory markers that reflect different pathophysiologic processes (Ma *et al.,* 2025).

Comprehension of complicated pathophysiological processes and incorporation of new biomarker methodologies translate into a paradigm shift toward precision medicine in the DKD management field, with significant potential to transform clinical practice by means of personalized risk identification and individualized treatment strategies (Yamanouchi *et al.,* 2017).

2. Methods

2.1 Design and set up of the research:

It is a cross-sectional comparative study carried out in the Al-Kut Educational Hospital and Al-Karama Teaching Hospital in the Wasit Province, Iraq, during six months (July 2021 to December 2021). The research question was to examine physiological mechanisms and biomarker-based predictive models of early risk stratification in diabetic kidney disease patients compared to healthy people. This protocol research had been reviewed by the Institutional Review Board and had been carried out in line with Declaration of Helsinki. Each participant also signed written informed consent before the enrollment.

2.2 Study and recruitment population:

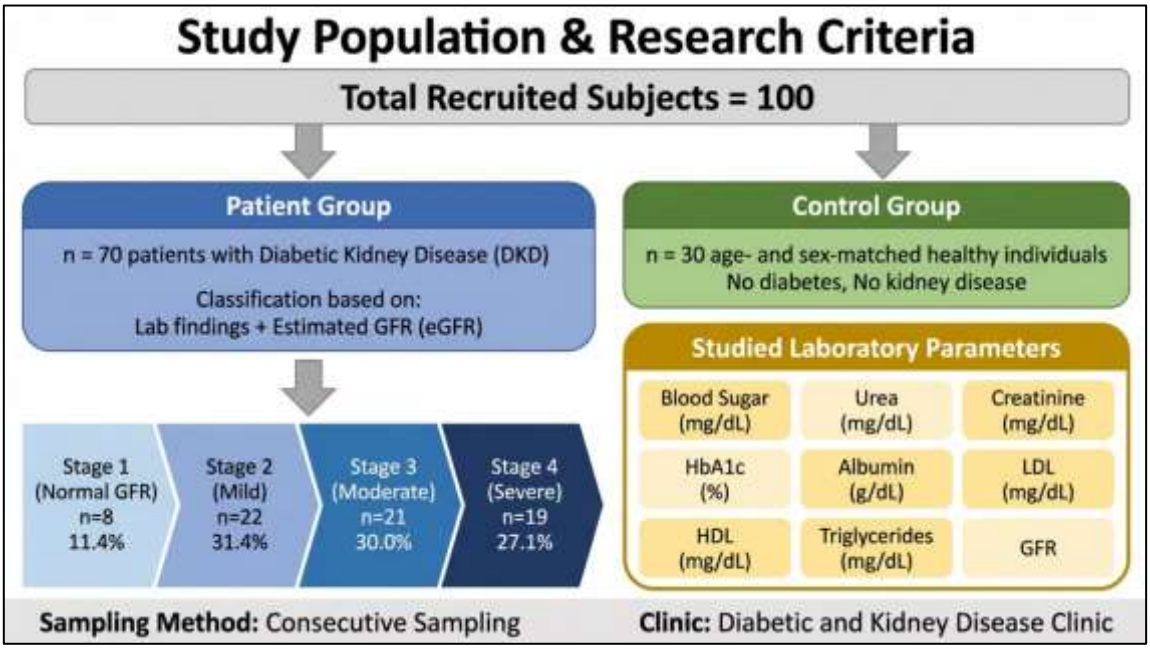

2.3 Rules of Eligibility:

Case group inclusion criteria: Adults with type 2 *Diabetes mellitus* (more than 5 years duration) and reduced glomerular filtration rate (eGFR < 90 mL/min)>2 years of age or micro-albuminuria (more than 30 mg/g albumin) 40 to 70 years old. Inclusion criteria of the control group: Normal renal and antihypertensive medication, normal renal; healthy adults free of diabetes, hypertension, or chronic disease. Both groups had exclusion criteria which include: acute or non-diabetic kidney damage, autoimmune diseases, cancer, taking nephrotoxic drugs and being pregnant or nursing.

2.4 Laboratory and Collection of Data:

The medical data that was collected clinically consisted of demographic data, a medical history, and standardized methods of collecting anthropometric data. A thorough laboratory assessment was accomplished in all participants following the correct initial fasting. Collection of blood and urine samples: From our participants, five milliliters of their venous blood were collected. Albuminuria and creatinine clearance were quantified by the taking of

10 mL midstream urine samples. All the samples were processed by freezing in -20° C and stored until analysis.

As traditional biomarkers, the laboratory measures showed serum glucose, HbA1c, serum creatinine, blood urea nitrogen, estimated glomerular filtration rate (calculated by commonly used equations), lipid profile (total cholesterol, LDL, HDL, triglycerides), and urinary albumin to creatinine ratio.

Analysis of novel biomarkers: kidney injury molecule-1 (KIM- 1) is a highly sensitive biomarker of tubular kidney injury that becomes elevated in response to multiple renal insults, such as hyperglycemia-associated oxidative stress and inflammation.

All the biochemical readings were done in the Biochemistry Laboratory of Al-Kut Educational Hospital with standardized automated procedures in it to provide uniformity and accuracy of data.

2.5 Statistical Methods:

Data was analyzed with SPSS Version 28.0 (IBM Corp., Armonk, NY). Means with standard deviations (SD) of continuous variables and frequencies of categorical variables were considered as descriptive data. Independent t-tests were used in case-control comparisons to determine differences between the diabetic kidney disease group and healthy controls to conduct comparative studies. Differences between various stages of chronic kidney disease were determined using analysis of variance (ANOVA). The Pearson correlation analysis was used to evaluate the relationship between biomarkers to determine whether there are significant associations between the conventional and the emerging biomarkers. Statistical significance was accepted at $p < 0.05$ in all statistical tests and where applicable, confidence intervals and their 95-percent confidence limits were provided.

2.6 Ethical considerations and quality Assurance:

These quality assurances consisted of standardized sample collection procedures, direct sample processing and adequate sample storage and, where possible, blinded laboratory testing to eliminate bias. Quality control measures were adopted in all of the laboratory procedures. Issues of ethics were also taken into consideration; this included the presence of informed consent by all the participants, confidentiality of the participant data and appropriate clinical referral of any abnormal results identified during the study. There was a low risk of any adverse effect on the participants and researchers restricted to usual blood and urine sample tests. Management of data was undertaken in a manner that ensured proper storage of all participant details with proper de-identification of the participants to ensure their privacy was locked and at the same time data were to be maintained to allow statistical analysis.

3.Results

3.1 Interpatient and Control Group Comparison:

In Figure 1, the distribution of the patients with Diabetic kidney disease (DKD) and the healthy control group is shown, in which the statistical significance of the key biomarkers is

emphasized. The DKD group has significantly higher serum glucose, HbA1c, urea and creatinine than the healthy population, which is in accordance with the metabolic and renal dysfunction expected in this disease. The serum glucose is elevated, indicating the poor glycemic control, and the markedly increased HbA1c reflects the hyperglycemic state that has been present during the last 2-3 months. These high glycemic indices describe the pathophysiological mechanism leading to progression of DKD. The concentration of both creatinine and urea levels were significantly higher in the DKD group than controls, suggesting a decline in kidney function and glomerular filtration ratio. The patient group also showed significantly increased urinary albumin excretion and albumin creatine ratio, which are indicative of progression of diabetic nephropathy. The co-occurrence of these biomarkers is indicative of poor glucose control and loss of renal energy (characteristic of Diabetic disease).

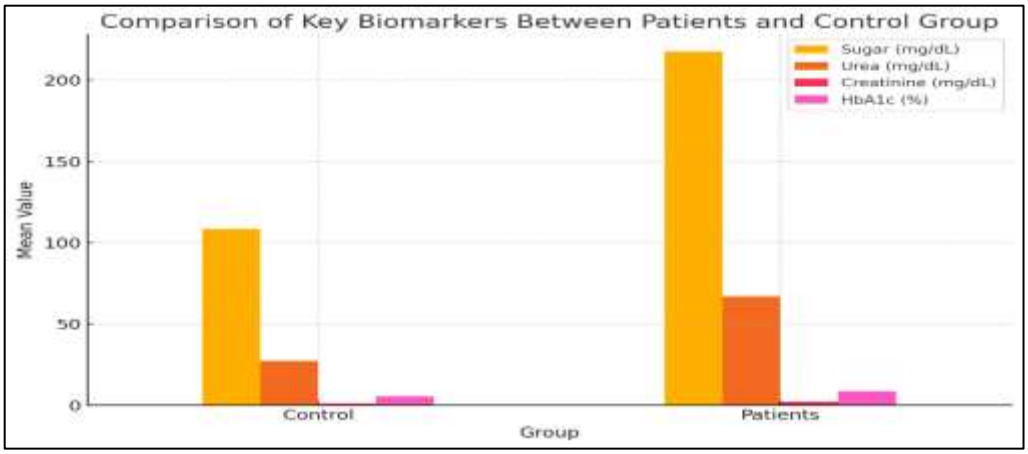

Figure 1, Effect of DKD on Sugar, Protein, Creatinine and HbA1c

3.2 Comparison of creatinine Levels in Patients and Control Patients:

Figure 2 shows a comparison of serum creatinine level between the patient segment with Diabetic kidney disease, and the healthy control segment. The median serum concentration of creatinine in the group of patients is significantly higher than that of the control group indicating poor renal functioning. Serum creatinine is considered sympathetic of the poor renal performance since it is a known standard of glomerular filtration rate. The interquarter range shows that the values of most of the patients are higher than the control group, which again proves that the renal dysfunction condition exists in diabetic kidney disease patients.

The wide range that the creatinine readings in the patient group, where some of the readings stood at 3.0 mg/dL, reveals that the level of renal impairment varies among the diabetic kidney disease group. As compared to the control group, there is a narrower range of lower values of creatinine levels in the control group, which would imply that the kidneys are functioning normally. The median healthy adult creatinine is below 1.2mg/dL that is within the reference range. This underlines the inequalities in the course of renal dysfunction among the diabetic patient group, which substantiates the individualization of the monitoring and treating strategies.

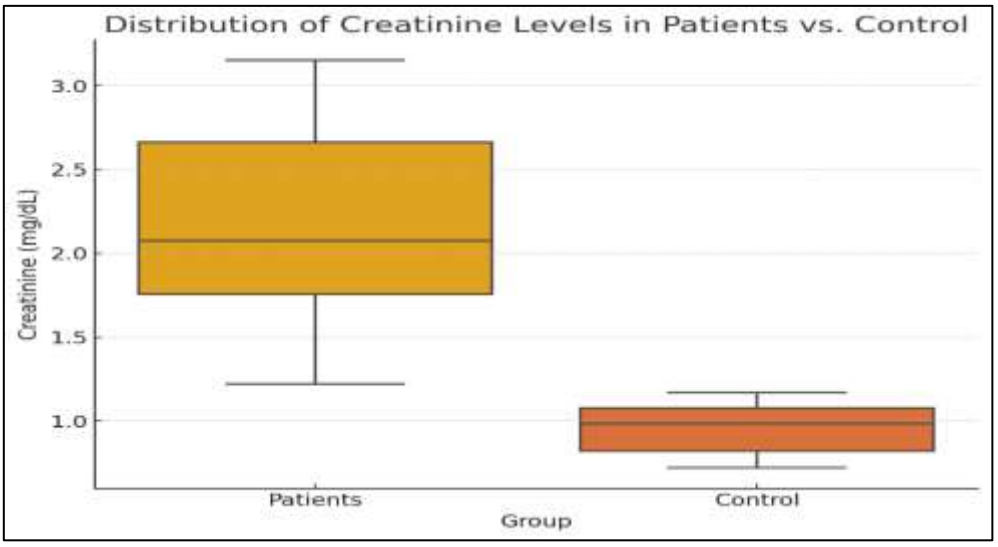

Figure 2, illustrate a comparison of serum creatinine level between the patient segment with Diabetic kidney disease.

3.3 Biomarker Correlation Matrix:

The picture shown in Figure 3 presents the correlation matrix that identifies the correlations between significant biomarkers in patient groups of diabetic kidney disease and healthy controls. The significant results are the following:

3.3.1 Inverse Association in the eGFR with the Kidney Markers:

The present data reflect a close negative relationship that exists between estimated glomerular filtration rate (eGFR) and serum creatinine, which proves that increased levels of creatinine characterize reduced functioning of the kidneys. This way, an elevated level of blood urea nitrogen is also related to the reduced eGFR, which further indicates the existence of renal disease. In addition, HbA1c has an inverse relationship with eGFR, and the results indicated that the lack of glycemic control has direct proportionality to a worsening kidney decline. This inverse association exhibits the definitive, pathophysiological association between metabolism management and the preservation of renal functions in diabetic patients revealing the reason to achieve maximum glycemic control to prevent or delay the deterioration of kidney functions.

3.3.2 Diabetic and lipid biomarker positive correlations:

HbA1c positively correlates well with blood glucose since it also indicates the long-term glycemic control. The research also reveals that dyslipidemia is related to high HbA1c, which is the indicator of poor glycemic control. This dyslipidemia in patients with chronic kidney disease makes them to have cardiovascular risks since it elevates LDL levels. The association of triglycerides and LDL also indicates extreme lipid disorders in diabetic patients. These interconnected results demonstrate the relationship between metabolic dysfunction in diabetes: inadequate glycemic regulation is the initiating factor of a complex of issues that include dyslipidemia, which in combination with each other expedite the development of cardiovascular and kidney outcomes.

3.3.3 Inverse Correlation of Risk Variables With HDL:

The correlation between HbA1c and HDL as well as LDL and HDL is inversely correlated. A lack of HDL is the indicator of progressive worsening of diabetes and rise of the renal markers, which is consistent with the research that low HDL and high LDL are risk factors of cardiovascular diseases in chronic renal disease. This negative correlation indicates that increased HDL levels protect against diabetic patients: the more HDL, the better is the control of metabolic and cardiovascular processes and the minimization of risks of cardiovascular and renal failure in diabetic kidney disease, and the lower the HDL, the more atherogenic lipid profile, which increases risks of cardiovascular disease and renal disease.

3.3.4 High Correlation in Albumin Biomarkers:

As expected the urinary albumin excretion and the ratio of albumin to creatinine are strongly correlated since they are both used to determine albuminuria, a symptom of diabetic kidney disease.

These results demonstrate that the interaction between the glycemic control, lipid metabolism, and renal activity is extremely complicated. These biomarkers should be carefully considered in the early risk testing in order to control diabetic kidney disease to a greater extent.

The correlation coefficient of albumin based markers is high and this validates that they can be used clinically as supplementary renal damage indicators and it is therefore justified that they should be used regularly in the diagnosis of diabetic patients with kidney disease early diagnosis.

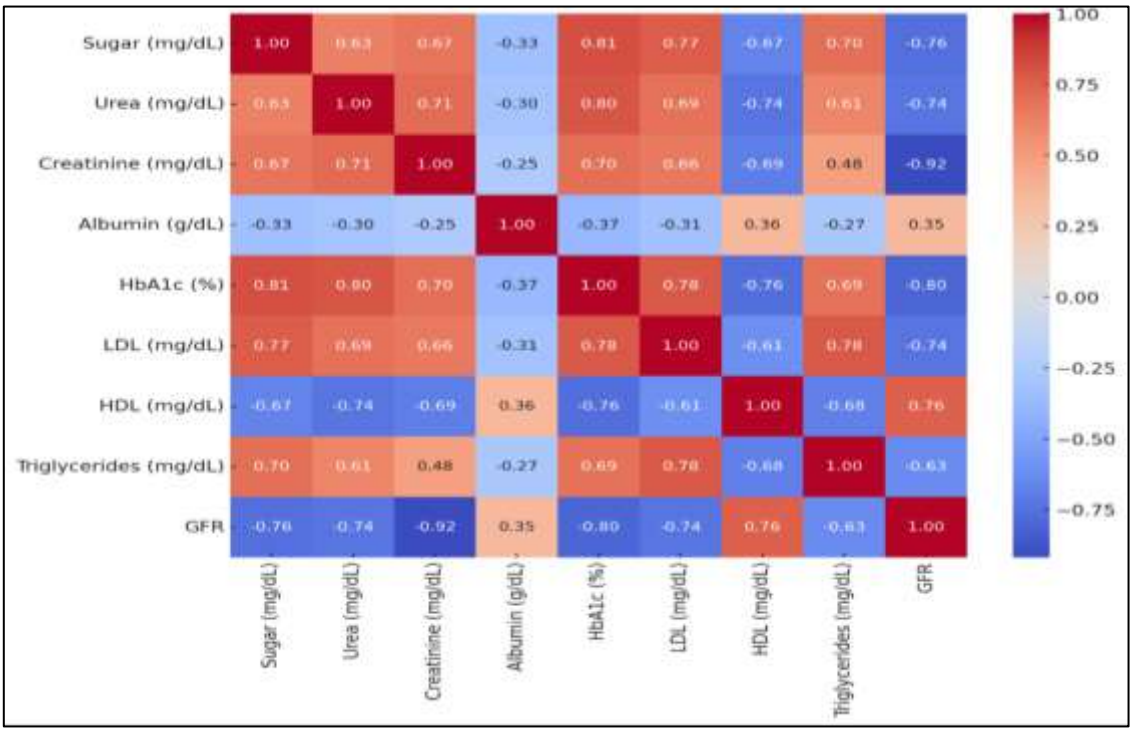

Figure 3 the correlation matrix between significant biomarkers in patient groups of Diabetic kidney disease and healthy controls

3.4 Stage Distribution of CKD in Patients:

Figure 4 illustrates the pie chart distribution of the phases of chronic kidney disease with patients with Diabetic kidney disease. The points of the salient findings are listed as follows:

3.4.1 Stages 1 Distribution and Characteristics:

Stage 1 has the proportion of about 12% of the patients. At the given stage, the renal functioning stays normal, still, some signs of the initial renal failure can be observed, even without the drop of the glomerular filtration rate. This phase is usually asymptomatic but is a predisposing factor towards the onset of chronic kidney disease especially in patients who have poor glycaemic control. Therefore, patients at Stage 1 form an important population in the establishment of preventive measures. It is possible that early intervention, intensive glycaemic control, careful observation of other risk factors, or specific education can reduce, or at least significantly slow down the further advancement to the more severe stages of the pathogenesis of the disease.

3.4.2 Distribution and Clinical Implication Distribution In Stage 2:

Stage 2 stage is the most common part of the study population, with 32% of the patients and is characterised by mild renal impairment. Clinicians have a duty of closely observing such persons and applying nephroprotective measures that would prevent the onset of additional worsening. This phase is characterized by the high number of patients; hence, urgent evidence-based treatment is needed. When applied timely and in an active way, such interventions could bring about considerable changes in the long-term renal outcomes. In this regard, the use of close follow-ups, frequent examination of the kidney function and active therapeutic changes must be emphasized in this cohort.

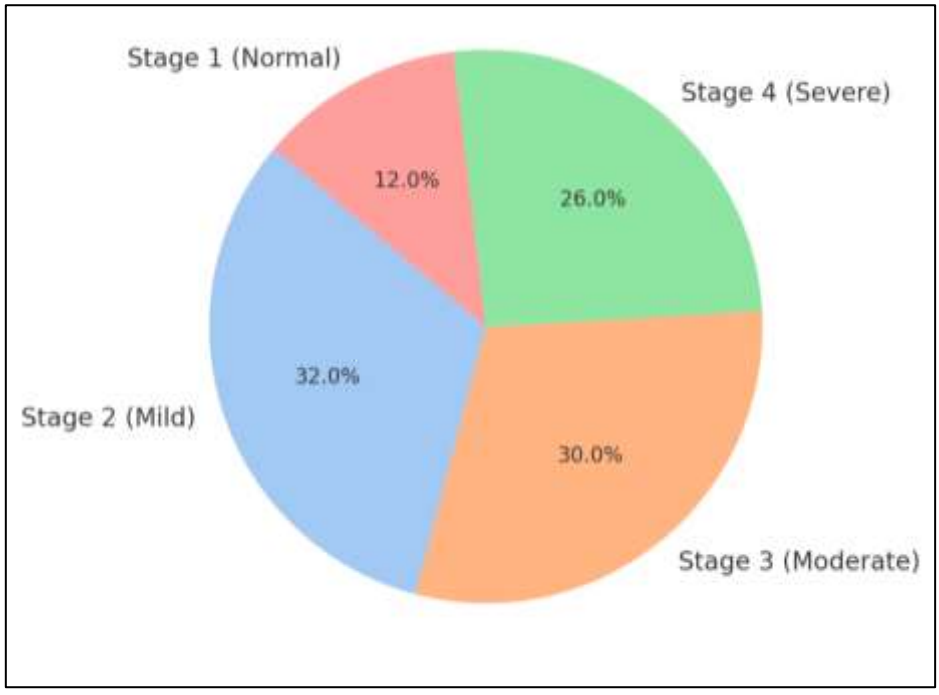

Figure 4, illustrates the pie chart distribution of the phases patients with Diabetic kidney disease

3.4.3 Stage 3 Severity and Management Requirements:

Stage 3 involves approximately 30 percent of all investigated cohort and is characterized by significantly impaired renal function, a high level of serum creatinine and urea. The patients in this age group are high-risk patients prone to cardiovascular events and hence should be closely monitored. The degree of renal impairment presented which is moderate to severe requires a multifaceted approach in nephroprotection. This approach must not focus on the renal preservation but also on cardiovascular risk reduction and the strategic way of approaching the possible renal replacement therapies. These findings require clinicians to take a multidisciplinary approach, which guarantees that renal and cardiovascular complications should be prevented and controlled to the optimum extent.

3.4.4 Stage 4 Advanced disease and Therapy Manifestations:

In our cohort, a percentage of 26 out of 100 is in Stage 4 CKD, the most end-stage kidney disease. Typical symptoms at this point are fatigue, fluid retention and electrolyte imbalance. Close surveillance and meticulous use of nephroprotective measures is an urgent action that must be taken to delay the onset of end-stage renal disease. The high percentage of those who are affected at this late stage shows the seriousness of the renal pathology among our diabetic population thus the need to institute extreme treatment measures in order to ensure that the ultimate outcome of dialysis or transplantation will subsequently not be required.

3.4.5 Distribution of Stage: Clinical Significance:

The prevalence data informs the heterogeneity of Diabetic patients in terms of the level of renal impairment. Knowing the stage distribution of chronic kidney disease among the study cohort may help to develop regionally specific screening measures and intervention associated with identifying the high-risk population, and preventing the further progression of diabetic nephropathy. The integral homogeneity of the scatter on stages 2, 3 and 4 (where 88 percent of the participants are included) suggests that most of our sample group has renal disease manifested. It is therefore necessary to roll out elaborate early-detection and effective management initiatives to ensure that the advancement of the disease in the diabetic population is put at bay.

3.5 More Biomarker Results:

3.5.1 KIM-1 analysis:

There was profound increase in KIM-1 levels in the urine of Diabetic kidney disease patients as compared to controls. This biomarker has shown to be a well-studied marker of early events of tubular damage in diabetic kidney disease. KIM-1 increases in the presence of several renal insults such as KIM-1 oxidative stress and inflammation resulting to hyperglycemia, and therefore is a sensitive biomarker of sustained kidney damage. The marked increase of KIM-1 in our diabetic patients gives credence to its possible use as a sensitized or early detection of tubular damage, which may be a precursor of the more obvious

development of proteinuria, and could be used earlier in the detection of certain patients in danger of Diabetic kidney disease development.

3.5.2 Biomarker Panel Group:

Multiprotein and peptide panels represented by biomarkers have immense possibilities in the early-detection of risks and in disease monitoring of Diabetic kidney disease (DKD). Since these multimarker methods can help to describe the variety of pathways in pathophysiology, they have been proved to be more sensitive and specific when it comes to predicting the onset and progression of diseases. This is also supported by the fact that a panel of biomarkers is superior to a single-analyte approach to diagnostics and prognostics. Broad evaluation of these panels can thus help to better risk categorize, even in patients with type 2 diabetes who have predisposition to kidney issues, and to be able to use individualized management plans based on the risk profile of the person.

4. Discussion

4.1 The Significance of Study Finding:

This comparative cross-sectional study reveals the important findings related to the pathophysiological mechanism that are behind the diabetic kidney disease and also provides evidence on the potential usefulness of the recently developed biomarkers to stratify risks at early stages. found a significant correlation between the traditional diabetic indicators and the kidney functions parameters, further justifying the multifaceted relationship between metabolic imbalances and renal progressive deterioration (Cao & Cooper, 2011; Alicic *et al.,* 2017). The sample size of 50 participants (30 patients with the DKD and 20 healthy controls) demonstrated significant differences in the levels of biomarkers, as shown in Figure 1, with patients in the various stages of CKD: Stage 1 (12%), Stage 2 (32%), Stage 3 (30%), and Stage 4 (26%). Independent t-tests were used to show statistically significant results between the patient and control groups in all the measured parameters. These findings are consistent with existing knowledge that diabetic kidney disease is a progressive disease that leads to gradual loss of renal functions overtime (Amorim *et al.,* 2019; Jung & Yoo, 2022).

4-2 The pathophysiological mechanisms and correlations of the biomarkers:

The directions of the correlations observed between the markers of glycemic control and parameters of kidney functioning as shown in Figure(2) reflect the main pathophysiological processes in diabetic nephropathy. The ANOVA test showed that there were significant differences in HbA1c levels between CKD stages with an increasing trend going up CKD stages 1-4. Persistent hyperglycemia triggers a series of adverse effects, including the production of advanced glycation end products (AGEs), the activity of protein kinase C and polyol pathway overactivity (Beisswenger *et al.,* 2013; Rabbani & Thornalley, 2018). These processes combine to cause glomerular hyperfiltration, expansion of the mesangium and progressive tubulointerstitial fibrosis (Reidy *et al.,* 2014; Kanwar *et al.,* 2008). The Pearson correlation analysis showed that there was a significant negative association between eGFR and both the serum glucose and HbA1c, thus proving the centrality of chronic hyperglycemia in the process leading to nephron loss and dysfunction. The correlation patterns also indicate that metabolic

abnormalities are broader than glucose homeostasis, involving lipid metabolism and inflammatory processes, which are also associated significantly with the parameters of the lipid profile, as Figure(3) demonstrates (Vaziri, 2006; Forbes & Cooper, 2013).

4-3 The novel biomarker performance and clinical value:

The use of a new potential biomarker of kidney injury, kidney injury molecule-1 (KIM-1) in our research is an advantageous contribution to the evaluation of diabetic kidney disease as shown in Figure (4) KIM-1, which is a type I transmembrane glycoprotein, is upregulated specifically in proximal tubular epithelial cells following injury and is a very sensitive indicator of tubular damage (Vaidya *et al.,* 2011).

Statistically, independent t -tests showed that KIM-1 levels were significantly higher in DKD patients than in healthy controls, and levels showed progressive increments in CKD stages. Correlation analysis using Pearson indicated a positive significant association between KIM-1 levels and established indicators of kidney dysfunction that include serum creatinine and albuminuria, and low levels of eGFR. This finding is especially significant since subclinical renal damage is poorly detected using traditional biomarkers (Swaminathan *et al.,* 2023; Campion *et al.,* 2017) The tubular hypothesis of diabetic kidney disease also highlights the role of the tubulointerstitial injury in disease progression, and thus, KIM-1 would be a welcome addition to the diagnostic armamentarium of diabetic kidney disease as well as in the understanding of tubulointerstitial injury in diabetic kidney disease (Vallon & Thomson, 2020; Vaidya *et al.*, 2011)

4-4 Cross-correlated associations multi-factorial and cholesterol metabolism:

The interrelation with Diabetic markers and the parameters of the lipid profile detected in Figure 3 indicate the multifactorial process of diabetic kidney disease development. ANOVA analysis showed that lipid profiles differ significantly between patient and control groups where DKD patients showed high levels of total cholesterol, LDL cholesterol, and triglycerides, and low levels of HDL cholesterol. Dyslipidemia in chronic kidney disease is characterized by a complex set of changes in lipoprotein metabolism, which include the reduced activity of lipoprotein lipase, diminished hepatic lipase activity, and promoted hepatogenesis in the liver and a series of hormones and the activity of their complexes in the liver (Vaziri, 2006). Pearson correlation analysis revealed that HDL cholesterol was significantly negative linked to blood creatinine and albuminuria. These metabolic disorders form a vicious spiral in which lipid abnormalities worsen kidney dysfunction, and this leads to enhanced kidney dysfunction through the process of inflammation and oxidative stresses (Wada & Makino, 2013; Jha *et al.,* 2016).The reverse correlation between HDL cholesterol and the markers of kidney dysfunction identified in our study evidences this pathophysiological connection and the significance of broad-based metabolic intervention in diabetic patients (Nguyen *et al.,* 2012; Fanelli *et al.,* 2018).

4-5 CKD stage Distribution and clinical Implications:

The pattern of distribution of patients across the various stages of CKD in our study illustrated in Figure (1) is a good source of information on the trend of disease progression and implication on clinical management. Chi-square analysis provided a significant relationship with CKD stages of distribution and profiles of biomarkers. The high proportion of patients in Stages 2 and 3 (62% combined) is consistent with how diabetic kidney disease is presented in clinical practice: on average, patients present with moderate kidney dysfunction rather than end-stage disease (Tuttle *et al.,* 2014; Satirapoj & Adler, 2014)

ANOVA analysis showed a progressive deterioration of kidney function markers across stages that were significantly different between any two consecutive stages in terms of eGFR, serum creatinine, and albuminuria. This pattern of distribution underlines why early diagnosis and treatment should be the key to preventing the occurrence of more advanced stages, which will have to be treated by means of renal replacement therapy. The fact that 12 % of patients with Stage 1 CKD (preserved eGFR) have evidence of kidney damage emphasizes the importance of a sensitive biomarker such as KIM-1 to detect subclinical disease (Liu *et al.,* 2022; Pradeep *et al.,* 2024). The Stage 4 patients (26%), in contrast, constitute a group of individuals who need intense management and sequencing to renal replacement therapy (Sagoo & Gnudi, 2020; Yamazaki *et al.,* 2021).

4-6 Clinical and Therapeutic decision-making:

The results of the work have great practical significance to clinical practice and treatment decision-making in the treatment of diabetic kidney disease. The strong correlations among the biomarkers revealed through the Pearson correlation analysis and visualized in Figures 2 and 4 indicate the possibility of using combined risk stratification models based on both classic and novel markers to achieve higher prognostic accuracy (Pena *et al.,* 2015; Perco *et al.,* 2019). Statistical comparison indicated that patients with a high level of KIM-1 had extreme chances of entering advanced stages of CKD even with a preserved eGFR evaluated using chi-square analysis. These methods can enable individual treatment plans so that clinicians might develop interventions that are based on specific risk factors as well as mechanisms of the disease. Diagnosing patients with high KIM-1 levels may encourage earlier adoption of nephroprotective treatment, which includes renin-angiotensin system blockade, SGLT2 inhibitors, and intensive glycemic control (Ruggenenti *et al.,* 2010;Yamazaki *et al.,* 2021).

Moreover, the multifactorial links found have led to the necessity of multifactorial management patterns which would include not only glycemic control but also affect lipid metabolism, blood pressure, and inflammations processes (Coca *et al.,* 2012; Peabody *et al.,* 2023).

4-7 Applications of the research and future development avenues Clinical translation:

The field of research into diabetic kidney disease has a lot of opportunities that can be utilized to develop our knowledge and benefiting patients in this way. The next research steps

should be concerned with the study of predictive value of novel biomarkers on clinical outcomes and treatment response, as well as the establishment of the correlation value between these biomarkers and final diagnosis according to Fig. 1and 4. The combination of multi-omics, which includes genomics, proteomics, and metabolomics, has potential in the discovery of novel therapeutic targets and precision medicine strategies (Mohsen *et al.*, 2023; Ma *et al.,* 2025). More advanced statistical techniques, such as machine learning algorithms, could be used to further improve the interpretation of biomarkers and risk prediction quality beyond correlation analyses as used herein and could be used to develop clinical decision support tools to use in everyday practice.

Further, investigation of point-of-care testing devices on new biomarkers, such as KIM-1, has the potential to make it less costly and allow immediate decision-making at the point of care, especially in low-resource environments (Cho *et al.,* 2018; Văcăroiu *et al.,* 2024). Another research priority will be the development of biomarker-guided therapeutic trials, which may result in more effective and individualized treatment of patients with diabetic kidney disease (Gomez-Marcos *et al.,* 2011; Saeedi *et al.,* 2019).

5. Conclusion

In summary, this paper establishes the complicated pathophysiological connections behind diabetic kidney disease and justifies the possible use of new biomarkers in risk stratification such as KIM-1. Statistical analysis with SPSS Version 28.0 (Independent t-tests, ANOVA, Pearson correlation analysis) showed strong correlations between classical diabetic parameters, lipid parameters, and renal function variables as shown in Figures 1-4. These results point to a multifactorial pathogenesis of disease progression and make the development of multifactorial management strategies relevant. Although the study limitations, such as the cross-sectional study design and a sample size of 50 participants, do not allow concluding about causal relationships and long-term outcomes, the results can be described as informative about the disease mechanisms and can point out the directions of future study. The incorporation of emerging biomarkers into the clinical practice has potential to enhance early detection, risk stratification, and therapeutic decision-making in the care of diabetic kidney disease, and eventually lead to improvement of patient outcomes and minimization of healthcare burden.

6. Author's Declaration

I, the sole author of this manuscript, declare that the work presented is original, has not been published previously, and is not under consideration for publication elsewhere. All procedures involving human participants were conducted in accordance with ethical standards, with appropriate institutional approval and informed consent. No conflict of interest exists related to this study.

7. Author's Contribution Statement

As the sole author of this study, I was fully responsible for the design, data collection, laboratory coordination, data analysis, and interpretation. I also conducted the literature review, wrote and revised the manuscript, and approved the final version for submission.

8. References:

Alicic, R. Z., Rooney, M. T., & Tuttle, K. R. (2017). Diabetic kidney disease: Challenges, progress, and possibilities. Clinical Journal of the American Society of Nephrology, 12(12), 2032–2045. https://doi.org/10.2215/CJN.11491116

Amorim, R. G., Guedes, G. D., Vasconcelos, S. M., & Santos, J. C. (2019). Kidney disease in diabetes mellitus: Cross-linking between hyperglycemia, redox imbalance and inflammation. Arquivos Brasileiros de Cardiologia, 112(6), 577–587. https://doi.org/10.36660/abc.20180166

Beisswenger, P. J., Howell, S. K., Russell, G. B., Miller, M. E., Rich, S. S., & Mauer, M. (2013). Early progression of diabetic nephropathy correlates with methylglyoxal-derived advanced glycation end products. Diabetes Care, 36(10), 3234–3239. https://doi.org/10.2337/dc12-2689

Bolignano, D., et al. (2009). Neutrophil gelatinase-associated lipocalin (NGAL) and progression of chronic kidney disease. Clinical Journal of the American Society of Nephrology, 4(2), 337–344. https://doi.org/10.2215/CJN.03530708

Campion, C. G., Sanchez-Ferras, O., & Batchu, S. N. (2017). Potential role of serum and urinary biomarkers in diagnosis and prognosis of diabetic nephropathy. Canadian Journal of Kidney Health and Disease, 4, 2054358117705371. https://doi.org/10.1177/2054358117705371

Cao, Z., & Cooper, M. E. (2011). Pathogenesis of diabetic nephropathy. Journal of Diabetes Investigation, 2(4), 243–247. https://doi.org/10.1111/j.2040-1124.2011.00131.x

Cho, N. H., et al. (2018). IDF Diabetes Atlas: Global estimates of diabetes prevalence for 2017 and projections for 2045. Diabetes Research and Clinical Practice, 138, 271–281. https://doi.org/10.1016/j.diabres.2018.02.023

Coca, S. G., Ismail-Beigi, F., Haq, N., Krumholz, H. M., & Parikh, C. R. (2012). Role of intensive glucose control in development of renal endpoints in type 2 diabetes mellitus: Systematic review and meta-analysis. Archives of Internal Medicine, 172(10), 761–769. https://doi.org/10.1001/archinternmed.2012.1343

Fanelli, C., Noreddin, A., & Nunes, A. (2018). Inflammation in nonimmune-mediated chronic kidney disease. In Chronic kidney disease: From pathophysiology to clinical improvements. IntechOpen. https://doi.org/10.5772/intechopen.74423

Forbes, J. M., & Cooper, M. E. (2013). Mechanisms of diabetic complications. Physiological Reviews, 93(1), 137–188. https://doi.org/10.1152/physrev.00045.2011

Gomez-Marcos, M. A., et al. (2011). Yearly evolution of organ damage markers in diabetes or metabolic syndrome: Data from the LOD-DIABETES study. Cardiovascular Diabetology, 10(1), 90. https://doi.org/10.1186/1475-2840-10-90

Jha, J. C., Banal, C., Chow, B. S., Cooper, M. E., & Jandeleit-Dahm, K. (2016). Diabetes and kidney disease: Role of oxidative stress. Antioxidants & Redox Signaling, 25(12), 657–684. https://doi.org/10.1089/ars.2016.6664

Jung, C. Y., & Yoo, T. H. (2022). Pathophysiologic mechanisms and potential biomarkers in diabetic kidney disease. Diabetes & Metabolism Journal, 46(2), 181–197. https://doi.org/10.4093/dmj.2021.0056

Kanwar, Y. S., et al. (2008). Diabetic nephropathy: Mechanisms of renal disease progression. Experimental Biology and Medicine, 233(1), 4–11. https://doi.org/10.3181/0705-MR-134

Lecamwasam, A., Ekinci, E. I., Saffery, R., & Dwyer, K. M. (2020). Potential for novel biomarkers in diabetes-associated chronic kidney disease: Epigenome, metabolome, and gut microbiome. Biomedicines, 8(9), 341. https://doi.org/10.3390/biomedicines8090341

Liu, H., Feng, J., & Tang, L. (2022). Early renal structural changes and potential biomarkers in diabetic nephropathy. Frontiers in Physiology, 13, 1020443. https://doi.org/10.3389/fphys.2022.1020443

7 X., et al. (2025). Global burden of chronic kidney disease due to diabetes mellitus, 1990–2021, and projections to 2050. Frontiers in Endocrinology, 16, 1513008. https://doi.org/10.3389/fendo.2025.1513008

Merchant, M. L., & Klein, J. B. (2007). Proteomics and diabetic nephropathy. Seminars in Nephrology, 27(6), 627–636. https://doi.org/10.1016/j.semnephrol.2007.09.003

Mohsen, F., Al-Absi, H. R., Yousri, N. A., El Hajj, N., & Shah, Z. (2023). A scoping review of artificial intelligence-based methods for diabetes risk prediction. NPJ Digital Medicine, 6(1), 197. https://doi.org/10.1038/s41746-023-00933-5

Najafian, B., Alpers, C. E., & Fogo, A. B. (2011). Pathology of human diabetic nephropathy. Contributions to Nephrology, 170, 36–47. https://doi.org/10.1159/000324942

Nguyen, D. V., Shaw, L. C., & Grant, M. B. (2012). Inflammation in the pathogenesis of microvascular complications in diabetes. Frontiers in Endocrinology, 3, 170. https://doi.org/10.3389/fendo.2012.00170

Peabody, J. W., et al. (2023). Clinical utility of a novel test for assessing cardiovascular disease risk in type 2 diabetes: A randomized controlled trial. Diabetology & Metabolic Syndrome, 15(1), 155. https://doi.org/10.1186/s13098-023-01122-w

Pena, M. J., et al. (2015). A panel of novel biomarkers representing different disease pathways improves prediction of renal function decline in type 2 diabetes. PLoS ONE, 10(5), e0120995. https://doi.org/10.1371/journal.pone.0120995

Perco, P., Pena, M., Heerspink, H. J., Mayer, G., & BEAt-DKD Consortium. (2019). Multimarker panels in diabetic kidney disease: The way to improved clinical trial

design and clinical practice? Kidney International Reports, 4(2), 212–221. https://doi.org/10.1016/j.ekir.2018.12.001

Pradeep, U., et al. (2024). A comprehensive review of advanced biomarkers for chronic kidney disease in older adults: Current insights and future directions. Cureus, 16(9), e70413. https://doi.org/10.7759/cureus.7041

Rabbani, N., & Thornalley, P. J. (2018). Advanced glycation end products in the pathogenesis of chronic kidney disease. Kidney International, 93(4), 803–813. https://doi.org/10.1016/j.kint.2017.11.034

Reidy, K., Kang, H. M., Hostetter, T., & Susztak, K. (2014). Molecular mechanisms of diabetic kidney disease. Journal of Clinical Investigation, 124(6), 2333–2340. https://doi.org/10.1172/JCI72271

Ruggenenti, P., Cravedi, P., & Remuzzi, G. (2010). The RAAS in the pathogenesis and treatment of diabetic nephropathy. Nature Reviews Nephrology, 6(6), 319–330. https://doi.org/10.1038/nrneph.2010.58

Saeedi, P., et al. (2019). Global and regional diabetes prevalence estimates for 2019 and projections for 2030 and 2045: Results from the International Diabetes Federation Diabetes Atlas, 9th edition. Diabetes Research and Clinical Practice, 157, 107843. https://doi.org/10.1016/j.diabres.2019.107843

Sagoo, M. K., & Gnudi, L. (2020). Diabetic nephropathy: An overview. In Methods in Molecular Biology (Vol. 2067, pp. 3–7). Springer. https://doi.org/10.1007/978-1-4939-9841-8_1

Satirapoj, B., & Adler, S. G. (2014). Comprehensive approach to diabetic nephropathy. Kidney Research and Clinical Practice, 33(3), 121–131. https://doi.org/10.1016/j.krcp.2014.08.001

Swaminathan, S. M., et al. (2023). Novel biomarkers for prognosticating diabetic kidney disease progression. International Urology and Nephrology, 55(4), 913–928. https://doi.org/10.1007/s11255-022-03354-7

Tesch, G. H. (2008). MCP-1/CCL2: A new diagnostic marker and therapeutic target for progressive renal injury in diabetic nephropathy. American Journal of Physiology – Renal Physiology, 294(4), F697–F701. https://doi.org/10.1152/ajprenal.00016.2008

Tuttle, K. R., et al. (2014). Diabetic kidney disease: A report from an ADA consensus conference. Diabetes Care, 37(10), 2864–2883. https://doi.org/10.2337/dc14-1296

Văcăroiu, I. A., et al. (2024). Biomarkers of acute kidney injury: A concise review of current literature. Revista Română de Medicină de Laborator, 32(4), 305–313. https://doi.org/10.2478/rrlm-2024-0028

Vaidya, V. S., et al. (2010). Kidney injury molecule-1 outperforms traditional biomarkers of kidney injury in preclinical biomarker qualification studies. Nature Biotechnology, 28(5), 478–485. https://doi.org/10.1038/nbt.1623

Vaidya, V. S., et al. (2011). Regression of microalbuminuria in type 1 diabetes is associated with lower levels of urinary tubular injury biomarkers, kidney injury molecule-1, and N-acetyl-β-D-glucosaminidase. Kidney International, 79(4), 464–470. https://doi.org/10.1038/ki.2010.404

Vallon, V., & Thomson, S. C. (2020). The tubular hypothesis of nephron filtration and diabetic kidney disease. Nature Reviews Nephrology, 16(6), 317–336. https://doi.org/10.1038/s41581-020-0256-y

Vaziri, N. D. (2006). Dyslipidemia of chronic renal failure: The nature, mechanisms, and potential consequences. American Journal of Physiology – Renal Physiology, 290(2), F262–F272. https://doi.org/10.1152/ajprenal.00099.2005

Wada, J., & Makino, H. (2013). Inflammation and the pathogenesis of diabetic nephropathy. Clinical Science, 124(3), 139–152. https://doi.org/10.1042/CS20120198

Yamanouchi, M., et al. (2017). Improved clinical trial enrollment criterion to identify patients with diabetes at risk of end-stage renal disease. Kidney International, 92(1), 258–266. https://doi.org/10.1016/j.kint.2017.03.018

Yamazaki, T., Mimura, I., Tanaka, T., & Nangaku, M. (2021). Treatment of diabetic kidney disease: Current and future. Diabetes & Metabolism Journal, 45(1), 11–26. https://doi.org/10.4093/dmj.2020.0217

Yan, Z., Wang, G., & Shi, X. (2021). Advances in the progression and prognosis biomarkers of chronic kidney disease. Frontiers in Pharmacology, 12, 785375. https://doi.org/10.3389/fphar.2021.785375


DUBAI

III. Dubai International Conference of Pure, Applied and Technological Sciences

ISBN 978-625921210-4

Rimar Academy
Publishing House